Electrochemical Studies of Cellulose Matrices: Absorption, Diffusion, Reactivity & Detection

Bonne, Michael

Award date:
2008

Awarding institution:
University of Bath

Electrochemical Studies of Cellulose Matrices: Absorption, Diffusion, Reactivity & Detection

Michael James Bonne

A thesis submitted for the degree of Doctor of Philosophy
University of Bath
Department of Chemistry
September 2008

_____
Michael James Bonne

"*… methinks both you and the chymists agree, that the surest way is to learn by experiments what differing parts particular bodies do consist of…*"

Robert Boyle, *Sceptical Chymist* (1661) p.434

"Alchemy, however, is a chaste prostitute, who has many lovers but disappoints all and grants her favours to none. She transforms the haughty fools, the rich into paupers, the philosophers into dolts, and the deceived into loquacious deceivers…"

Trithemius, *Annalium Hirsaugensium Tomi II*, S. Gallo (1690) p.141

Abstract

Electrochemical techniques are used to investigate a variety of novel and natural cellulose materials. Novel cellulose architectures are formed using electrodeposition of cellulose microfibrils (from spruce tree) and by the layer-by-layer deposition or solvent casting of cellulose nanofibrils (from sisal). Pure cellulose (with a crystal structure of cellulose-I) constitutes the majority of all architectures, however additional properties were incorporated via the addition of polymers (polydiallyldimethylammonium chloride, chitosan), nanoparticles (TiO_2) or binding molecules (boronic acid dendrimer). Cotton fabric, a natural form of cellulose, was also investigated via the physical attachment to the electrode surface of graphite flake modified cotton samples using a course lycra membrane. All samples are characterised using a combination of scanning electron microscopy, atomic force microscopy and small and wide angle x-ray scattering.

The absorption, diffusion and detection of charged species in cellulose materials is studied using voltammetry under aqueous conditions. Firstly, architectures are probed using charged metal species like $Fe(CN)_6^{3-/4-}$ and $Ru(NH_3)^{3+/2+}$ in order to construct a model of diffusion and absorption. Later, target analytes such as environmental molecules (triclosan, sodium dodecylsulfate) and physiological type molecules (alizarin red S) are detected within a typical range of 10^{-6} – 10^{-3} M. Approximations of Fick's Laws are used to calculate membrane diffusion co-efficients. Langmuir type binding is assumed and the binding of species in the cellulose architectures is quantified.

The reactivity of molecules in cellulose matrices is studied. Methyl viologen ($MV^{2+/+}$) is shown to form aggregates in when partitioned in a cellulose environment. Methemoglobin undergoes a novel demetallation when in a charged nanocellulose-TiO_2 matrix. The reactivity of a well-known catalase model system, the dinuclear manganese metal complex $[Mn(IV)_2(\mu\text{-}O)_3L_2](PF_6)_2$ (with L = 1,4,7-trimethyl-1,4,7-triazacyclononane), is shown to be affected by the presence of a cellulose matrix.

Acknowledgements

Firstly, I would like to thank all the people who gave me technical support during this PhD including: Unilever Research & Development at Port Sunlight for the PhD stipend (money) and the support of Dr. Matthew Helton, Dr. Anthony McKee and Matthew L. Parry; Wim Thielemans for the supply of nanofibrils of cellulose; Matt Wasbrough and Dr. Karen J. Edler who helped me with taking (and interpreting!) the SAXS/WAXS data; Alan Carver for help with iron elemental analysis; Ewan Galbraith and Dr. Tony James, for the synthesis of the boronic dendrimer; Konstantina Tsourounaki and Elefteria Psillakis for my time in Greece working on environmental chemistry; and summer project student James Taylor for help with the cotton electrode.

The electrochemistry research group who made the lab a bearable place over the years especially PhD students Liz Milsom, Stuart Macdonald and Rob French – cheers for the beers! My project students should also get a mention so cheers Charlie and the guys. Everyone in the Bath Chemistry Department who I have annoyed with my presence over lunch, beers, competitions etc. especially Andy Kirk, Alberto Fattori, Nathan Hollingsworth (team Vistech!).

A big thank you to those of you who made this thing remotely possible (in a non-chemistry way) with their love and support: my family Mum, Dad, Greg, Noni and Omi. My non-chemistry friends who are Jax and Neil, JP, Bobby, Stew CS, Matty, Leo, Nines and loads of other who have been just great.

And finally, Dr. Frank Marken without whose support, depth of knowledge and friendship this whole endeavour never would have even begun.

Thank you all!

Contents

Chapter 1 : Introduction

1.1 Cellulose: Omnipresent Polymer of Nature

Cellulose is the most abundant biomaterial in the world. The backbone of plants and trees, it is a polymeric carbohydrate of D-glucose with a β-glycosidic bond joining consecutive sugar monomers (Figure 1.1). It was discovered in 1838 by the French chemist Anselme Payen who described it as a fibrous solid that remains behind after the various treatment of plant tissues with acids and ammonia, followed by extraction with water alcohol and ether [1]. Cellulose is a homopolymer with a highly functionalized linear stiff-chain. It is characterized by its hydrophilicity, chirality, and biodegradability. Its ability to form versatile semicrystalline fiber morphologies has made it the 'backbone' of the natural world. It is cellulose that gives the plant cell wall its structural rigidity by forming hierarchical microstructures with high strength and stiffness called 'microfibrils'. These are ultimately arranged into amorphous and crystalline regions in biostructures that are prevalent in the natural world.

The breakdown of these cellulose structures has been of great interest for the production of general purpose materials and as a potential biofuel such as cellulosic ethanol. Pure cellulose can be generated via biosynthetic routes or harsher chemical acid-hydrolysis of natural sources of cellulose such as sisal [2]. The biosynthesis of cellulose takes place not only in plants, but also in bacteria (such as Acetobacter, Acanthamoeba, and Achromobacter spp.), algae (Valonia, Chaetamorpha spp.), and fungi [3]. Cellulose produced from sisal (a type of grass found in India) is used to explore the nanoscale world of this polymer. Sisal is a commonly occurring plant with an annual worldwide fibre production reported to attain 4.5 million tons [4]. Cellulose content of sisal varies between 49.6 wt% and 61 wt%, depending on the age of the plant [5]. Sisal fibre length is found to be between 1 and 1.5 m, with average diameters of 200 μm [6]. Sisal was used in this work as a novel source of cellulose whiskers. These cellulose nanofibrils can obtained from native cellulose source by acid hydrolysis which removes the amorphous regions. The remaining particles are individualized nanosize monocrystalline particles.

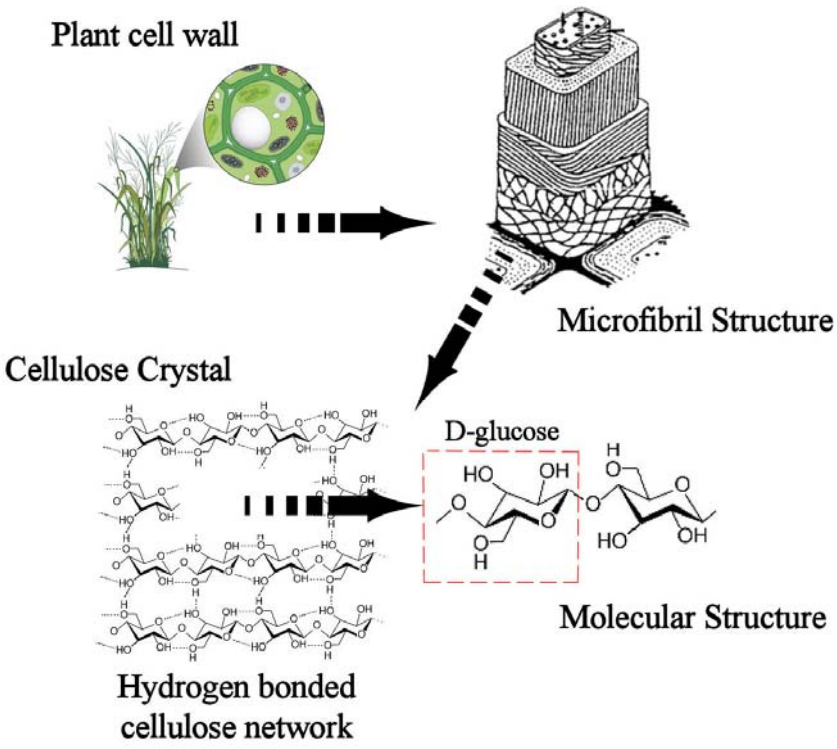

Figure 1.1 Cellulose and its derivation from natural resources, via a microfibril structure to individual crystals of cellulose. The structure of cellulose is hydrogen bonded β-glycosidic linkage chain of the D-glucose monomer units.

Macroscopic cellulose systems such as cotton remain a relatively unexplored area when looking at the chemistry occurring within them in processes such as dyeing and bleaching. Current methods are reliant upon macroscopic observations rather than molecular studies; does the material take the colour of the dye? Are the chromophores of the stain removed by the bleaching agent? By analyzing in situ data it might be possible to answer more specific questions about the thermodynamics and kinetics of cellulose chemistry. What is the binding energy of the dye to the cotton? What is the mechanism for the bleaching agent? Does the cellulose incur a 'matrix effect' upon the binding/bleaching?

In order to fully understand these integrated chemical systems, an element of controlled design needs to be applied to the study of integrated cellulose chemical systems. Nanotechnology enables the controlled formation of chemical environments, making it possible to create geometries which can be accurately modeled thus yielding quantitative rather qualitative information. The advantages to nanotechnology in this instance are two-

fold: the formation of a mimetic cellulose architecture can act as a precursor to the development of new materials with a multitude of new applications.

A chemical sensor has the ability to yield information about its environment, via its make-up of a physical transducer and a chemically selective layer [7]. In this thesis cellulose has been used as the fundamental component of that layer, be it in a form more recognisable such as the material cotton, or in its base form as a micro- or nano-fibril. As a mimetic cellulosic system or in a modified state, this omnipresent natural polymer shows great versatility when providing a solid state matrix which can influence the electrical properties of a chemical environment.

The manufacture of natural and artificial cellulose architectures is achieved using a number of different methods throughout this thesis. Natural architectures enable the exploration of synthetic and biological chemical systems through mimetics, whilst artificially constructed architectures offer the possibility of utilising the unique and robust properties of cellulose in new applications. Electrochemistry is a powerful tool for making in situ measurement, therefore methodologies for coupling the cellulose architecture to the electrode surface need to be addressed to fully utilise it.

New frontiers of science where cellulose is used have been created so that its innate properties can be ascertained for any given scenario it is found in. With areas including environmentally friendly cellulose fiber technologies, bacterial cellulose biomaterials, and in-vitro syntheses of cellulose, this brings fresh perspectives on this most versatile of materials. In view of the considerable increase in interdisciplinary cellulose research and product development over the past decade worldwide, this thesis takes a new approach to the chemistry of cellulose by looking at it from an electrochemical perspective.

1.2 Electrochemical Theory

1.2.1 Thermodynamics of Chemical Systems

An integrated chemical system can be described when at its most dynamic as a set of reactants and products that interchange with each other. The introduction of dynamism suggests intrinsically that there is an element of change over a given period of time that is occurring in the system. When a set of reactants (be they solid, liquid or gas) are mixed, they are often not at their most stable, especially as mixing implies the addition of surplus energy into a chemical system. It is at this point that it is stated that a reaction occurs within the chemical system. An equilibrium is established when this energy change is dissipated throughout the system, typically through a rearrangement of its components to form a set of products. Predictions can be made about the direction (but not the rate) in which these chemical reactions proceed through the use of the axioms of thermodynamics [8]. In chemistry we may represent the physical changes in the system by writing it as a chemical equation, for example,

Equation 1.1

$$A + B \rightleftharpoons C + D$$

where reactants A and B are introduced to each other to form products C and D. The energy of this system may also be described mathematically. Any given isolated physical system must obey the laws of conservation that state that "…energy cannot be created or destroyed, only changed in its form or transferred from one body to another, but ultimately remaining constant." This remains equally as true for the thermodynamic energy of a chemical system. The Gibbs energy, G_{sys}, describes the total energy of the system, including that of the reactants, products and additional energy sources (heat, light, etc.) at constant pressure. Equilibrium can be defined as the point where G_{sys} is at its lowest possible level. Therefore, at the point at which equilibrium becomes established,

Equation 1.2

$$dG_{sys} = 0$$

Each of the species A, B, C and D in this example will have a quantifiable number of fundamental elements (atoms, molecules) associated to them that is essential to the balancing of this equation under constant pressure and temperature. The concept of chemical potential can be used to describe the amount of energy present when all elements

of the species are taken into account. Therefore, at equilibrium, the chemical potentials of the reactants and the products must also equal one another. Mathematically this can be described as,

Equation 1.3

$$\mu_j = \left(\frac{\partial G}{\partial n_j} \right)_{T, n_i \neq n_j}$$

where μ_j (J mol^{-1}) is the chemical potential of species j (j = A,B,C…), T is the absolute temperature and n_i is the number of moles of i (i = A,B,C…). It follows that at equilibrium that

Equation 1.4

$$\mu_A + \mu_B = \mu_C + \mu_D$$

For this to be true the system must remain under constant pressure and temperature. Gibbs suggested that the chemical potential of a solution system when expressed in individual chemical potentials is

Equation 1.5

$$\mu_j = \mu_j^0 + RT \ln \left(\frac{[j]}{[j]^0} \right)$$

where μ_j is the standard chemical potential of j, R is the universal gas constant (8.314 J K^{-1} mol^{-1}), T is the temperature, [j] is the concentration of species j and $[j]^0$ is the standard concentration (typically 1 molar). It therefore follows that μ_j^0 is the energy of one mole of j when at equilibrium comparative to the standard concentration. The general equilibrium constant can be used to describe the balance of reactants and products in a chemical reaction. The general equilibrium constant (for the reaction in Equation 1.1) is

Equation 1.6

$$K_C = \frac{\text{products}}{\text{reactants}} = \frac{\left(\frac{[C]}{[j]^0} \right) \left(\frac{[D]}{[j]^0} \right)}{\left(\frac{[A]}{[j]^0} \right) \left(\frac{[B]}{[j]^0} \right)}$$

Therefore, when this is combined with Equation 1.5 we can derive an expression for the energy in the system

Equation 1.7 $$\mu_j - \mu_j^0 = RT \ln K_c$$

This expression is the fundamental law of thermodynamics and combines all of the laws of thermodynamics (0^{th}, 1^{st} and 2^{nd}) into one expression that can be applied to any chemical system. Next, the implications of these general thermodynamics principles are explored with regards to their application in electrochemistry.

1.2.2 Electrode Thermodynamics

When looking at an electrochemical equilibrium, there is not only a balance of chemical potentials but also electrical energies. Electrical energies or potentials are defined from one species to another by their electronic structure. In the chemical systems studied in this work, reactants and products are usually in different phases (solid and liquid) and are typically a conducting material i.e. a metal or carbon, and a solution phase ion. For example, when looking at a metal, the electronic structure involves electronic 'conduction bands'. The electrons are free to move throughout the solid, thus binding the metal cations together. The energy levels in these bonds can reach a total energy called the Fermi level. Conversely, the ions in the solution phase have discrete electronic energy levels constituting the molecular orbitals of the ion.

When electrons are transferred into and out of this electronic structure, they enter the lowest un-occupied molecular orbital (LUMO) or leave the highest occupied molecular orbital (HOMO). Consistent with the idea of equilibria being established when the energies of a system are at their lowest possible levels, the filling and emptying of these energy levels works in the same way. Subsequently, if a metal is introduced to an ionic species the difference in energy between the electronic structures creates a potential difference in the system. This potential difference is the driving force for the exchange of electrons between the metal and ions in solution. Ultimately, the electrons in the system must occupy all of the lowest energy levels available in the system (Figure 1. 2).

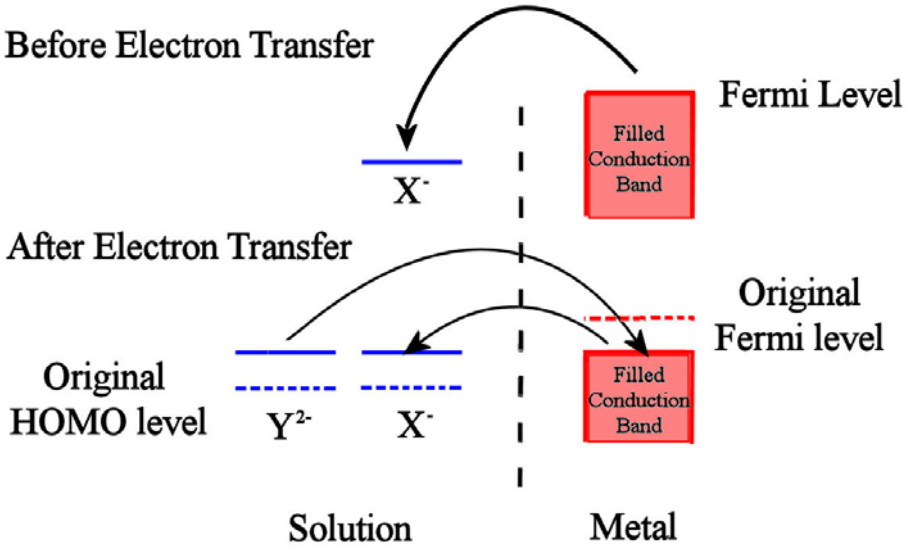

Figure 1. 2 A representation of the energy levels in the solution and electrode phases before and after electron transfer has occurred.

In order to account for the electrical energies now present in the system it is necessary to define an electrochemical potential, $\overline{\mu_j}$, of a species *j*,

Equation 1.8

$$\overline{\mu_j} = \mu_j + Z_j F \phi$$

where μ_j is the chemical potential and Z_j is the charge on molecule *j*, *F* is the faraday constant (the charge on one mole of electrons, 96487 Coulombs) and ϕ is the potential of the particular phase – electrode or solution – in which species *j* is found. At equilibrium the electrical potential of an electrochemical reaction must obey the laws of conservation therefore if we take an example electrochemical reaction

Equation 1.9

$$X^-(aq) + e^-(m) \rightleftharpoons Y^{2-}(aq)$$

where X^- is an ion in aqueous solution which when introduced to a metal electrode which has a conduction band with a Fermi level higher than the LUMO of X^-. Equilibrium is therefore established when the chemical and electrical potential are at their lowest possible energy levels, causing the transfer of an electron to X^- forming species Y^{2-} in the aqueous phase, with a new electrical charge. Mathematically, as with the chemical potential it implies that

Equation 1.10

$$\overline{\mu}_{X^-} + \overline{\mu}_{e^-} = \overline{\mu}_{Y^{2-}}$$

In Equation 1.8 we can see that the electrical potential is the sum of the chemical potential and the potential of the phase multiple by the charge on the species in that particular phase. Therefore by substituting Equation 1.10 into Equation 1.8 it can be said that

Equation 1.11

$$\left(\mu_{X^-} + 1F\phi_s\right) + \left(\mu_{e^-} - F\phi_m\right) = \left(\mu_{Y^{2-}} + 2F\phi_s\right)$$

where ϕ_m and ϕ_S are the potential of the metal electrode and the solution respectively. The driving force of an electrochemical reaction is the applied potential, the difference in potential between the electrode and the solution $(\phi_m - \phi_s)$. If Equation 1.11 is now rearranged to obtain the driving term and inserted into Equation 1.7 you arrive at the expression

Equation 1.12

$$\phi_m - \phi_s = \frac{\Delta\mu^0}{F} + \frac{RT}{F}\ln\left(\frac{Y^{2-}}{X^-}\right) \quad \text{where } \Delta\mu^0 = \Delta\mu^0_{X^-} + \Delta\mu_{e^-} - \Delta\mu^0_{Y^{2-}}$$

which at constant temperature and pressure is called the Nernst Equation. In electrochemistry it is termed that when an electrochemical reaction occurs if an electron is gained by a species it is *reduced* or alternatively an electron is lost it is *oxidized*. This leads to the general electrochemical reaction

Equation 1.13

$$O(aq) + ne^-(m) \rightleftharpoons R(aq)$$

For this general case it is now possible to express the Nernst equation in its more familiar form of

Equation 1.14

$$E_e = E^{0'} + \frac{RT}{nF}\ln\frac{[O]}{[R]}$$

where E_e is the equilibrium potential of the electrode which is resultant from the standard electrode potential of the reaction, $E^{0'}$ (the activity co-efficient is assumed to be equal to 1). The standard electrode potential is characterized by the chemical and electrical potential of the reaction (Equation 1.11). Equilibrium electrochemical measurements

enable thermodynamic parameters (free energies, entropies and enthalpies, equilibrium constants) to be ascertained. Before equilibrium is reached, the rate at which an oxidation or reduction might occur is proportional to the energy needed to promote electron transfer. If Equation 1.13 is at the equilibrium potential E_e (no net current is flowing) it follows that

Equation 1.15

$$k_{red}[O]_O = k_{ox}[R]_O$$

where the rate of reduction, k_{red}, and the rate of oxidation, k_{ox}, when multipled by the concentration of oxidised and reduced species respectively are equal to each other. In the transition state theory, a transition state intermediate is form at the point before the reactants becomes a product. The transition state intermediate is usually of a higher energy than either that of the reactant or product (in this case, the oxidized and reduced species). The transition state theory therefore states that the rate of electron transfer for a reduction process (k_{red}) is

Equation 1.16

$$k_{red} = A\exp\left(\frac{-\Delta G_{red}^{\mp}}{RT}\right)$$

where $\Delta G_{red}^{\mp}$ is the free energy of activation for electron transfer ($\mp$) and A is a frequency factor which in this instance is an additional energy function for the electroactive species. Figure 1.3 shows the reaction co-ordinate diagram for the reduction of O to R (Equation 1.13).

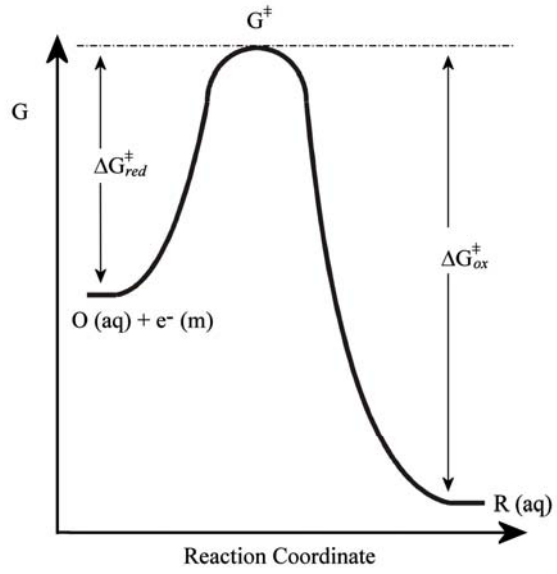

Figure 1.3 Free energy plot for a simple one electron reduction of a species O(aq).

It follows for a fixed temperature and pressure the energy of formation of the reduced species, $\Delta G_{red}^{\mp}$, is equal to the energy of the transition state, $G^{\mp}$, minus that of the oxidized species (G_{ox}) and vice versa. For any other applied potential where $E \neq E_e$ the electrochemical system is no longer at equilibrium making the electron-transfer thermodynamically viable. The deviation of E from the equilibrium potential means that a new parameter, η, needs to be introduced to describe the potential when a current is flowing (when the cell is active). Therefore, the 'over-potential' is

Equation 1.17

$$\eta = E - E_e$$

Over-potentials are important in electron-transfer as they describe the direction of the reaction, where oxidation occurs its sign is negative and reduction when it is positive. The Butler-Volmer equation can be derived by looking at the relationship between the over-potential and the net current. Although not explored thoroughly here, this relationship is important due to the conclusions it draws, especially when looking at the extreme cases of large and small standard exchange currents, i_o, which is directly proportional to the overall rate of electron transfer, k^o. When k^o is large, little or no over-potential is needed to drive the electrochemical reaction; this is said to be the *reversible* case as current is as likely to flow in either of the anodic (oxidation) or cathodic (reduction) direction depending upon the sign of the over-potential. Conversely, when k^o is small, this is the *irreversible* case as

a high over-potential is required to drive the reaction. The use of Tafel analysis (involving the plotting of ln(i) against E) allows the elucidation of the standard exchange currents and hence the reversibility of any given electrochemical reaction. However, it must be noted that the results of such experiments are only relative to the transport of material in and out of the interfacial region. From this point it shall be assumed that k^o is large and that all systems are reversible and mass transport (*vide supra*) is the rate determining factor of electron-transfer.

1.2.3 Current Flux in Electron Transfer

By altering the equilibrium potential of the electrode in a reaction, the relative ratio of oxidized species to reduced species may also be altered i.e. the reaction co-ordinate is said to be altered, determining the direction of the equilibrium (Equation 1.13). The number of electrons transferred at the solution:metal interface now becomes the point of focus in the electrochemical reaction. If the number of electrons transferred, N, is multiplied by the number of electrons per reaction, n, and the charge on one mole of electrons, F, you get the total charge of the reaction, Q.

Equation 1.18

$$N \times nF = Q$$

This process will be time dependent as the electrons are not transferred instantaneously. The rate at which the charge of electrons is monitored with respect to time (the electron-transfer rate) is referred to as the current, i, therefore

Equation 1.19

$$i = \frac{dQ}{dt}$$

When the number of moles electrolysed is considered with respect to time, it is then possible to combine Equation 1.8 and Equation 1.19 to give

Equation 1.20

$$\frac{dN}{dt} = \frac{i}{nF}$$

where dN/dt in standard units describes the number of moles electrolysed per second which is directly proportional to the rate of change in the charge (the current). Unlike a homogeneous reaction, electron transfer is heterogeneous thus implying that there is added complexity to the process with it dependent on mass transport to the surface of the electrodes and various surface effects, in addition to the usual kinetic variables (*vide supra*). It is at this point that the experimental set up of electron-transfer first manifests itself in this derivation with a need to define the electrode:electrolyte interface, the electrode area.

Equation 1.21

$$\frac{dN}{dt} = \frac{i}{nFA}$$

By using this equation and the Nernst equation (Equation 1.14) it can now be understood not only how a reaction occurs but also how fast it will occur. Information about an electrode reaction is often gained by determining the current as a function of the potential (*i*-*E* curves). From these curves it can be seen that the electrolytic current may dependent predominately upon two variables

- The rate of the heterogeneous electron transfer (rate determining **electrode kinetics**)
- The transport to, or products from, the electrode surface (rate determining **mass transport**)

In this work on the effect of cellulose matrices on electrodes surfaces, it is important to point out that the electrode kinetics are dependent upon the ion in solution once at the electrode surface. It is therefore more relevant to examine the effect of mass transport in this system, as the cellulose will inhibit or promote mass transport in the system. However, it is still necessary to have an understanding of the processes of electron transfer kinetics as they are fundamental to the understanding of the current-potential curves that are the cornerstone of electrochemical measurements.

1.2.4 Diffusion

There are three modes of mass transport which are significant in electrochemical systems and they are diffusion, convection and migration [9]. Previously it has been proved that electrical current is the result of electron transfer and that it is proportional to the number of species at a specified electrode surface during a given period of time. Flux, j, is often used to describe the flow of a reactant undergoing electron-transfer at an electrode with a surface area A and can be substituted into Equation 1.18 to give

Equation 1.22 $$i = FAj$$

It is this same flux which Fick used over 150 years ago, but instead of the flow of electrons, it was the flow of molecules in a system. It is evident that diffusion will take place down a concentration gradient where a volume containing many species will diffuse to an area where there are fewer species (obeying the principles of entropy). Therefore, at any point x in a 1-dimensional model, there will be a diffusive flux quantified by Fick's 1st Law:

Equation 1.23 $$j = -D\frac{\partial c}{\partial x}$$

where j is the flux of a number of molecules passing through a unit area. The two terms on the right-hand side of this equation specifically relate to the local concentration gradient at point x, $\partial c/\partial x$, and D is known as the diffusion co-efficient. Points of note in Fick's 1st law are firstly that the sign of the flux is negative, which is coherent with the concentration having a down gradient. Secondly, the diffusion co-efficient is intrinsic of the species it describes. Typically, as later suggested by the Stokes-Einstein relation, diffusion co-efficients are inversely proportional to molecular size and lie in a region between $10^{-9} – 10^{-10}$ m^2 s^{-1} when experiments are carried out in thermostatically controlled conditions.

In practice, it is necessary to know what the concentration at x is as a function of time. This leads to the derivation of Fick's 2nd Law, which is achieved by considering the variation of concentration of a substance within a region defined by planes of equal area, A, at x and (x + dx) during a time interval, dt (Figure 1.4).

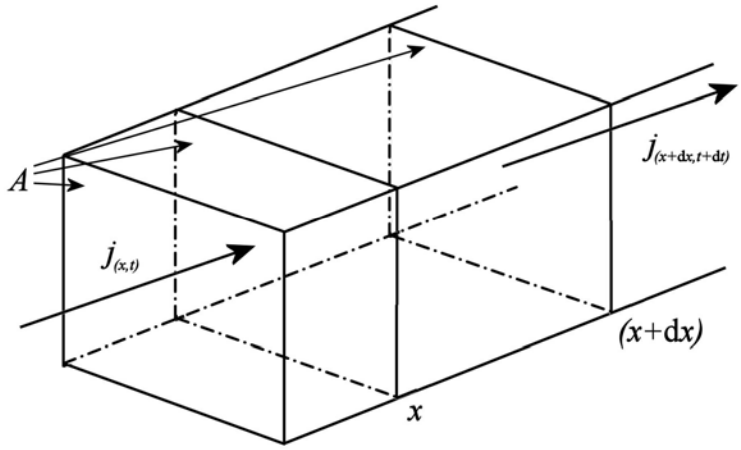

Figure 1.4 Schematic of the flux of a species into and out of a zone bounded by two planes separated by a distance d*x*.

A statement of mass conservation whereby the difference in flux of *c* entering through the plane at *x* and the flux leaving at plane (*x* + d*x*) during time d*t* may be expressed as

Equation 1.24

$$c_{(x,t+dt)}Adx - c_{(x,t)}Adx = j_{(x,t)}Adt - j_{(x,t+dt)}Adt$$

This expression may be rearranged and the flux from Equation 1.23 may be substituted in it so that

Equation 1.25

$$\frac{\partial c}{\partial t} = D\left(\frac{\partial^2 c}{\partial x}\right)$$

This expression is Fick's 2nd Law for one dimension (*x* in the Cartesian axes; this expression may also be derived for all three axis or in cylindrical or polar co-ordinates depending upon the size and geometry of *A*). It enables the prediction of diffusion via differentials of concentration with respect to both time and distance. However, this does not account for the other forms of mass transport, migration and convection.

Convection is movement of molecules caused by natural convection and mechanical force e.g. stirring, rotation, sonication, etc. Natural convection occurs within the solution due to vibration, thermal gradients and/or density differences within the solution. These could be due to the electrochemical reaction itself being exo/endothermic for example. Mechanical force is sometimes deliberately introduced in order to 'swamp out' natural convection. It is

also possible to describe mathematically some systems where artificial convection is introduced as it can reduce a number of the observable variables (*vide supra*).

Migration in an electrochemical system is important as it also used to describe the effect of an electrical field upon the movement of charge species. At the electrode/solution interface there exists and external field as a result of the drop in potential between two phases. Typically, in electrochemical experimentation is advantageous to eliminate the effects of migration as it often makes the interpretation of a system more complex. This is made possible by the introduction of a supporting electrolyte, usually a salt that is chemically and electrochemically inert, which is added to solutions in high concentrations. The reasoning behind this addition may be explained by examining the electrode/solution interface during the exchange of electrolytic ions.

1.2.5 The Electrode/Solution Interface

When an electrochemical reaction occurs there is a redistribution of electrical charges in the bulk solution. For a reaction where k^o is high and is being driven to reduction, there will become an excess of negatively charged ions at the electrode/solution interface and an excess of unreacted positively charged ions in the bulk solution. The supporting electrolyte will have components with both positive and negative charges that are fully dispersed at both the electrode/solution interface and in the bulk solution. This neutralizes the charge in the system, hence when the potential difference at the electrode/solution interface is such that electron-transfer occurs, the new imbalance in the concentrations of the electroactive species is cancelled out by the presence of an excess of neutral charge. Although there will still be an electrode/solution potential difference, the distance that this penetrates into the bulk is typical in the order of 1-2 nm (the so-called ‘double layer’). These effects have two results: (i) the absence of potential gradients outside of this narrow region prevents migration effects and (ii) the distance is short enough to be comparable with the tunneling of electrons between electrode and reactant.

The double layer has now been established as volume with a depth of ca. 1-2 nm and the cross section of the electrode surface. It is here that all electron transfer reactions occur. It is characterized by the electrode/solution boundary and the subsequent forces that are

imposed upon it. The double layer is of fundamental importance as it affects the forces that govern the behaviour of the bulk solution. The difference in potential at the interface induces electrostatic interactions between the electroactive ions and the electrode. There is even a cause to look at the effect of its distance upon the solvent molecules whose dipole moments are also affected within this range.

There are many theories that have attempted to describe the structure and behaviour of the double layer, the first of these was by Helmholtz. In his model (and subsequent attempts) it is assumed that no electron transfer reactions occur directly at the surface of the electrode. Instead, there are charge densities attributed to the electrode, q_m, and to the solution, q_s. Again, conservation of energy suggests that there should be overall charge neutrality so

Equation 1.26 $$q^m = -q^s$$

This charge is the result of the redistribution of electrolyte ions at the interface and the re-orientation of dipoles in solvent molecules and is driven by electrostatic interactions. Helmholtz describes this redistribution as the attraction of an ion to the electrode, where its distance from the electrode is limited by the thickness of its solvation shell. In later theories (e.g. the Grahame models) this is described as the Outer Helmholtz Plane (OHP), whilst the penetration of ions through the solvation shell to the electrode surface is described as the Inner Helmholtz Plane (IHP). The ions in the IHP are said to be 'specifically adsorbed' (Figure 1.5).

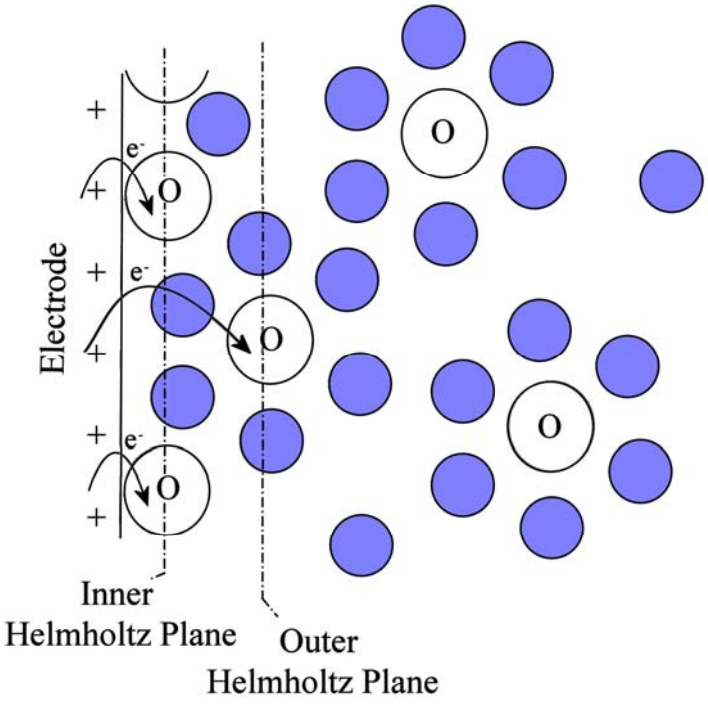

Figure 1.5 Schematic representation of the Outer (adjacent to the electrode surface with solvation shell) and Inner (specifically adsorbed to the electrode surface) Helmholtz Plane.

This double layer is the equivalent to an electrical capacitor. This is only a model and further work has been done on improving this model so that it more accurately portrays the electrode solution interface (a more modern approach is to use statistical mechanics).

After the double layer, the next zone that is appreciable to the changes that occur during electron-transfer is the Nernst Diffusion layer. What happens to the products of electron transfer once they are formed in the double layer? Electron transfer occurs for species that are in the double layer and beyond as there is a continuum of exchange of ions from the bulk solution into the double layer. As mentioned previously, coupled to electron transfer are the elements of mass transport in an electrochemical system. It is due to this mass transport that further quantities of ions are able to get close enough for electron tunnelling to occur. As migration has been limited by the presence of supporting electrolyte, convection and diffusion transport ions to the site of electron exchange. As the rate constant of electron transfer is assumed to be large, it is these elements that become the rate determining parameters.

Consider an electrode of area, A, and the reaction in Equation 1.13. Before any potential difference is applied to the system, it is assumed that there is a uniform bulk concentration

of oxidized species, [O]* throughout the solution. If the electrode is then connected to a potential source, the reaction is driven to completion and the oxidized species in the double layer are able then to be reduced. As a result a concentration gradient is induced between the concentration of O at the surface (where [O] = 0 after electron transfer occurs) and the bulk solution (where [O] = [O]*). The concentration gradient is perpendicular to the x-axis thus inducing an influx of oxidized species to replace those that have been reduced towards the electrode surface. This is the point at which a diffusion layer is first defined in the system giving it three distinct zones. At the electrode surface in the double layer where [O] = 0, the diffusion layer where [O] ≠ [O]* and [O] ≠ 0 and finally the bulk solution where [O] = [O]* (Figure 1.6).

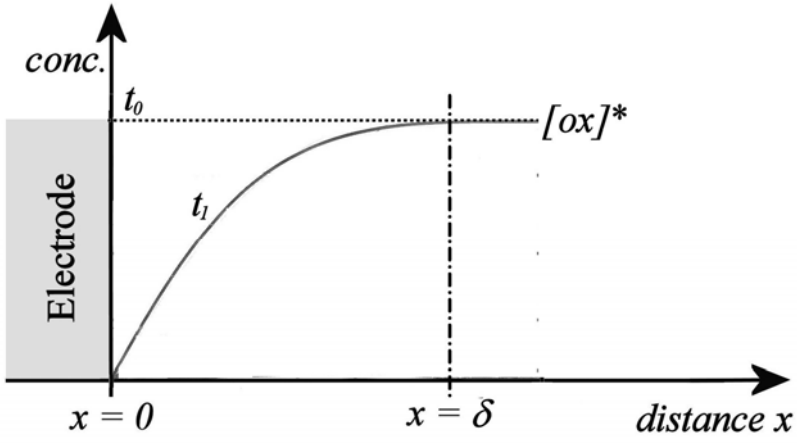

Figure 1.6 The Nernst diffusion layer thickness is $x = \delta$ at time t_1 and does not exist at time t_0.

The size of the diffusion layer grows proportionally to the length of time as electron-transfer consumes more and more of the oxidized species. This growth could occur infinitely however natural convention prevents as it competes by bringing new oxidized species from the bulk solution. This provokes the development of a steady-state at the diffusion layer/bulk solution boundary. It is called the Nernst diffusion layer as he first suggested an estimate for measuring the thickness of the diffusion layer. The definition of the diffusion layer is said to be the distance over which the concentration goes from the bulk value to zero at the electrode surface. By monitoring the current when a steady-state has been established, i_{lim}, the diffusion layer thickness, δ, may be calculated as

Equation 1.27

$$\delta = \frac{DFA[O]^*}{i_{\lim}}$$

The current measure here is an example of a *limiting current*, which flows when the electrode potential drives the electrode reaction to completion at the electrode surface. It is termed limiting as it is the point at which the reaction reaches a steady-state and the current is limited by the experimental parameters. There are a number of simplifications in this model. It is assumed that the electrode area is large enough for it to be termed a 'macroelectrode', therefore the diffusion is planar and only the x-axis need be considered when looking at the concentration profile. Secondly, it is assumed that the diffusion co-efficient of the oxidized species is equal to that of the reduced species. Finally, the electron transfer rate constant is assumed to be fast enough and the over-potential large enough for the concentration of oxidized species at the electrode surface to be equal to zero.

1.2.6 Voltammetry

The use of monitoring electrochemical processes becomes particularly apparent when monitoring changes in current as a function of the working potential. This experimentally is referred to as voltammetry and may encompass the study of electron transfer kinetics as well as diffusional motion in an integrated chemical system as discussed previously. From this point forward, all examples of studies at electrode surfaces are assumed to be occurring at the primary electrode's surface, the *working electrode*. The simplest approach to measuring the current/voltage characteristic of a system is to use a two electrode cell, where the second electrode, *the counter*, completes the circuit to ensure a flow of electrons. However, this set-up has a distinct disadvantage as it not only monitors the potential difference between working electrode and solution, but all the components of the cell. It is also a function of the product of the current flowing between the electrodes and its subsequent resistance and the potential difference between the counter electrode and the solution phase. For this reason it is necessary to introduce a third electrode, the *reference electrode*. This acts as a cell within the main cell and monitors the additional parameters introduced. When the three electrode cell is coupled with electronics (such as a potentiostat) which compensate the measured potential at the working electrode with that found at the reference electrode, it then becomes possible to focus on processes occurring at the working electrode.

Voltammetry may take many different forms depending upon the mathematical function used to alter the potential. In this thesis cyclic voltammetry (a modification of its simpler relative, linear voltammetry) is the experimental method used. By altering the potential linearly as a function of time and reversing the sign of the gradient at chosen potential intervals, the current response is observed.

Equation 1.28 $$E(t) = E - v_s t$$

where v_s is the sweep or scan rate of the potential (noting that at $t = t_0$ then $E = E_1$, at $t = t_1$ then $E = E_1$ and at $t = t_2$ then $E = E_2$). The form of this potential function may be seen in Figure 1.7A. The form of the current response takes up an altogether more complex form called the cyclic voltammogram.

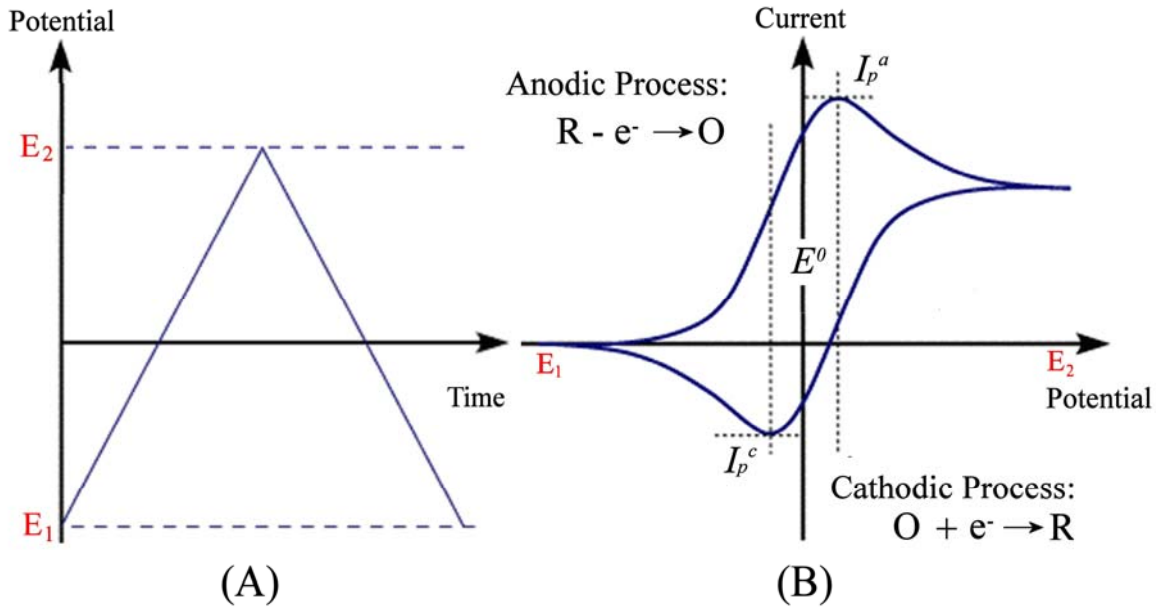

Figure 1.7 (A) Variation of potential with time during a cyclic voltammetry experiment. (B) Basic cyclic voltammogram for reversible one electron reduction and oxidation.

When studying a voltammogram, it is necessary to have in mind what process is occurring at the working electrode/solution interface. Once again looking at Equation 1.13, the over-potential must exceed the standard potential of the reaction in order for oxidation to occur and current to flow.

$$R(aq) \rightleftharpoons O(aq) + ne^-(m)$$

Thus when the standard potential is reached, there is an increase in the current response. However, when looking at the voltammogram there is a peak rather than an infinite increase in current proportional to potential. The appearance of a peak is due to the growth of the Nernst diffusion layer. This means there is a limited amount of the reduced species near enough to the double layer for electron transfer to occur. When equilibrium has been established then there is a constant exchange of reduced and oxidised species between the bulk solution and the Nernst diffusion layer.

In Figure 1.7B there is also a current flowing before E^0 is reached. This violates the principle that current only flows when E^0 has been exceeded. This is because this does not take into account the relative size of k^0 to the diffusion co-efficient. It has been previously mentioned that when k^0 is small the electron transfer reaction is said to be irreversible. In this case, the principle would hold that current will only flow when E^0 is exceeded. In the figure we have the opposite, the reversible case, where k^0 is large and electron transfer is fast. In this instance, as soon as electron transfer becomes viable, current begins to flow. The voltammogram potential-current peak can be divided into two zones, where at the beginning of the peak the signal is kinetically controlled and at the maxima where it is diffusion controlled.

The newly introduced variable of the scan rate has a marked affect upon the resulting voltammograms. When the scan rate is increased, the potential of the peak current shifts for an irreversible reaction but remains constant for the reversible case. There is also an effect on the peak current. In Equation 1.22 and Equation 1.23, it was noted that the current or flux of electrons is directly proportional to the concentration gradient at the electrode solution interface. When the scan rate is altered so is the length of time, *dt*, that the concentration gradient is measured over. Therefore at fast scan rates *dt* is very small, resulting in a large current response. Ultimately, by combining the Butler-Volmer expressions of electron transfer and Fick's laws of diffusion it can be proved that for the reversible case

Equation 1.29

$$\left|i_p\right| = 0.4663^{\frac{3}{2}} nAFD^{\frac{1}{2}} v_s^{\frac{1}{2}} [ox]_{bulk}$$

Therefore a diffusion limited species with reversible electron transfer characteristics will have a direct proportionality of the peak current with the square root of the scan rate. This is as true for a reduction as much as it is for an oxidative process and is called the Randles-Sevcik equation.

Voltammograms are labelled specifically for each species that is undergoing electron transfer at the working electrode. The peaks resulting from the limitations of diffusion in the cell are called the anodic (oxidation) and cathodic (reduction, when the potential sweep is reversed) peak currents, I_p^a and I_p^c. Although the shape of the peaks is identical, the potential at which they occur is not the same for the anodic and cathodic processes. Instead there is a shift to a more positive potential of E^0 for the anodic response and more negative for the cathodic signal. This so called peak-to-peak separation is characteristic of cyclic voltammograms and for a reversible 1-electron transfer the peak separation is 59 mV at 25°C and independent of scan rate. The potentials at which these peaks occur can be summed then divided by two yielding the mid-point potential, E_{mid}, which is equivalent to the standard potential of the reaction. The potential must always be defined with a corresponding reference value. In this work, all voltammetry has been conducted using a calomel reference electrode with the potential axes on any voltammograms label accordingly (V vs. SCE).

One instance when there is no peak-to-peak separation is when the species under going electron-transfer is not diffusion controlled. Instances of this are typical when a redox active species is immobilised on the surface of the working electrode. A species may be attached via a process such as adsorption and the most common way of explaining this process is described by the Langmuir Isotherm. Langmuir-type adsorption has three specific criteria: (i) that binding sites are non-specific (no one site is more favourable for binding than another), (ii) that binding is independent of prior or subsequent binding and (iii) that only a monolayer layer of the substance forms on the substrate. With a finite area assumed for the electrode surface, it is possible to introduce a new variable of the surface coverage, Γ_{total}, measured in mol cm^{-2}. By assuming that the species has undergone the same Nernstian electron transfer behaviour it is possible to derive an expression similar to the Randles-Sevcik equation for diffuse species.

Equation 1.30

$$I_p = \frac{F^2}{4RT} v_s A\Gamma_{total}$$

This difference between adsorbed and diffuse species is immediately apparent as the cyclic voltammogram of an adsorbed species will have a characteristic symmetry to its anodic and and cathodic peak response (Figure 1.8A). Through integration of this peak signal it is also possible to calculate the charge of the signal. This is a direct representation of the number of adsorbed species on the electrode surface as all species are expected to have under gone electron transfer.

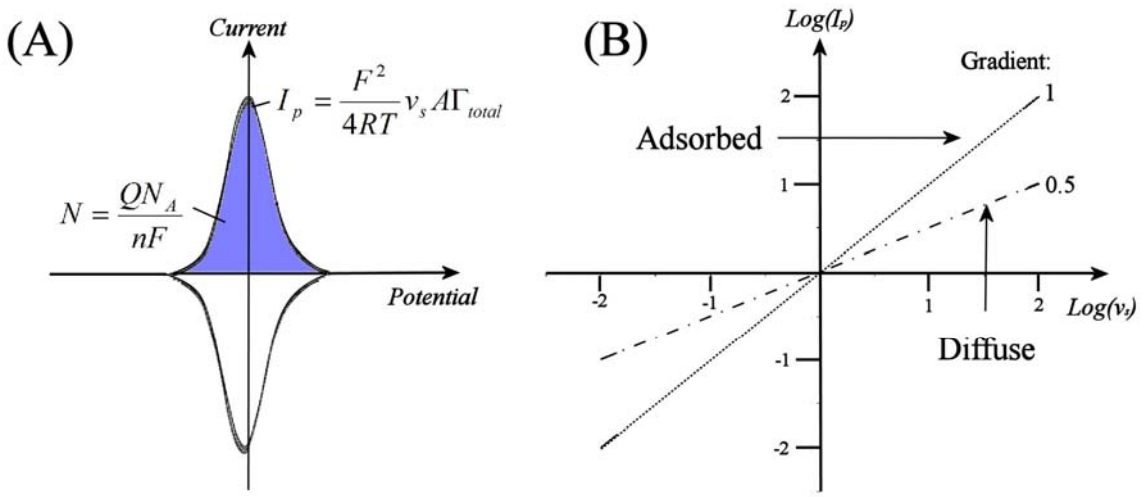

Figure 1.8 (A) Cyclic voltammogram for an adsorbed species under Nernstian conditions. (B) The logarithmic plots of current vs. scan rate for an (i) adsorbed and (ii) a diffuse electron active species. Axes are accurate when $F^2 A\Gamma_{total} = 4RT$ for adsorbed species and $1 \cong \log(A^2 F^2 [ox]^2_{bulk} D)$ for diffuse species.

This behaviour allows a distinction to be made between the respective peak currents of diffuse and adsorbed species as the proportionality with respect to the scan rate is square rooted. When plotting the logarithm of the current-scan rate the gradient of the corresponding line can be used to determine whether the species is diffuse or adsorbed (Figure 1.8B).

1.2.7 Rotating Disc Electrode Voltammetry

Until this point it has been assumed that the three modes of mass transport are apparent in the cell, that diffusion brings species to the electrode/solution interface, natural convection

stirs the bulk solution and migration is limited by the presence of a supporting electrolyte. These modes are again in the voltammetric signals obtained during experimentation and can often convolute information making it difficult to attain accurate quantitative measurements. Rotating disc electrode (RDE) voltammetry is the first instance where, by purposefully introducing convection, natural convection can be controlled and the Nernst diffusion layer may be altered. This essentially means that forms of mass transport are distinctly represented on the voltammogram; the limiting current is indicative of limits of diffusion.

In a typical RDE experiment, a disc electrode is rotated at speeds of between 0 and 50 Hz. This induces an alteration to the hydrodynamics of the cell as the electrode begins to act like a pump, pulling solution towards the disc. Upon reaching the disc, the solution is perturbed by the presence of the electrodes and fluid moves away from the central axis of the disc. The concentration flow profile can now be clearly defined as planar diffusion to the electrode surface (see Figure 1.9).

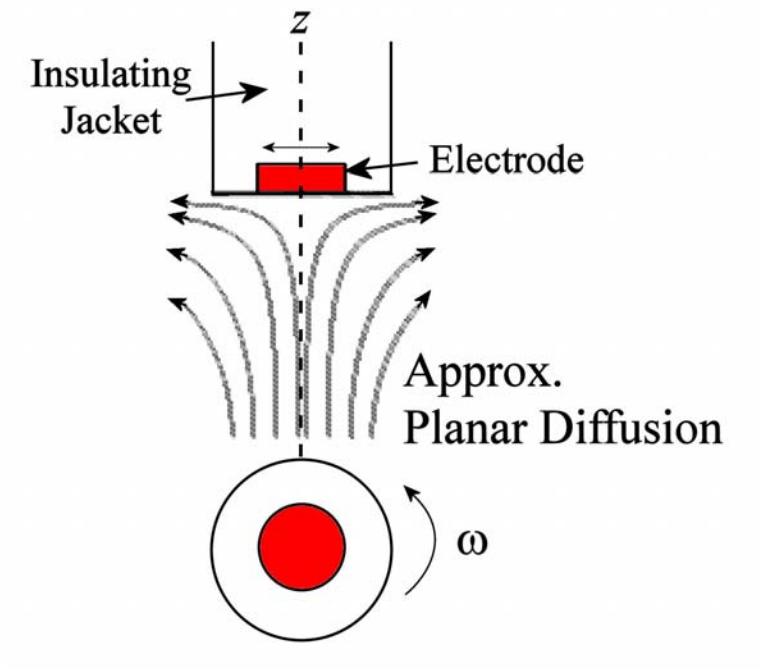

Figure 1.9 Schematic of rotating electrode and the flow patterns of the solution.

The velocity component, v_z, of the solution near the electrode surface can be described as being approximately

Equation 1.31

$$v_z \approx -0.510\omega^{\frac{3}{2}} v_{bulk}^{\frac{1}{2}} D^{\frac{-1}{3}} z^2$$

where ω is the speed at which the electrode is rotated, v_{bulk} is the kinematic viscosity of the bulk solution and z is a distance on the axis normal to the electron surface. The velocity component is analogous to the diffusion co-efficient when looking at Fick's 1st Law for convection (similar in its composition to Equation 1.23 for diffusion). When mass transport is under steady-state conditions, the convective and diffusive components sum to equal zero and it is assumed that there is enough background electrolyte to negate migration effects. The equation may be resolved if it is also assumed that the concentration of the species at the electrode is equal to zero, a result of electron transfer. The limiting current for the reaction in Equation 1.13 maybe now be evaluated as being

Equation 1.32

$$i_{\lim} = 0.62nFA[ox]_{bulk} D v_{bulk}^{\frac{-1}{6}} \omega^{\frac{1}{2}}$$

which is known as the Levich equation for RDE experiments and predicts the limiting current as a function of the square root of the rotation speed. It is another way of describing a diffusion layer similar to that of the Nernst diffusion layer, however this time the experimentalist has control over the thickness of the layer. The diffusion layer thickness, δ, can be predicted by

Equation 1.33

$$\delta = 1.61 D^{\frac{1}{3}} v_{bulk}^{\frac{1}{6}} \omega^{\frac{-1}{2}}$$

where the inverse proportionality of the diffusion layer thickness to the speed of rotation rationalises that the gradient of the concentration profile will be steeper. This in turn explains why the limiting current is larger at fast rotation as the flux is being driven by the steeper gradient. The ability to control and monitor the diffusion layer at the electrode surface is an important tool when looking at the behaviour at the electrode surface. By being able to experimentally control the solution phase dimensions of the systems, it is possible to now include further modifications to the solid phase electrode.

1.2.8 Electrochemical Processes at Modified Electrodes

The chemical processes that occur at modified electrode surfaces are analysed electrochemically in order to determine the thermodynamic properties of the layer, the kinetics of electron transfer at the layer-electrode and layer solution boundaries and the kinetics of mass- and charge-transfer within the layer (this is predominately for layers of 1-micron thickness and above).

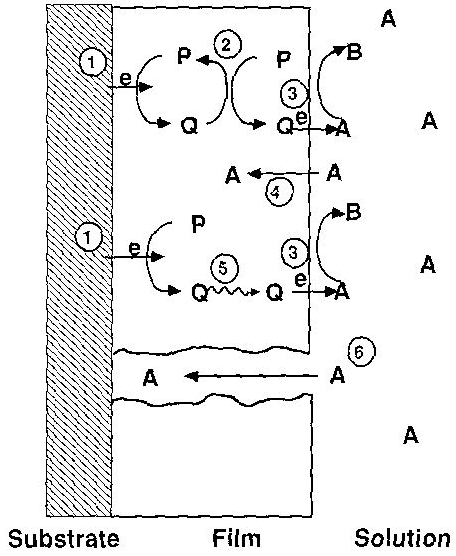

Figure 1.10 Schematic diagram of several processes that can occur at a modified electrode. P represents a reducible substance in a film on the substrate surface and A, a species in solution. The contributions and rates of these processes can be probed by electrochemical techniques [10].

There are 6 processes that may be studied electrochemically within a film at an electrode surface (all numerical points refer to Figure 1.10).

(1) Heterogenous electron transfer from electrode substrate to P, a species in the film.
(2) Electron transfer between different species within the film (also termed 'electron-hopping').
(3) Electron transfer at the film/solution interface between species in either media.
(4) Penetration of A, a species from solution, into the film (a so called 'membrane extraction process').
(5) Mass transport of any species within the film.
(6) Movement of A through a channel directly to the electrode surface, by-passing the film altogether.

When considering such systems, a primary assumption is made that the film is not electrochemically active or conductive and that any electrochemical signal is due a penetrative electro-active species. As well as the behaviour of such species, further information pertaining to the thickness of the layers, the physical make-up (such as organised assemblies) and the extent to which the electrode surface is covered by the film can be established. Two mass mass-transport limited models, the pin-hole and membrane models are essential to understanding the basic processes occurring within the films and how they may be characterised. These models are highly complex and achieving a like for like match with a model system and experimental results is often hard.

1.2.9 "The Pin-hole Model"

The 'Pin-hole Model' usually assumes a thin film formation at the surface of the substrate which does not cover all of the available substrate area. Instead, the non-conductive polymer covers a fraction, $(1-\theta)$, of the total electrode area, A, making this part of the surface electrochemically inactive. The active region, θ, consists of pin-hole pores (active sites) of radius, a, uniformly distributed across A at a distance greater than that of a. The active region of the electrode is the only site at which electron transfer occurs. For the pinhole model to be valid, the diameter of the pores must be larger than the double layer thickness (1 - 2 nm).

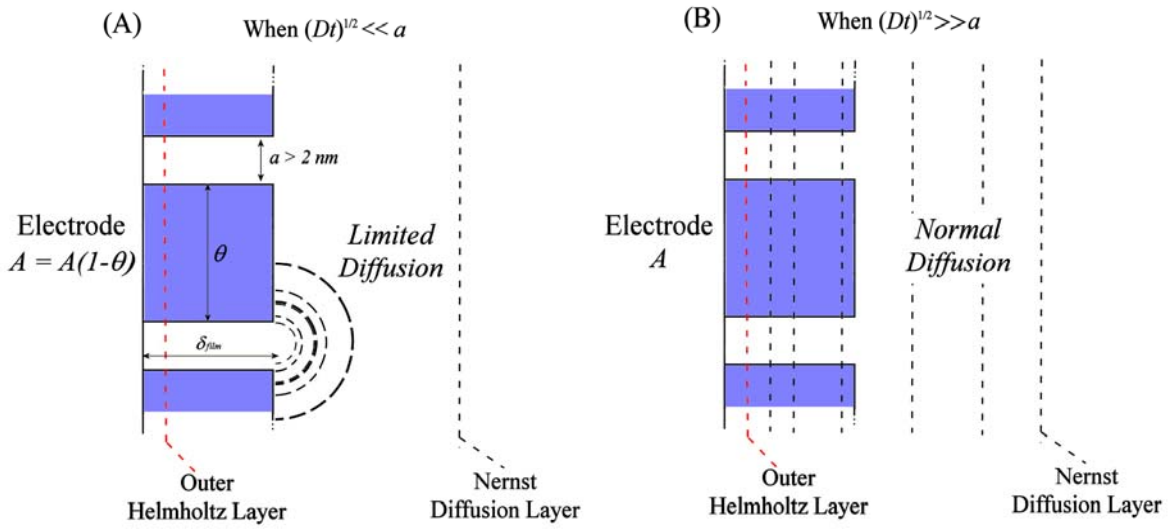

Figure 1. 11 Schematic of pin-hole model where the the electrode surface area is covered by θ m2 of film. Mass transport is (A) **diffusion limited when** $(Dt)^{1/2} << a$ **and** (B) **normal when** $(Dt)^{1/2} >> a$.

The electrochemical signal is thus limited by this assigned geometry which affects all of the kinetic variables in the system and can be described by the relationship between $(Dt)^{1/2}$ and a, where D is the diffusion co-efficient of a species moving within the solution phase and t is the length of time in which a species can be oxidised/reduced at any active site. When the time period is varied so that $(Dt)^{1/2} << a$, a normal electrochemical response is seen for a electrode reduced in area by $(1-\theta)$ and the signal is said to be mass transport limited. However, if the time period is large and $(Dt)^{1/2} >> a$, the coverage of the electrode becomes irrelevant and as the concentration contours overlap the sampling time is so large that mass transport is no longer a limiting factor. There is enough time for the species to diffuse to the active site, for a redox process to occur, and to diffuse away again leaving the site vacant for further redox to occur at a rate paralleled by an unmodified electrode. There are two electrochemical methods that are applicable to this model, chronoamperometry and rotating disc-electrode.

Chronoamperometry allows t to be kept small so that the signal is mass transport limited. The current-time curve for a bare electrode of area A follows the Cottrell equation:

Equation 1.34

$$\frac{i_d(t)}{nFAD^{1/2}[ox]} = (\pi t)^{-1/2}$$

Where $i_d(t)$ is the current during a potential step for the reduction of a mass-transport limited species with a concentration of $[ox]$ and a diffusion co-efficient D. This behaviour is altered by the presence of a film at the surface as described before and can be modelled in various ways. Work by Saveant [11] describes the film as a network of hexagons with a radius of R, which covers the majority of the electrode making it inactive. At the centre of each hexagon is a circular pore of radius a, which constitutes the active areas of the electrode. When the new current is normalised to the bare electrode current a number of parameters are introduced to an altogether more complicated function. The point of note is that when the time is short the current ratio is at the limiting value of $(1-\theta)$. When it is long, and the diffusion layer is large when compared to R, the ratio approaches unity. The location of the intermediate region is dependent upon the values of a and θ and a plot of the current ratio against time can be used to estimate these parameters.

A similar experiment can also be carried out using a rotating disc electrode (RDE). The diffusion layer thickness is limited by the convection caused by the rotation of the disc electrode, ω. At faster rotations the thickness is reduced inversely proportionally to $\omega^{1/2}$. For the same electro-reduction of a species at a modified electrode, the limiting current is dependent upon the size and geometry of the pores as they are mass-transport limiting. An example of the method is the one used by F. Scheller et al. [12] in 1970. Other methods have been used to determine the effect of the presence of a non-conductive membrane at the surface of an electrode, in particular the use of cyclic voltammetry which is a common electrochemical tool. The basic approach is similar in all cases put forward here, however the effects of heterogeneous catalysis need to be considered, affecting the accuracy of estimates of the pore size and fractional electrode coverage.

1.2.10 "The Membrane Model"

An alternative to the pin-hole model is the 'Membrane Model', which is assumed to be pinhole free in this case (all pores are smaller than the double layer, a < 2 nm). Electrochemical signals are assumed to be caused by electro-active species extracted from the solution phase into the uniform membrane where it can diffuse to the electrode surface. The film is usually treated as having a physical make-up not too dissimilar to that of an immiscible liquid at the surface of the electrode (a model similar to liquid-liquid phase boundary diffusion [13]) into which a substance, *[O]*, maybe extracted into. If the extraction rate is rapid enough, the system can equilibrate so that a constant can be established for the variation between the concentration of $[O]_{sol}$ in solution and $[O]_{mem}$ in the membrane such that:

Equation 1.35

$$[O]_{mem}(\phi,t) = \kappa[O]_{sol}(\phi,t)$$

Where κ is the partition coefficient and $\phi^{+/-}$ are positive and negative positions along the axis of diffusion, which at point ϕ the boundary between membrane and solution is located (Figure 1.12). This type of film can also be examined using electrochemical techniques.

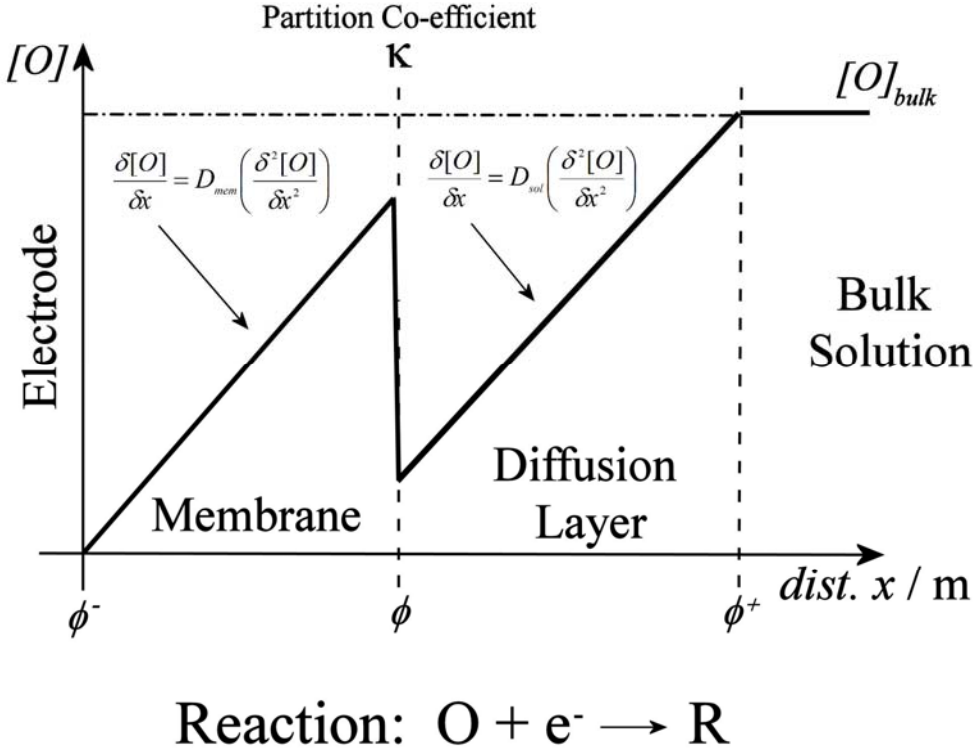

Figure 1.12 Plot showing the change in concentration of an oxidised species upon reduction at an electrode as a function of a distance x normal to the electrode.

Potential step [14] and RDE [15] experiments are the most popular characterisation techniques for this model and can be used to examine the dynamics of the equilibrium established at the film/solution interface. The key to all of these techniques in the amount of time the membrane modified electrode is given to establish equilibrium conditions with its surrounding solution. At short times, when the diffusion layer is small compared to the membrane thickness it can be assumed that electron-transfer occurs exclusively in the membrane. Any diffusion occurring at this time is solely dependent upon D_{film} and the initial concentration in the film, $\kappa[O]_{bulk}(\phi^{-},t)$. At long times the diffusion layer extends into the solution phase as can be seen in Figure 1. 11. However, it is often difficult to vary the time spans enough in order to get a good set of data for chronoamperometry as *t* needs to be very small in order to minimise the size of the mass transport diffusion layer.

Rotating disc experiments make it easier to limit the mass transfer diffusion layer by introducing a convective current that limits the value of ϕ^{+}. By varying the rate of rotation and plotting this square rooted against the limiting current, i_{lim}, a linear relationship is seen

Equation 1.36

$$\alpha \frac{-i_{\lim}}{\omega^{1/2}} = \frac{\phi}{\kappa D_{film}}$$

Equation 1.36 has been derived from the Levich equation and describes the thickness of the film, ϕ, the partition coefficient, κ, and diffusion coefficient of the electro-active species within the film, D_{film} (α is a constant calculated from all the invariable constants in the system). The membrane, by trapping species at the surface of the electrode, extracts the species from solution by an amount dependent upon the equilibrium determined by the partition co-efficient. This equilibrium can be driven in the opposite direction by changing the model to the species diffusing out of the membrane where the concentration wants to be lower when introduced to the aqueous phase.

There are some fundamental assumptions with all of these models that would affect the parameters that have supposedly been calculated from them. They assume 100% electron transfer at the electrode surface and that the diffusion kinetics are independent of the electron transfer kinetics, in effect setting the electron transfer kinetic constant to zero. It is assumed that no charge transfer occurs within the cellulose (electron hopping) or by the cellulose itself (that the cellulose can transfer electrons from the species to the electrode surface, something that an insulating polymer like cellulose cannot do). There is no account of the transfer kinetics at the film/solution phase boundary; the only parameter taken into account is the partition co-efficient that assumes that equilibrium is instantly attained at the boundary. Finally, no catalytic properties are assumed of the cellulose at the substrate surface.

The pin-hole and membrane models are very precise mathematical models of modified electrode systems that need very specific experimental conditions for the assumptions to be made valid. This is not always possible, for example there are times when the geometry of the electrode films is complicated and cannot be described as either a uniform membrane or a uniform film with equally spaced pin-holes. In these cases it is best to use approximate methods in order to establish roughly what the system parameters are.

1.3 Formation and Application of Cellulose Film Electrodes

1.3.1 Constitution of Cellulose Architectures

Electrodes have been chemically modified by layers and films since the early 1970's. They form an integrated chemical system in which advantageous conditions for electrochemical investigation of these films may be undertaken. Techniques prior to this remained rudimentary and lacked the ability to supply more dynamic information pertaining to the materials in question. The very first modified electrode systems consisted of common conductive substrates with covalently attached monolayers. Later in this decade, thicker polymer layers were introduced to these substrates and the possibility of using such electrodes as 'analytical sensors' was first realised. The coupling of electrochemical techniques with polymers/layers/films/etc. has meant that processes (such as electron- and mass-transport) have been studied in detail, to the point where their properties can be used in many tools that are now common place in everyday life.

There are two main components in a modified electrode system, the substrate and the binding film itself. The substrate needs to have a high electrical conductivity and be resistant to chemical attack and corrosion. The primary substrate used in this work has been carbon due to it high chemical stability. It can take various forms including basal plane pyrolytic graphite (BPPG) and boron-doped diamond (BDD) or glassy carbon; each of these options yielding different electrode properties.

The films themselves then need to be bound to the surface of the substrate and this too can be done in a number of different ways depending upon both component parts. Binding thin-films to electrode surfaces is usually done using either adsorption or covalent attachment. Adsorption processes usually only form monolayers (singular atomic/molecular layers covering the whole surface evenly) which when adsorbed often have an electrochemical signature signal for the adsorbed species. Examples of this include the adsorption of ions from aqueous solution (halides, SCN^-, CN^-, etc.) or organic compounds with conjugated electron systems (aromatic rings, double bonds, etc.). Covalent attachment is where the film is chemically bonded by the attachment of specific functional groups to the surface of the substrate through chemical reaction with the substrate. The species covalently bonded more often than not will have electro-active

components, where complementary species in solution can interact with them at the electrode surface, thus altering the chemical signal obtained.

The development of a simple *in situ* electrochemical method for monitoring accumulation, diffusion and reactivity of chemical species in cellulose matrices, is dependent upon the ability to put cellulose on an electrode. Such methods resulted in novel effects caused by the cellulose matrices on aqueous chemical processes (e.g. those in laundry catalysis chemistry). However, the results of these rudimentary methods are hard to interpret with any degree of certainty. Issues arise due to the macro-constituent nature of materials such as cotton on an electrode. Inter- and intra-fiber diffusion differentiation and an inability to regulate the dimensions of materials inhibit further quantitative interpretation of the data beyond the initial qualitative result that an interaction had occurred. A new type of electrode ss needed to explain the exact interaction between chemical species and cellulose matrices with more certainty.

The formation of these modified electrodes is contingent upon a number of intermolecular interactions that contribute to the ability to (i) create cellulose architectures, (ii) attach them to an electrode surface and (iii) the subsequent interaction when they are being studied in a dynamic chemical system. The strength and effectiveness of these interactions is variable and they affect the behaviour of the chemical system differently.

Covalent bonding: This is the most obvious and strongest method of binding the cellulose and attaching it to the electrode surface. However, this would necessitate altering the chemical composition of the cellulose surface which when looking at a mimetic system would cause misleading experimental observations.

Electrostatic interactions: These occur via ion exchange, such as the replacement of one ion by another in a polyelectrolytic material, via ion pairing, or via donor-acceptor interactions. This mode is important in ion exchanging polymers, such as Nafion® and also in clays and zeolites. Layer-by-layer formation of nanoarchitectures is a prime example of the use of electrostatic interaction used in electrode construction.

Hydrogen bonding: Although the energy of an individual hydrogen bond is small, intermolecular interaction may be very strong, because it involves the formation of a large

number of hydrogen bonds between species. Hydrogen bonds are especially prevalent in biological systems. In cellulose matrices there are a large number of hydrogen bonds due to the high degree of functionality in the glucose monomer. This functionality is readily available at the surface of any cellulosic substance. By using functionalised electrodes, it would also be possible to achieve good adhesion to the surface.

Van der Waals forces: The weakest of the main intermolecular interactions present in any possible cellulose integrated chemical system. They may be involved in physical adsorption of species in the cellulose matrix rather than overly contributing to formation and electrode adhesion.

Physical entrapment: Methodologies where the cellulose is physically held at the electrode surface would facilitate the ability to study macroscopic forms of cellulose without further modification. As an interaction in a chemical system, the physical presence of a cellulose matrix means that species can be held inside pores. (For example, micelles containing species held via a hydrophobic interaction can be entrapped in a polyacrylamide matrix [16]).

The ability to manipulate cellulose as a nano-building block enables the creation of thin-film architectures on electrode surfaces. Methods of producing such architectures include layer-by-layer deposition and solvent evaporation deposition (vide supra). This allows control over the film thickness on a nanometer length scale, a higher amount of control over the film morphology, and control of general composition. Once formed, the architectures need to be verified by characterisation methods. Quartz Crystal Microbalance (QCM) techniques, atomic force microscopy, scanning electron microscopy and small/wide-angle X-ray scattering experiments are amongst some of the techniques used in this study.

1.3.2 Cellulose Architecture Formation Methodologies

Methods of preparation for modified electrode vary widely, with some having better reproducibility or better binding than others. The main considerations when creating a new architecture are: (i) the quality of the reproducibility, (ii) the ease of the methodology, (iii)

its cost and (iv) the resultant architecture's properties. In this thesis, four different methodologies are used to create cellulose architectures at electrode surfaces. These were chosen for their varying abilities to look at different types of cellulose, from macroscopic cotton, through refined microfibrils to nanocellulose and nanocellulose composites.

Electrodeposition: The use of electrodeposition is a key technique where polymers are created by either the oxidation or reduction of a dissolved polymer from a solvent in with the product of the polymerisation process is insoluble. A classic example is the electrodeposition of poly-vinyl ferrocene dissolved in methylene chloride solution with $Bu_4N^+ClO_4^-$ salt present. The polymer formed is $PVF^+ClO_4^-$ which is then transferred to acetonitrile in which it is insoluble so that electrochemical analysis of process within the polymer maybe carried out [17].

Electrostatic Layer-by-Layer Deposition: The term self-assembly implies the spontaneous absorption of molecules or nanoparticles in a mono-layer, onto a substrate. Self-assembled multilayer films are formed by the absorption of subsequent monolayers of molecules or nanoparticles (see review [18]). The act of self-assembly of molecules has been known for over a century and can be traced conceptually to the molecular organisation of simple surfactants. In 1891 Agnes Pockel developed techniques for handling surfactant monolayers but it was Irving Langmuir and Katherine Bloggett who demonstrated that compressed monolayers of surfactants could be transferred, layer-by-layer, onto solid substrates to form ultrathin stable films, now known as Langmuir-Blodgett films. Development by Sagiv [19] in the 1980's then led onto the construction of self-assembling monolayers (SAMs), which obviate the need for surfactant compression in a Langmuir trough, but require strong chemical interactions to anchor the functionalised surfactant to the substrate surface. Since that time the construction of monolayers and self –assembled films has extended to include larger molecules and supramolecular assemblies [20], incorporating fullerenes [21], polyelectrolytes [22], polystyrene microspheres [^{23}], silylated glass beads, and surfactant coated metallic, semi-conducting, magnetic and ferroelectric nanoparticles.

Layer-by-layer deposition based on non-covalent interactions has been applied to cellulose architecture for this work. This method has increased in popularity over the past decade due to the ease of film preparation, low cost, fast preparation time and high diversity of

nanocomposites that can be produced. A simple technique devised by Decher [24] in the early 1990's means that, unlike Langmuir-Bloggett films, little specialist equipment is required and unlike the preparation of SAMs, formation relies solely on the electrostatic interactions of component parts.

The formation of multilayered structures is achieved simplistically from solutions of polyions or other charged molecular or colloidal particulates. The basis for the preparation of layer-by-layer nanocomposite films is shown schematically in Figure 1.13 below. The layers are built up sequentially by immersing a substrate such as silicon or glass slides with a negatively charged surface into a positively charged nanoparticle solution (Step (i)). A rinsing step follows to remove any loosely bound material followed by immersion into the negatively charged ion solution (Step (ii)). Layers of ions can then be built up in a cyclic procedure that can either be carried out manually or by an automated device.

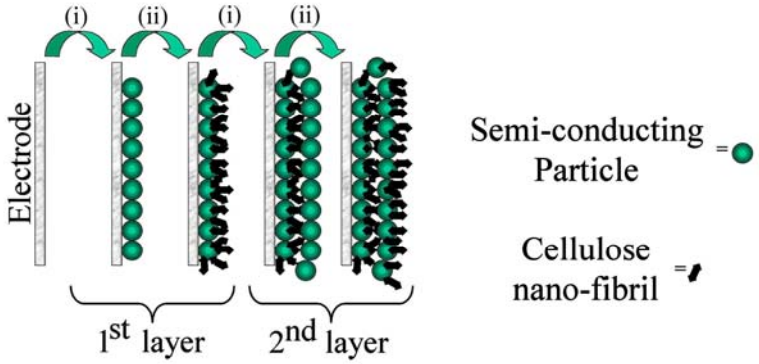

Figure 1.13 Layer-by-layer deposition process involving (i) immersion of a negatively charged, conducting substrate into a positively charged semi-conducting nanoparticle solution, followed by rinsing then (ii) immersion into the negatively charged cellulose nano-fibril solution.

Because the process only involves adsorption from solution in ordinary beakers there are, in principle, no restrictions with respect to substrate size and topology. Similarly there are no real restrictions on the type of ionic solution used as long as the principle of surface charge reversal is achieved so that another layer can be adsorbed on top. Typical adsorption times of charged molecules range from minutes in the case of polyelectrolytes to hours in the case of gold colloids. Diversity in the structure, film morphology and surface properties of different multilayer films has been widely studied and can be achieved by altering shielding and adsorption conditions. It has been shown that the electrostatic interactions between the ions in solution and the surface are key in determining the final structure if the film. However secondary shorter range forces also

play a role in determining the film thickness, final morphology, surface properties and even whether the films are stable. Secondary interactions include hydrophobicity, hydrogen bonding and dispersion forces in these systems.

Solvent Evaporation Deposition: Similar to the layer-by-layer method, solvent evaporation deposition employs a poly-ionic solution where instead of dipping the substrate into this solution, a droplet is deposited onto the substrate. Morphology of the films can be affected by temperature of evaporation, the volatility of the solvent, the concentration of the deposition solution and the ionic species present. By incorporating multiple components to the deposition solution, additional functionality can also be incorporated into thin film architectures. This method is the simplest of evaporation/condensation techniques, with others such as chemical vapour deposition (CVD) allowing further scope for varying the deposition materials (e.g. heavy metal ions) but needing vastly more complicated and expensive equipment. This method has been used to create thin-film metal [25], semi-conductor, natural polymer [26], and poly-electrolyte [27] architectures on electrode surface. Casting and dip coating the electrodes is probably the simplest and cheapest method of producing films, but reproducibility of films is low as obtaining consistent thicknesses can be a problem.

1.3.3 Electrochemistry in Textiles

A textile is a cloth or fabric that has been manufactured by weaving or knitting fibres (synthetic or natural) together into one piece. Experimentation with textiles has varied greatly with the majority of work looking at treatments such as dyeing and adsorption processes [28] as well as more dynamic techniques where the textile is used as a separation membrane. By using electrochemical techniques it is hoped that it will be possible to ascertain new information about processes within textiles that have previously eluded researchers. In situ investigation at fibril sites would allow the effect a textile environment has on chemical reactivity to be explored beyond purely looking as resistive properties of textiles (a typical technique used on textiles). Further to this, electrochemistry is a non-invasive technique which only goes to further mimic the real life systems being modeled by electrochemical parameters.

Kinetic data such as diffusion processes and adsorption of electro-active species, for example metal centred catalysts, can be examined along with thermodynamic information which is a fundamental aspect of electrochemistry. The standard electrode potential, E_0, of a species means that the Gibbs Energy, enthalpy and entropy of a textile system can all be calculated directly. Electrochemistry is a well established, reliable and popular analytical tool which has a body of work whose ideas can be readily manipulated to explore textile chemistry. Its methods are quick and cheap, which is a good economy for any technique, and its reproducibility and robustness mean that gaining corroborative results is just a simple repeat procedure away.

Electrochemistry and textiles is a new partnership that has only just begun. Already, sensors are being produced with a wide range of application that could be essential to everyday life in the future. The common place nature of textiles in our clothes, packaging, tools, etc. means that studying their effect electrochemically allows integral parts of our life to be brought into the digital era. "Smart" clothing is an example where electrochemistry and textiles can be used in conjunction with each other to detect problems with even our own human biology. The genetic disease Muco-viscidosis (cystic fibrosis) affects the quality of life of 0.02% of the world's population, with as many as 5% being carriers of the genetic mutation. This disease has already been investigated using textile modified electrodes to monitor the salt content in sweat to a high accuracy [29]. Previous methods used to detect this illness have involved invasive in-vitro tests on new born babies and basic sweat testing, both of which are not only expensive but also have a high amount of inaccuracy. Inaccuracy in such a serious situation is only going to create further unnecessary mental anguish for people who may have had the misfortune to receive false positive results. Further examples such as this sensor could be developed into a whole new area of sensing that has, up until now, been an untapped resource of chemical information.

1.4 References

[1] A. Payen, C. R. Hebd, *Seances of the Academy of Sciences* 7, **1838**, 1125;

[2] N.L.G. de Rodriguez, W. Thielemans, A. Dufresne, *Cellulose* 13, **2006**, 261.

[3] a) E. J. Vandamme, S. De Baets, A. Vanbaelen, K. Joris, P. DeWulf, *Polymer Degradation Stability* 59 ,**1998**, 93. b) R. Jonas, L. F. Farah, *Polymer Degradation Stability* 59, **1998**, 101. c) R. E. Cannon, S. M. Anderson, *Critical Review of Microbiology* 17, **1991**, 435.

[4] N. Chand, R.K. Tiwary and P.K.Rohatgi. *Journal of Material Science 23,* **1988**, 381.

[5] N. Chand and S.A.R. Hashmi. *Methods in Material Processing* 5, **1993**, 51.

[6] Y. Li, Y.-W. Mai and L. Ye, *Composite Science Technology* 60, **2000**, 2037.

[7] J. Janata, A. Bezegh, *Analytical Chemistry* 60, **1988**, R62-R74.

[8] R. G. Compton and Craig E. Banks, "Understanding Voltammetry", *World Scientific Publishing Co. Pte. Ltd*, Singapore, **2007**.

[9] A. C. Fisher, "Electrode Dynamics", *Oxford University Press*, **1996**.

[10] A. J. Bard, "Integrated Chemical Systems: A Chemical Approach to Nanotechnology", *John Wiley & Sons, Inc., NY,* **1994**, p. 185.

[11] J. M. Saveant, *Journal of Electroanalytical Chemistry* 302, **1991**, 91-101.

[12] F. Scheller, .R Landsber, H. Wolf, *Electrochimica Acta* 15, **1970**, 525.

[13] M. J. Bonne, C. Reynolds, S. Yates, G. Shul, J. Niedziolka, M.Opallo, F. Marken, *New Journal of Chemistry* 30, **2006**, 327-334.

[14] P. J. Peerce, A. J. Bard, *Journal of Electroanalytical Chemistry* 114,**1980**, 89-115.

[15] T. Ikeda, R.Schmehl, P. Denisevich, K. Willman, R. W. Murray, *Journal of the American Chemical Society* 104, **1982**, 2683-2691.

[16] A. J. M. Valente, A. Y. Polishchuk, H. D. Burrows, M. G. Miguel, V. M. M. Lobo, *European Polymer Journal* 39, **2003**, 1855-1865.

[17] A. L. Nguyen, J. H. T. Luong, *Applied Biochemistry and Biotechnology* 43, **1993**, 117-132.

[18] G. Decher, M. Eckle, J.Schmitt, B. Struth, *Current Opinion in Colloid & Interface Science* 3, **1998**, 32-39.

[19] R. Maoz, J. Sagiv, *Journal of Colloid and Interface Science* 100, **1984**, 465-496.

[20] A. C. De Souza, J. P. Kamerling, "Functional Glycomics", *Elsevier Academic*

Press Inc: San Diego, **2006**, Vol. 417, p 221-243.

[21] K. I. Matsuoka, T. Akiyama, S. Yamada, *Journal of Physical Chemistry C* 112, **2008**, 7015-7020.

[22] S. V. P. Barreira,; V. Garcia-Morales, C. M. Pereira, J. A. Manzanares, F. Silva, *Journal of Physical Chemistry B* 108, **2004**, 17973-17982.

[23] S. Habicht, R. J. Nemanich, A. Gruverman, *Nanotechnology* 19, **2008**, 4.

[24] G. Decher, J. B. Schlenoff, "Multilayer Thin Films", *Wiley-VCH*, **2003**.

[25] Y. Yamauchi, and K. Kuroda, *Electrochemical Communications* 8, **2006**, 1677.

[26] M.A. Murphy, G. D. Wilcox, F. Marken, *Indian Journal of Chemistry A*, 44, **2005**, 924.

[27] C. W. Lee, D. H. Nam, *Sensors and Actuators B - Chemistry* 109, **2005**, 334.

[28] R. S. Blackburn, A. Harvey, L. L. Kettle, J. D. Payne, S. J. Russell, *Langmuir* 22, **2006**, 5636-5644.

[29] P. Westbroek, "Analytical Electrochemistry in Textiles", *Woodhead Publishings* **2005**, p. 274.

Chapter 2: Microcellulose Modified Electrodes

Electrodeposition of Cellulose Microfibrils

2.1. Introduction

Electrodeposition occurs where an electrical current is applied to a solution in order to yield a solid deposit upon an electrode surface. It is a methodology that has been applied to precious metals [1], galvanostatic metal coating [2] and the formation of protective polymer layers [3]. More recently electrodeposition has been used to form novel nano-architectures [4,5] and in detection techniques when coupled with stripping voltammetry [6].

In this chapter, electrodeposition is used to accumulate cellulose microfibrils at boron-doped diamond electrodes. Films of cellulose are of interest in this instance as a generic architecture that can be used to mimic a number of natural and synthetic integrated cellulose systems. Plain cellulose films are a good starting point for developing more advanced architectures. In order to produce reconstituted celluloses, the natural fiber has to be dissolved first into a microfibrilar form. Methods for the dissolution of cellulose rely on reagents which break-up the strong hydrogen bonding pattern in natural cellulose-I. Rayon from alkaline Cu^{2+} is a well known [7] example of cellulose dissolution and reconstitution. Other methods which have been developed are based on the solvent N-methylmorpholine-N-oxide [8], the use of thiourea in alkaline aqueous solution [9], and recently the use of ionic liquids [10] to dissolve cellulose. Here, the dissolution of cellulose in alkaline aqueous solution in the presence of thiourea is used to create conditions suitable for the anodic electro-deposition of cellulose onto polished and mechanically stable diamond substrates.

This chapter describes the anodic electro-deposition of thin cellulose films at electrode surfaces. An alkaline aqueous solution in the presence of thiourea is employed to create conditions under which electrochemical oxidation of thiourea [11,12] results in the reconstitution of cellulose directly at the electrode surface. Boron-doped diamond [13] is

employed as a particularly smooth and inert substrate material to allow well-defined films to be formed and characterised.

A simple voltammetric method for the control of the cellulose film thickness based on a cyclic potential sweep is described and films of typically 1 to 4 μm thickness are generated. These films are shown to exhibit macro-pores (ca. 10 μm) and micro-pores (suitable for molecular and ion diffusion) and they affect electrochemical processes at the electrode surface. Partitioning between the aqueous and the cellulose phase allows redox active species to be accumulated or, as shown for the case of the reduction of methylviologen^{2+}, products from the reduction process to be bound into the membrane. Electrodeposited cellulose and cellulose composite films may be of interest in sensor development and for the protection of sensor electrodes against interferences.

Electrochemical methods have commonly been employed to characterize cellulose films [14] or related membrane [15] or textile materials [16]. Cellulose based membranes can be employed to control release of reagents [17], to protect electrode surfaces [18,19], or to control permeation in biosensors [20].

2.2. Experimental

2.2.1. Reagents

1,1'-Dimethyl-4,4'-bipyridinium dichloride or methyl viologen (MV^{2+}), KCl, $Ru(NH_3)_6Cl_3$, NaOH, and thiourea were obtained from Aldrich and used without further purification. The source of cellulose was 1-15 μm diameter refined spruce tree fibrils from Fluka. Demineralised and filtered water was taken from an Elgastat water purification system (Elga, High Wycombe, Bucks) with a resistivity of not less than 18 MOhm cm.

2.2.2. Instrumentation

For voltammetric studies a microAutolab II potentiostat system (EcoChemie, Netherlands) was employed with a Pt gauze counter electrode and a saturated Calomel (SCE) reference electrode (Radiometer, Copenhagen). The working electrode was a 5 mm × 5 mm square highly polished boron doped diamond (BDD, Windsor Scientific) electrode mounted in epoxy. Experiments were conducted after de-aerating with high purity argon (BOC) for at least 15 minutes. The temperature during experiments was 20 ± 2 ^{o}C.

SAXS/WAXS (simultaneous small-angle x-ray scattering and wide-angle x-ray scattering) pattern of the electro-deposited cellulose was obtained on a SAXSess system using a PW3830 X-ray generator and the x-ray image plates were observed using a Perkin Elmer Cyclone Storage Phosphor System. A thick film of cellulose (20 deposition cycles) was produced for SAXS measurements. The cellulose film was washed then transferred from the electrode to the diffractometer using 'Magic' scotch tape (3M). The patterns with Cu Kα radiation ($\lambda = 1.5406 \times 10^{-10}$ m^{-1}) at 40 kV and 50 mA were recorded in the region of 2θ from 5° to 25° with an exposure time of 45 minutes. Scanning electron microscopy (SEM) images were obtained with a JEOL JSM6310 system. The samples were all gold sputter coated for 30 seconds before images were obtained. A tilt of 40° was used in order to get a side profile scratches in the electro-deposited cellulose films for measuring film thickness.

2.2.3. Preparation of Thin-Film Electro-deposited Cellulose

A solution of cellulose was produced following a literature recipe [5]. Briefly, aqueous 1.5 M NaOH with 0.65 M thiourea was used to dissolve cellulose particles of varying size (1-15 μm) from spruce in 3 wt.%. This solution was then equilibrated and refrigerated (4^{o}C) for a minimum of 24 hours before being used without further purification. The electrodeposition was performed on boron-doped diamond (BDD) electrodes immersed in the deposition solution after being thoroughly polished and then rinsed in de-ionised water. The three-electrode cell was activated and the working electrode potential cycled between -0.1 V and 0.5 V vs. SCE continuously at a scan rate 10 mV s^{-1}. Deposition of cellulose occurred immediately during the first cycle and the number of potential cycles was used to control the thickness of the resulting cellulose film deposit. After deposition, the electrode was transferred into alkaline wash solution (30 minutes) and then rinsed with deionised water and dried in air. Each deposition cycle resulted in an increase of the average film thickness by approximately 0.4 μm (estimated by SEM).

2.2.4. Treatment of Data Describing the Diffusion and Release of Reagents from the Cellulose Film

After accumulation of a redox system into the cellulose film, cyclic voltammetry was used to monitor the release back into pure buffer solution. In a typical "leaching" experiment the concentration at the electrode surface will change with time in a characteristic way depending on the thickness of the membrane (parameter *l*). Due to slow diffusion within the cellulose film, the concentration of reagent in the aqueous phase can be assumed to be effectively zero at all times. Therefore, in first approximation only diffusion in the membrane is important. An approximate equation to solve this case for a thin homogeneous membrane was derived by Carslaw and Jaeger [21] (see Equation 2.1).

Equation 2.1

$$\frac{C}{C_0} = 1 - \left[\exp(-\beta t) \frac{\cos x(\beta/D)^{1/2}}{\cos l(\beta/D)^{1/2}} \right] - \frac{16\beta l^2}{\pi} \sum_{n=0}^{\infty} \left[\frac{(-1)^n \exp(-D(2n+1)^2 \pi^2 t / 4l^2)}{(2n+1)\{4\beta l^2 - D\pi^2 (2n+1)^2\}} \cos \frac{(2n+1)\pi x}{2l} \right]$$

In this equation C is the concentration of the diffusing reagent, C_0 is the initial concentration, β (here set to 2 s^{-1}) denotes the time constant for a fast step of the solution concentration to a new non-equilibrium value, D is the diffusion coefficient in cellulose, l is the thickness of the membrane, x is the position for which the concentration is calculated, and n denotes the degree of the term used in this approximation. Here calculation with n = 3 gave satisfactory results and data fitting was possible with a Microsoft Excel spreadsheet.

2.3. Results and Discussion

2.3.1. Formation and Characterisation of Electro-Deposited Thin Film Cellulose

The dissolution and reconstitution of cellulose is commonly used to manufacture films or fibers [3]. Cellulose is soluble in media such as alkaline copper tetrammine solutions (the Cuprammonium process [22]), N-methylmorpholine-N-oxide (the Lyocell process [23]), in some ionic liquids [24], and in alkaline thiourea media [25]. Here, the dissolution of cellulose in alkaline aqueous media in the presence of thiourea has been chosen for the electro-deposition of cellulose. Thiourea is known to undergo facile oxidation in alkaline media [15] and it was assumed that under the right conditions this would lead to electro-deposition of reconstituted cellulose at the electrode surface.

A solution of 3 wt% cellulose in 1.5 M NaOH and 0.65 M thiourea was prepared following a literature procedure [5] (see Experimental). Electrodes immersed in this solution gave a clear oxidation response commencing at ca. 0.2 V vs. SCE. It is believed that the thiourea is oxidized resulting in a potential difference between the cellulose suspension and the electrode surface. Initial tests showed that film deposition did occur and that polished boron-doped diamond electrodes are suitable substrates for the deposition and study of these films. Figure 2.1A shows typical multi-cycle voltammetric responses for the electro-deposition process at a 0.25 cm^2 boron-doped diamond electrode.

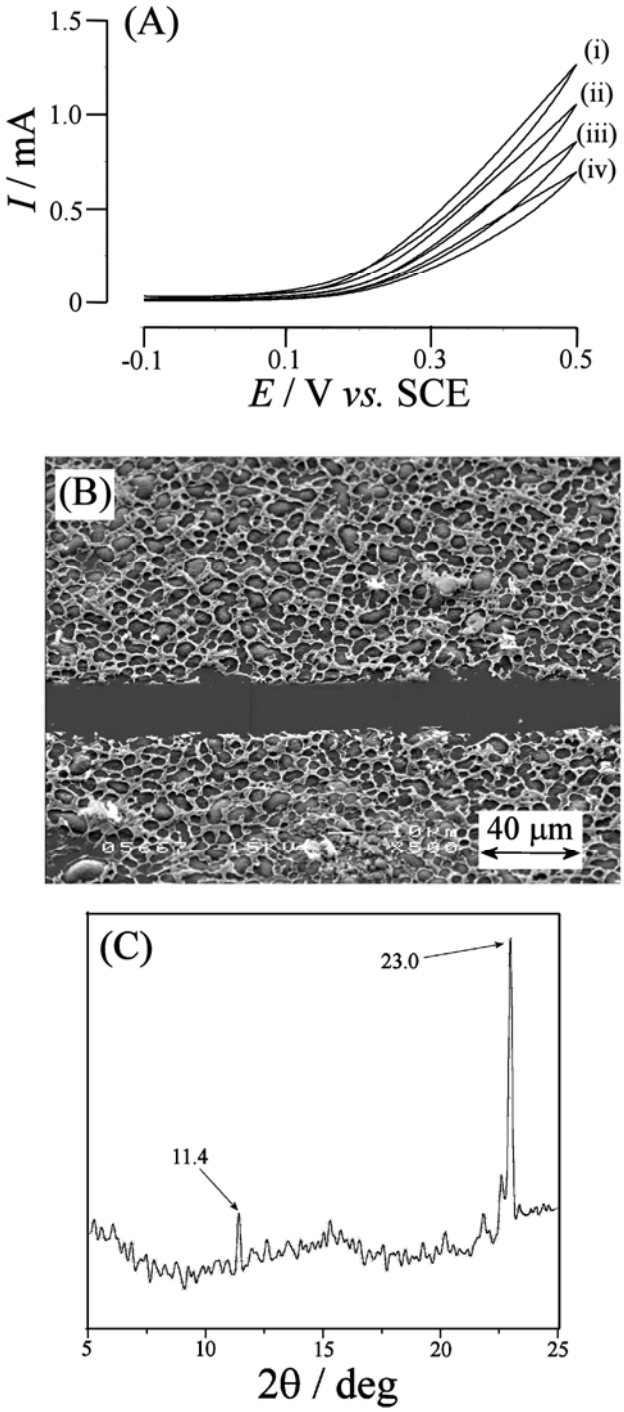

Figure 2.1 (A) Cyclic voltammograms (scan rate 10 mV s^{-1}) for the electro-deposition of (i) 1st-cycle, (ii) 3rd-cycle, (iii) 7th-cycle and (iv) 10th-cycle layer of cellulose at the surface of a 0.25 cm^2 boron-doped diamond electrode submerged in 1.5 M NaOH and 0.65 M thiourea with 3 wt.% cellulose (15 μm refined spruce tree fibrils). (B) Scanning electron microscopy images of boron-doped diamond electrode surfaces modified with ca. 4 μm-thick (10 layers) electro-deposited cellulose films with a scratch line. (C) SAXS/WAXS pattern for a 20-layer sample of electro-deposited cellulose film (data has been processed to maximize peak definition).

The electro-deposition of cellulose films continued upon continuous cycling of the electrode potential, although the deposition current decreased with each deposition cycle (see Figure 2.1A). After electro-deposition, electrodes were transferred into an alkaline wash solution to remove excess thiourea and salts (30 minutes), rinsed with deionised water, and dried in air (see Experimental).

SEM images of the electro-deposited cellulose films suggest formation of a highly porous deposit (see Figure 2.1B). Both (i) a film-like deposit and (ii) a net-like deposit with about 10 μm pores are observed. The average thickness of a film produced with 10 deposition cycles is ca. 4 μm and the number of deposition cycles roughly correlates with film thickness. A scratch line demonstrates that the cellulose material is readily removed from the diamond surface with a scalpel. Cellulose films of more than 20 deposition cycles started to become mechanically unstable during rinsing and drying steps.

The mechanism of topography formation for this intriguing net pattern may be linked to the pattern of "bubbles" visible within some pores. A continuous film of cellulose forming at the electrode initially is likely to undergo a mechanical change during reconstitution and re-crystallization of cellulose fibrils and the formation of a net-like structure may be preferred. Once the pores have opened new deposit forms at the electrode surface and this will further strengthen the net-like topography. A very similar "net" topography for reconstituted cellulose films was reported by Ruan et al. [25].

In order to investigate the crystal structure of the electro-deposit, a SAXS/WAXS X-ray diffractogram was recorded for a free-standing film (produced after 20 deposition cycles and transfer onto an adhesive tape). Figure 2.1C shows the peak features observed for the crystalline components in the cellulose electro-deposit. When comparing the diffractogram for the electro-deposited cellulose film to literature data [26] it appears that the cellulose formed at the electrode has at least two components. The peaks at $2\theta = 11.4°$ and 23.0° can be attributed to reconstituted cellulose (cellulose-II) and non-reconstituted cellulose (cellulose-I), respectively [27]. The electro-deposited films are therefore likely to consist of amorphous and crystalline regions with both cellulose-I and cellulose-II components. Due to the mild

deposition conditions, the "redox state" of the resulting cellulose film is likely to be similar to conventional reconstituted cellulose.

2.3.2. Cellulose Absorption and Release of the $Ru(NH_3)_6^{3+/2+}$ Redox System

In order to explore the ability of the cellulose film to adsorb and retain redox active ions, two redox systems were studied. First the $Ru(NH_3)_6^{3+/2+}$ system is investigated. This redox system is known to undergo a reversible one electron transfer (Equation 2.2).

Equation 2.2

$$Ru(NH_3)_6^{3+}(aq) + e^- \rightleftharpoons Ru(NH_3)_6^{2+}(aq)$$

The cellulose modified boron-doped diamond electrode was immersed in 2 mM $Ru(NH_3)_6^{3+}$ in 0.1 M KCl and cyclic voltammograms recorded as a function of cellulose film thickness. Figure 2.2A shows the voltammetric response with a reversible potential of $E_{1/2}$ = -0.19 V vs. SCE. The data demonstrate that the main effect of the cellulose film is to partially block the access to the electrode surface. Upon increasing the thickness of the cellulose film the peak current for reduction and re-oxidation of $Ru(NH_3)_6^{3+}$ is reduced in spite of the permeability of cellulose to aqueous solutions. In addition, a minor shift of the reversible potential to more negative values is observed (vide infra). These effects are due to the uptake and slower diffusion of $Ru(NH_3)_6^{3+}$ within the cellulose material.

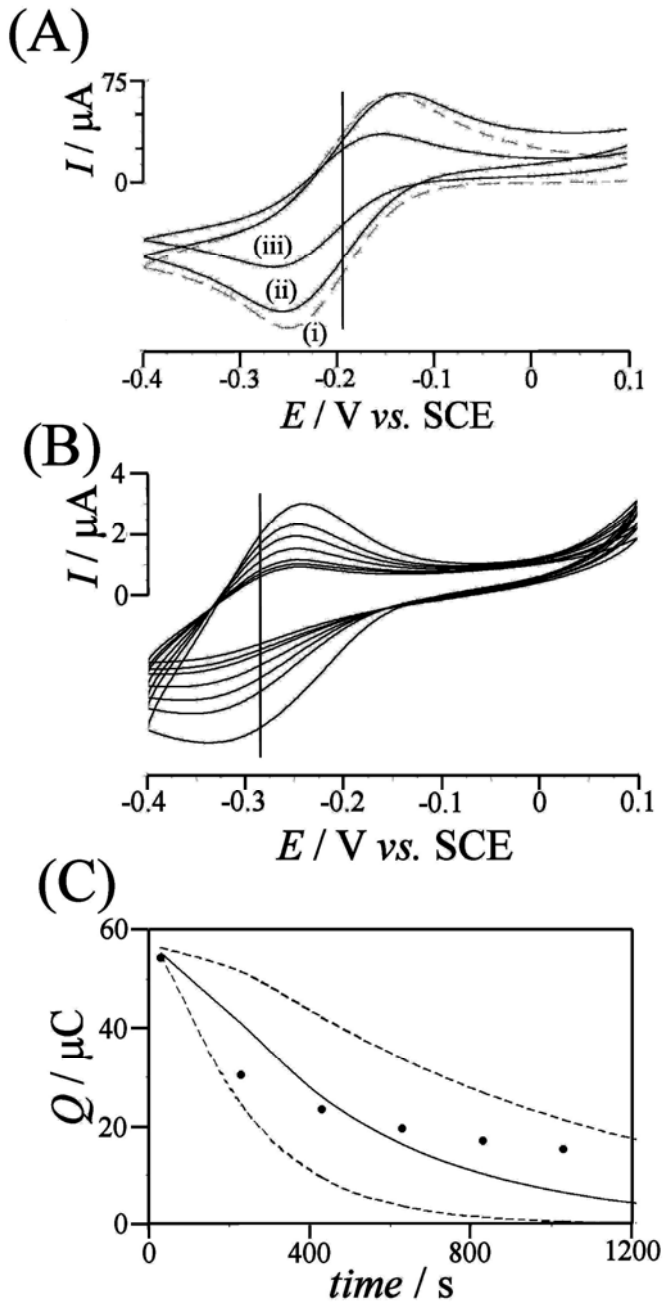

Figure 2.2 (A) Cyclic voltammograms (scan rate 100 mV s^{-1}) for the reduction and re-oxidation of 2mM $[Ru(NH_3)_6]^{3+}$ in 0.1M KCl solution (after 10 minute equilibration) of a (i) 0 μm-thick (dashed line), (ii) 2 μm-thick, and (iii) 4 μm-thick cellulose film modified boron-doped diamond (0.25 cm^2) electrode surface. (B) Cyclic voltammograms (scan rate 10 mV s^{-1}) for the reduction and re-oxidation of $[Ru(NH_3)_6]^{3+}$ (immobilized in cellulose by immersion into 2 mM $[Ru(NH_3)_6]^{3+}$ for one hour followed by rinsing and transfer) in 0.1M KCl solution at the surface of a 4μm-thick cellulose film modified boron-doped diamond electrode surface monitoring the concentration present with respect to time. (C) Plot of the charge under the $Ru(NH_3)_6^{3+}$ reduction response as a function of time for Q_{expt} (raw experimental data) and calculated decay curves (see Experimental) for the assumed diffusion coefficients 0.85×10^{-14} m^2s^{-1}, 1.7×10^{-14} m^2s^{-1}, and 3.5×10^{-14} m^2s^{-1}.

Next, the cellulose modified electrode (10 deposition cycles or ca. 4 μm thickness) was equilibrated in 2 mM $Ru(NH_3)_6^{3+}$ in 0.1 M KCl for one hour. The electrode is then rinsed and transferred into aqueous 0.1 M KCl for voltammetric measurements. Figure 2.2B shows typical voltammetric responses recorded with this electrode over a period of 20 minutes. A new voltammetric response at $E_{1/2}$ = -0.28 V vs. SCE is observed and with time this voltammetric response is decaying. The shift in reversible potential may indicate that $Ru(NH_3)_6^{3+}$ is preferentially adsorbed into cellulose when compared to $Ru(NH_3)_6^{2+}$. However, double layer effects due to the cellulose matrix may also contribute to the effect. The charge under the initial reduction response is approximately 55 μC which corresponds to ca. 0.55 nmol (or a concentration of at least 5.5 mM within the film).

The slow release of the $Ru(NH_3)_6^{3+}$ from the cellulose film can be explained with a slow diffusion process within the cellulose film. Diffusion in the aqueous solution is considerably faster and therefore a simplistic diffusion model based only on diffusion within the cellulose can be applied (see Experimental). Figure 2.2C shows experimental data points and calculated concentration decay curves for three diffusion coefficients. From these data the diffusion coefficient for $Ru(NH_3)_6^{3+}$ within the cellulose can be estimated as 2×10^{-14} m^2s^{-1}. When compared to literature values for ion diffusion in cellulose acetate [28], this is a realistic diffusion coefficient and diffusion within cellulose appears to be roughly 5 orders of magnitude slower when compared to diffusion in aqueous solution. The magnitude of the voltammetric response may be explained (at least in part) based on "intermolecular electron hopping" within the cellulose film rather than based on simple diffusion.

2.3.3. Cellulose Absorption and Release of the Methyl Viologen ($MV^{2+/+}$) Redox System

The absorption and accumulation of an organic redox system such as methylviologen (MV^{2+}) into cellulose is likely to be effective. Studies highlighting the adsorption and reactivity of methylviologen in cellulose in the presence of light [29] and in the presence of microwave radiation have been reported [30]. The hydrophobic MV^{2+} redox system has therefore been chosen as a system to provide further insight into the effects of the cellulose film.

Methylviologen dications are reduced in a reversible one electron process to give radical mono-cations [31] (Equation 2.3). A second one electron reduction which occurs at more negative potentials is not further considered here [32].

Equation 2.3 $MV^{2+}(aq) + e^- \rightleftharpoons MV^{+}(aq)$

This reduction is associated with a dimerisation (or oligomerisation) process in which association of the mono-cation occurs [33] (Equation 2.3).

Equation 2.4 $2\ MV^{+}(aq) \rightleftharpoons (MV)_2^{2+}(aq)$

Voltammograms obtained at a 0.25 cm^2 boron-doped diamond immersed in 2 mM MV^{2+} in 0.1 M KCl are shown in Figure 2.3A. A well-defined reversible reduction (Equation 2.3) occurs at $E_{1/2}$ = -0.67 V vs. SCE. A weak and broad oxidation signal at -0.2 V vs. SCE appears only at higher scan rates and this additional process is here tentatively attributed to the oxidation of the dimer (Equation 2.4). In the presence of the cellulose film (Figure 2.3B) three dramatic changes occur: (i) an additional reduction current is observed at a potential negative of the reduction of $MV^{2+}(aq)$, (ii) the peak current for the oxidation of $MV^{+}(aq)$ is considerably smaller, and (iii) a new broad oxidation response is detected at ca. -0.1 V vs. SCE. This new oxidation process observed in the presence of the cellulose can be attributed to the dimer (or oligomer) within the cellulose film $(MV)_2^{2+}$(cellulose). The rapid partitioning of the more hydrophobic dimeric form of the methylviologen mono-cation radical into the cellulose film is proposed (Equation 2.5).

Equation 2.5 $(MV)_2^{2+}(aq) \rightleftharpoons (MV)_2^{2+}(cellulose)$

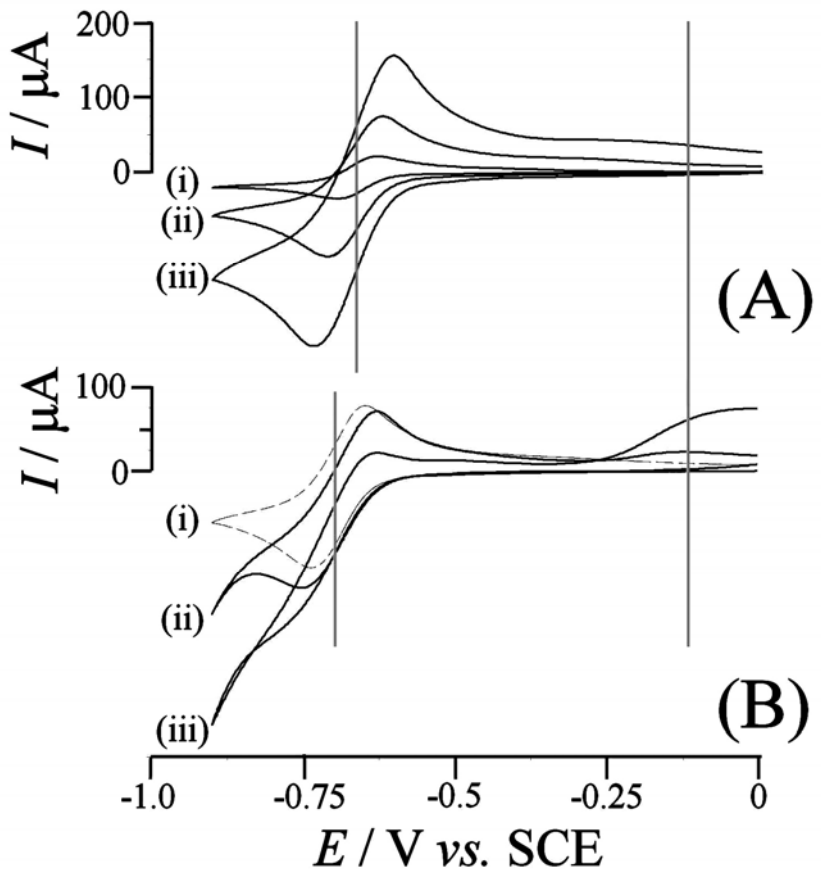

Figure 2.3 (A) Cyclic voltammograms obtained at a 0.25 cm^2 boron-doped diamond electrode for the reduction and re-oxidation of 2 mM methyl viologen (MV^{2+}) in 0.1 M KCl solution (after 10 minute equilibration) at varying scan rates of (i) 10, (ii) 100 and (iii) 500 mV s^{-1}. (B) Cyclic voltammograms (scan rate 100 mV s^{-1}) for the reduction and re-oxidation 2 mM methyl viologen (MV^{2+}) in 0.1 M KCl solution (after 10 minute equilibration) and (i) at a bare boron-doped diamond electrode, (ii) in the presence of a 2-layer cellulose film, and (iii) in the presence of a 5-layer cellulose film (ca. 2 μm-thickness).

This process becomes even more apparent when the scan rate during the methylviologen reduction process is altered. Figure 2.4 shows the effect of scan rate for a 5-layer cellulose film (ca. 2 μm thickness). The highly irreversible nature of the MV^{2+}(aq) reduction at slow scan rate can clearly be seen.

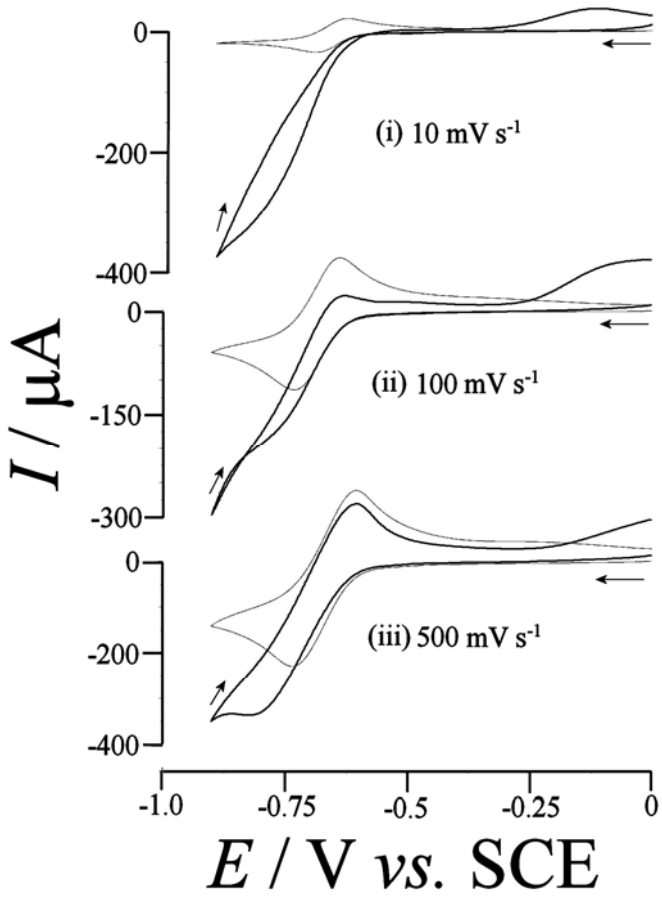

Figure 2.4 Cyclic voltammograms obtained at a 0.25 cm^2 boron-doped diamond electrode for the reduction and re-oxidation of 2 mM methyl viologen (MV^{2+}) in 0.1 M KCl solution (after 10 minute equilibration) at scan rates of (i) 10 mV s^{-1}, (ii) 100 mV s^{-1}, and (iii) 500 mV s^{-1} in the presence of a ca. 2 μm-thick cellulose film (5-layer deposit). Also shown are the voltammetric responses obtained in the absence of the cellulose film.

It is proposed that the fast formation of the dimer within the cellulose film, $(MV)_2^{2+}$(cellulose), is responsible for the absence of the re-oxidation peak for MV^+(aq). This irreversible nature of the reduction of MV^{2+}(aq) also has implication for the direct reduction of MV^{2+}(cellulose). It is likely that propagation of electrons within the cellulose film via intermolecular electron hopping is slow (irreversible) due to the dimer formation. Therefore the direct reduction of MV^{2+}(cellulose) is sluggish and occurs at more negative potential (Figure 2.3B). Obtaining a direct electrochemical measure of the amount of MV^{2+} accumulated into the cellulose film is not possible.

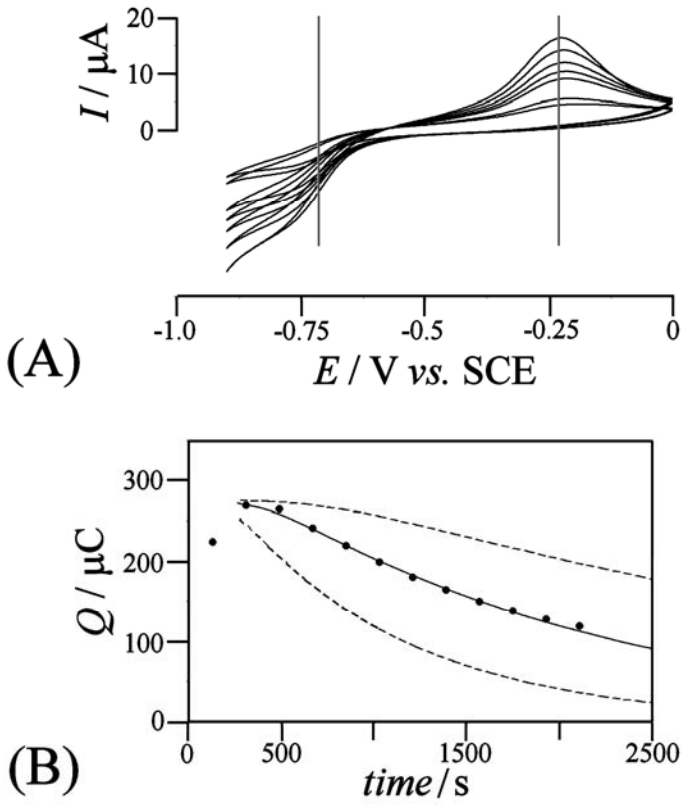

Figure 2.5 (A) Successive cyclic voltammograms (scan rate 10 mV s^{-1}) obtained at a 0.25 cm^2 boron-doped diamond electrode for the reduction and re-oxidation of methyl viologen (MV^{2+}) (immobilized in cellulose by immersion into 2 mM MV^{2+} for one hour followed by rinsing and transfer) in 0.1 M KCl solution in the presence of a 10-layer deposit of cellulose (4 μm thickness). Voltammograms were recorded at regular time intervals. (B) Plot of the charge under the MV^{2+} oxidation response as a function of time (Q_{expt} shown as data points) and calculated decay curves (see Experimental) for diffusion coefficients of 0.17×10^{-14} m^2s^{-1}, 0.35×10^{-14} m^2s^{-1}, and 0.70×10^{-14} m^2s^{-1}.

Next, a cellulose film equilibrated in a solution of 2 mM MV^{2+}(aq) in 0.1 M KCl is rinsed and transferred into 0.1 M KCl. Voltammetric signals recorded for this film (see Figure 2.5) are similar to those obtained directly in MV^{2+}(aq) solution (compare Figure 2.3). However, the magnitude of the currents is reduced and a characteristic decay due to loss of MV^{2+}(cellulose) into the solution is observed. When followed over 30 minutes the loss of MV^{2+}(cellulose) from the film into the aqueous solution phase can be monitored and again an estimate for the diffusion coefficient within the cellulose film can be obtained (Figure 2.5). The approximate diffusion coefficient for MV^{2+}(cellulose) is ca. 4×10^{-15} m^2s^{-1} and therefore somewhat slower when compared to the value for $Ru(NH_3)_6^{3+}$(cellulose).

2.4. Conclusions

It has been shown that thin porous cellulose films are readily electro-deposited onto electrode surfaces such as boron-doped diamond. Cationic redox systems such as $Ru(NH_3)_6^{3+}$ and MV^{2+} are absorbed and accumulated within the cellulose. Mass transport via diffusion within the cellulose environment is approximately 5 orders of magnitude slower when compared to diffusion in aqueous solution. Chemical processes such as the dimerisation of MV^{+} are affected by the presence of the cellulose film due to preferential partitioning. In future, the electro-deposition approach may be used to generate thin sensor films on various types of electrode surfaces. By changing the deposition conditions other film types, composites, or topographies may be accessible.

2.5. References

[1] J. A. Harrison, J. Thompson, *Electrochimica Acta* 18, **1973**, 829-834.

[2] K. I. Popov,; M. G. Pavlovic, M. D. Maksimovic, *Journal of Applied Electrochemistry* 12, **1982**, 525-531.

[3] P. I. Zubov, I. A. Krylova, *Uspekhi Khimii* 48, **1979**, 2240-2261.

[4] L. P. Bicelli,; B. Bozzini,; C. Mele,; L. D'Urzo, *International Journal of Electrochemical Science* 3, **2008**, 356-408.

[5] M. Lai, D. J. Riley, *Journal of Colloid and Interface Science* 323, **2008**, 203-212.

[6] C. M. Welch, M. E. Hyde, C. E. Banks, R. G. Compton, *Analytical Sciences* 21, **2005**, 1421-1430.

[7] C. Woodings (ed.), "Regenerated Cellulose Fibers", *Woodhead Publishing Ltd., Cambridge, UK,* **2001**.

[8] B. Niekraszewicz, P. Czarnecki, *Journal of Applied Polymer Science* 86, **2002**, 907.

[9] D. Ruan, L.N. Zhang, J.P. Zhou, H.M. Jin, H. Chen, *Macromolecules in Biosciences* 4 **2004**, 1105.

[10] S.D. Zhu, Y.X. Wu, Q.M. Chen, Z.N. Yu, C.W. Wang, S.W. Jin, Y.G. Ding, G. Wu, *Green Chemistry* 8 **2006**, 325.

[11] M.A. Ghanem, B.A. Coles, R.G. Compton, F. Marken, *Electroanalysis* 18 **2006**, 793.

[12] N. Spataru, T. Spataru, A. Fujishima, *Electroanalysis* 17 **2005**, 800.

[13] R.G. Compton, J.S. Foord, F. Marken, *Electroanalysis* 15 **2003**, 1349.

[14] A.K. Tiwari, S. Ahmad, *Journal of Colloid Interface Science* 298 **2006**, 274.

[15] M.I. Vazquez, R. de Lara, P. Galan, J. Benavente, *Journal of Membrane Science* 256 **2005**, 202.

[16] P. Westbroek, G. Priniotakis, P. Kiekens, "Analytical Electrochemistry in Textiles", *Woodhead Publishing Ltd., Cambridge, UK*, **2005**.

[17] R. Maki, E. Suihko, O. Korhonen, H. Pitkanen, R. Niemi, M. Lehtonen, J. Ketolainen, *European Journal of Pharmaceutical and Biopharmaceuticals* 62, **2006**, 163.

[18] F. Pariente, J.L. Alonso, H.D. Abruna, *Journal of Electroanalytical Chemistry* 379, **1994**, 191.

[19] H. Palchetti, S. Laschi, M. Mascini, *Anal. Chim. Acta* 530, **2005**, 61.

[20] A. Gill, G. Lillie, G. Farace, P. Vadgama, *International Journal of Environmental Analytical Chemistry* 85, **2005**, 699.

[21] J. Crank, "The Mathematics of Diffusion", *Oxford University Press, Oxford* **2004**, p. 53.

[22] K. Kamide, K. Nishiyama, in C. Woodings (ed.), "Regenerated Cellulose Fibers", *Woodhead Publishing Ltd., Cambridge, UK*, **2001**, p. 88.

[23] P. White, in C. Woodings (ed.), "Regenerated Cellulose Fibers", *Woodhead Publishing Ltd., Cambridge, UK*, **2001**, p. 62.

[24] S.D. Zhu, Y.X. Wu, Q.M. Chen, Z.N. Yu, C.W. Wang, S.W. Jin, Y.G. Ding, G. Wu, *Green Chemistry* 8, **2006** 325.

[25] D. Ruan, L.N. Zhang, Y. Mao, M. Zeng, X.B. Li, *Journal of Membrane Science* 241, **2004**, 265.

[26] A. Isogai, M. Usuda, T. Kato, T. Uryu, R.H. Atalla, *Macromolecules* 22, **1989**, 3168.

[27] L.N. Zhang, D. Ruan, S.J. Gao, *Journal of Polymer Science B* 40, **2002**, 1521.

[28] H. Ohya, S.I. Semenova, A. Sawada, S. Fukaya, Y. Suzuki, M. Aihara, Y. Negishi, *Desalination* 140, **2001**, 235.

[29] M. Kaneko, J. Motoyoshi, A. Yamada, *Nature* 285, **1980**, 468.

[30] M. Maeda, M. Kaneko, *New Journal of Chemistry*, 18 **1994**, 1241.

[31] F. Marken, Y.C. Tsai, B.A. Coles, S.L. Matthews, R.G. Compton, *New Journal of Chemistry* 24, **2000**, 653.

[32] F.L. Qiu, R.G. Compton, F. Marken, S.J. Wilkins, C.H. Goeting, J.S. Foord, *Analytical Chemistry* 72, **2000**, 2362.

[33] K.Y. Tam, R.L. Wang, C.W. Lee, R.G. Compton, *Electroanalysis* 9, **1997**, 219.

Chapter 3: Nanocellulose Composite Electrodes I

TiO_2 Nanoparticle-Nanocellulose Composite Electrodes

3.1. Introduction

If integrated chemical systems are to be more wholly understood the microscopic components of the system need to be broken down into their respective nano-scale constituents. Cellulose can be degraded into nanocrystalline cellulosic materials and then re-assembled into novel synthetic biocomposites [1,2]. Nanocellulose fibrils or "whiskers" have been produced [3] and employed for example for smart materials [4] and in functional nanocomposites [5]. By designing cellulose architectures from the nano-scale up, we hope to gain further understanding of the microscopic electrode modification.

Here it is shown that a novel porous cellulose nanocomposite material can be formed using the layer-by-layer film deposition technique [6]. Negatively charged cellulose nanofibrils with ca. 4 nm diameter and a few 100nm length are assembled from aqueous solution with a positively charged TiO_2 nanoparticle binder (ca. 6 nm diameter). These uniform film deposits (which grow by approximately 16 nm during each deposition cycle) are the first demonstration of a specifically designed and controlled cellulose nano-architecture. The film exhibits electrical characteristics similar to those for mesoporous TiO_2 and enlarged pores which are defined by the cellulose backbone. In this chapter the biocompatibility of cellulose nano-architectures is examined through the immobilization of a redox protein, methemoglobin, in the TiO_2-cellulose film. Typically, aqueous phosphate buffer is used as a physiological buffer solution in protein immobilization studies [7]. However at pH 5.5 phosphate buffer rather than simple electrochemical processes, demetallation and more complex redox phenomena are observed.

Hemoglobin electrochemistry has been studied in many types of film electrodes (for example in surfactant films [8], clay films [9], mesoporous silicates [10], ZrO_2-collagen composites [11], gold nanoparticle assemblies [12], Fe_3O_4 nanoparticle composites [13], mesoporous TiO_2 [14], hydroxyethylcellulose films [15], and others) and used for a range of

electrocatalytic processes (oxygen reduction [16], H_2O_2 reduction [17], trichloroacetate reduction [18], NO detection [19], nitrite reduction [20], etc.). Hemoglobin is a fairly sensitive protein (in particular under non-physiological conditions [21,22]) and both the loss of the prosthetic hemin group [23] as well as demetallation of hemoglobin or hemin [24] have been previously reported. In fact, the re-constitution of hemoglobins with new metal centers and structural modifications has been of considerable interest in hemoglobin research [25]. Surfactants, both cationic and anionic, have been shown to cause release of the hemin group from hemoglobin [26]. In thin film electrochemical systems it is often difficult to unambiguously establish the state of an adsorbed redox protein and there is considerable discussion in particular for the case of the widely used but sensitive hemoglobin system [27].

In this chapter a novel TiO_2-cellulose film electrode is assembled and characterized. Methemoglobin is employed as a test redox system to establish the ability of the film to bind larger proteins and to conduct electrons at sufficiently negative potentials. The observed demetallation process of methemoglobin in phosphate buffer was unexpected and it might be of wider significance for a better understanding of the redox chemistry of hemoglobin and hemin systems.

3.2. Experimental

3.2.1. Chemical Reagents

Sodium hydroxide, potassium phosphate (monobasic), acetic acid, and hemoglobin (from bovine blood, CAS 9008-02-0) were obtained from Sigma-Aldrich and used without further purification. Cellulose nanofibrils 0.69 wt% solution (4 nm average diameter and 250 nm average length nanofibrils derived from sisal, prepared by W. Thielemans [3]) and TiO_2 sol (ca. 6nm diameter anatase, 30% in aqueous HNO_3, ca. pH 1, TKS-202, obtained from Tayca Corp., Japan) were used for deposition solutions. Demineralised and filtered water was taken from an Elgastat water purification system (Elga, High Wycombe, Bucks) with a resistivity of not less than 18 MOhm cm. Argon from BOC (Pureshield) was employed to de-aerate solutions. All experiments were performed at T = 20 +/- 2 ^{o}C.

3.2.2. Instrumentation

For voltammetric studies a microAutolab II potentiostat system (EcoChemie, Netherlands) was employed with a Pt gauze counter electrode and a KCl-saturated calomel (SCE) reference electrode (Radiometer, Copenhagen). The working electrode was prepared from ITO coated glass (tin-doped indium oxide films, sputter-coated, active area 10 mm × 10 mm, resistivity 15 Ω per square) obtained from Image Optics Components (Basildon, Essex, UK). Cleaning of the ITO surface prior to experimentation was achieved by rinsing the surface with first ethanol then water. Heating the electrode surface for 30 minute to 500 °C in an Elite tube furnace in air followed by re-equilibration of the ITO electrodes to ambient conditions for at least 12h. Quartz crystal micro-balance experiments were conducted with 9.1 MHz AT-cut and ITO-coated quartz crystals (Part no. QA-A-9M-ITOM, Advanced Measurement Technology, Wokingham, Berks, UK). A quartz crystal oscillator circuit (Oxford electrodes) was connected to a frequency counter (Fluke, PM6680B). The sensitivity factor for the ITO coated quartz crystal was calculated [[28]] to be $\Delta m/\Delta f$ = 0.5 ng Hz^{-1}. Atomic Force Microscopy (AFM) images were obtained using (i) an Asylum Research AFM system in AC mode (Asylum Research, Oxford,

UK) and (ii) with a Digital Instruments Nanoscope IIIa MultiMode Scanning Probe Microscope in contact mode (only for film thickness measurements).

3.2.3. Layer-by-Layer Formation of TiO_2-Cellulose Nanocomposite Films

The clean ITO-coated glass electrode was (i) submerged in 3 wt.% TiO_2 sol for 10 seconds, then (ii) thoroughly rinsed with deionised water. Excess water was removed, and then the electrode was (iii) submerged into the aqueous 0.069 wt.% cellulose nanofibril solution for 60 seconds. The electrode was taken from the solution (iv) rinsed and dried in air at a temperature of 50 °C. This completed a single layer deposition (ca. 16 nm thickness per layer as determined by AFM) and the deposition cycle was repeated in order to deposit thicker films. This method was also used for the deposition of the TiO_2-cellulose nanocomposite film onto the ITO-coated quartz crystal. Bovine methemoglobin protein (ca. 68 kDalton) was immobilized into the TiO_2-cellulose films by immersion into 15 μM (or another concentration as specified) methemoglobin solution in 0.1 M phosphate buffer pH 5.5 at 4^oC and over a period of typically 12 hours.

3.3. Results and Discussion

3.3.1. Formation and Characterisation of TiO_2-Cellulose Nanocomposite Films

Film deposits were formed in a layer-by-layer assembly procedure (see for example [6]) and they were initially characterized by tapping mode AFM. Figure 3.1A shows cellulose nanofibrils deposited from aqueous solution without binder directly onto an ITO substrate. In Figure 3.1B a 20-layer film deposit of TiO_2-cellulose is imaged.

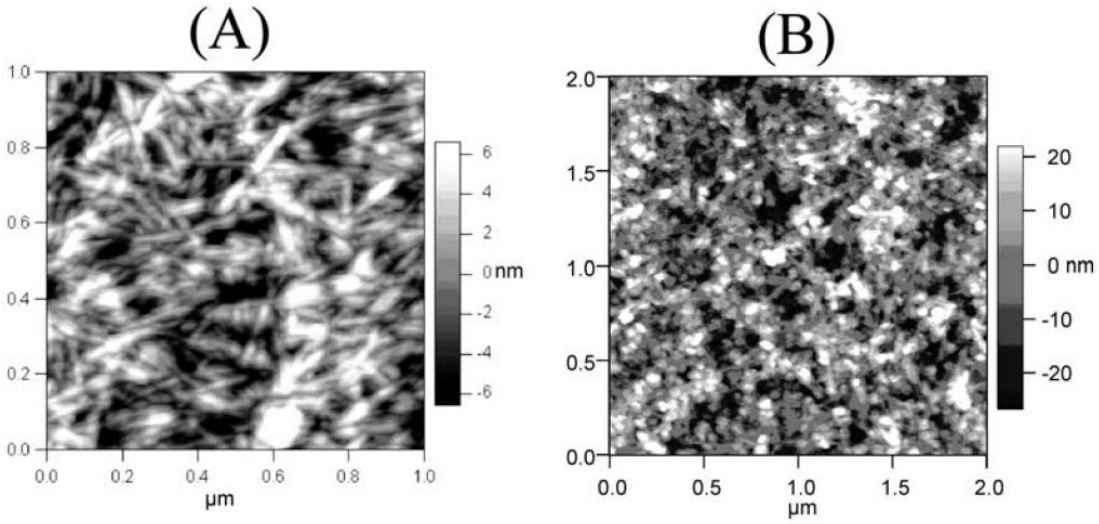

Figure 3.1 Atomic force microscopy (AFM, tapping mode) images of (A) cellulose nanofibrils deposited by solvent evaporation from aqueous solution onto an ITO substrate and (B) a 20-layer TiO_2-cellulose nanocomposite film.

In the nanocomposite film, both TiO_2 nanoparticles and cellulose nanofibrils can be identified. The TiO_2 nanopaticles are assembled into aggregates cross-linked by cellulose. Compared to purely inorganic TiO_2, the film is mechanically soft due to the cellulose component. The thickness of the film has been determined by scratching and AFM-imaging the step height from substrate to film. Consistently a thickness increase of 16 nm per layer deposited was measured for films ranging from 1 to 20 deposition layers.

Electrochemically, the TiO_2-cellulose films exhibit the characteristics expected for porous TiO_2 films [29]. A current response (see Figure 3.2, Process P1 in Equation 3.1) is observed at

-0.8 V vs. SCE which is consistent with the sequential filling of electronic states within the oxide [30] (Equation 3.1).

Equation 3.1 P1: $Ti(IV)(TiO_2) + e^-(ITO) + H^+(aq) \rightleftharpoons Ti(III)(TiO_2) + H^+(TiO_2)$

Similar to experimental results for pure mesoporous TiO_2 films, the voltammetric response increases proportional to film thickness and exhibits a peak current approximately proportional to the scan rate. Scanning the potential more negative (see Figure 3.2B) increases the reversible voltammetric response.

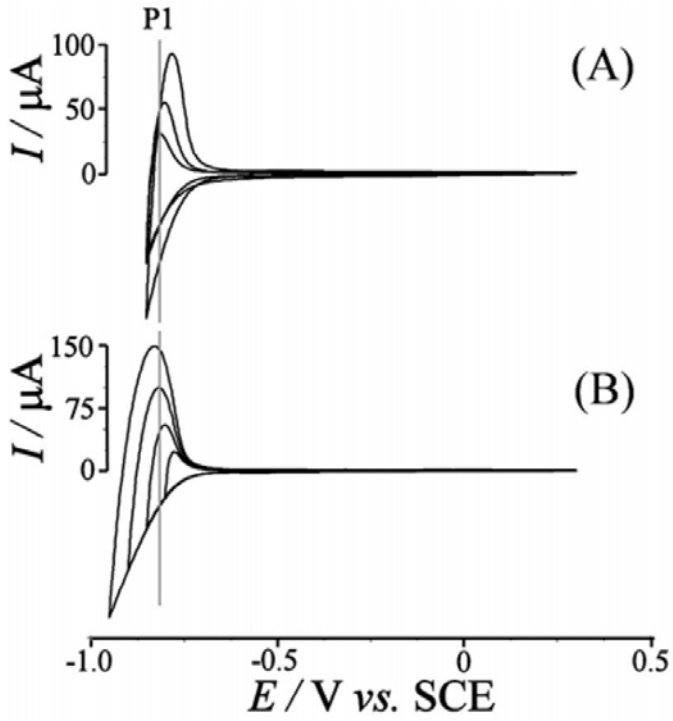

Figure 3.2 (A) Cyclic voltammograms (scan rate 100 mVs^{-1}) for an ITO electrode (area 1 cm^2) with (i) a 5 layer, (ii) a 10 layer and (iii) 20 layer TiO_2-cellulose nanocomposite films immersed in 0.1M phosphate buffer solution pH5.5. (B) Cyclic voltammograms (scan rate 100 mV s^{-1}) with varying potential windows for a 10 layer TiO_2-cellulose nanocomposite film on ITO immersed in 0.1M phosphate buffer solution pH 5.5.

A quartz crystal microbalance system was employed to determine the average mass per layer of the TiO_2-cellulose nanocomposite films. The frequency change per layer deposited is in average 1.7 kHz (see Figure 3.3) corresponding to a mass of 0.9 μg (0.72 μg TiO_2 and 0.18 μg

cellulose). The porosity of the film, ca. 82 % open pores, can be estimated from the densities (anatase [31] 3.9 g cm^{-3} and cellulose [32] of 1.72 g cm^{-3}).

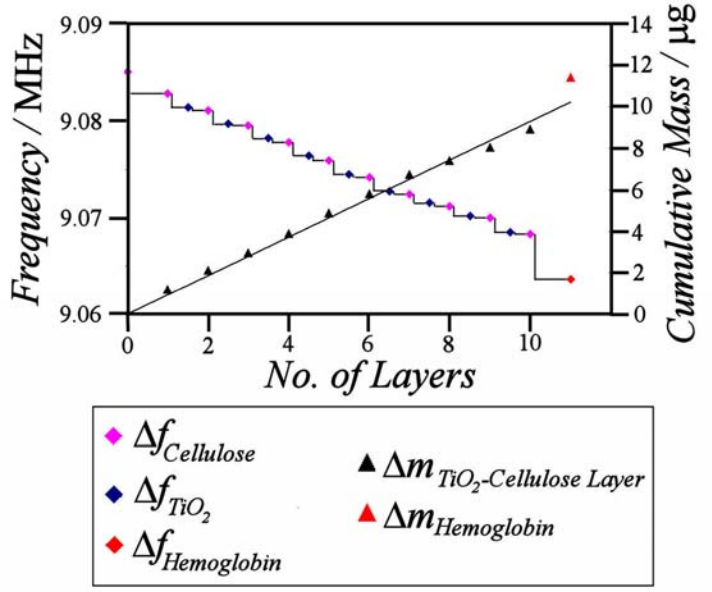

Figure 3.3 Plot of the resonance frequency change for an ITO coated quartz crystal during alternate deposition of TiO_2 and Cellulose nanoparticles (left axis). The corresponding mass change is shown on the right axis (sensitivity factor 0.5 ng Hz^{-1}). Also shown is the mass change after hemoglobin adsorption (1 mg mL^{-1} or 15 µM bovine methemoglobin in 0.1 M phosphate buffer pH5.5, 72hrs).

3.3.2. Immobilisation and Electrochemical Properties of Methemoglobin and Fe^{3+} in Cellulose-TiO_2 Nanocomposite Films

Methemoglobin when immobilized into the TiO_2-cellulose film from a phosphate buffer solution pH 5.5 produces a new voltammetric response (see Figure 3.4A). During the first potential cycle a reduction is observed at -0.8 V vs. SCE followed by the characteristic TiO_2 signal (P1). During the second and successive potential cycles a new reversible electrode process is observed at a potential of -0.1 V vs. SCE (process P3). This new process is dominating and, when monitored over several hours, the signal P3 is only gradually decreasing (not shown). The charge under the reduction peak for P3 amounts to ca. 400 pmol electrons which is in good agreement with the number of iron atoms (ca. 500 pmol) expected based on the weight of hemoglobin immobilized in this film (*vide supra* Figure 3.3).

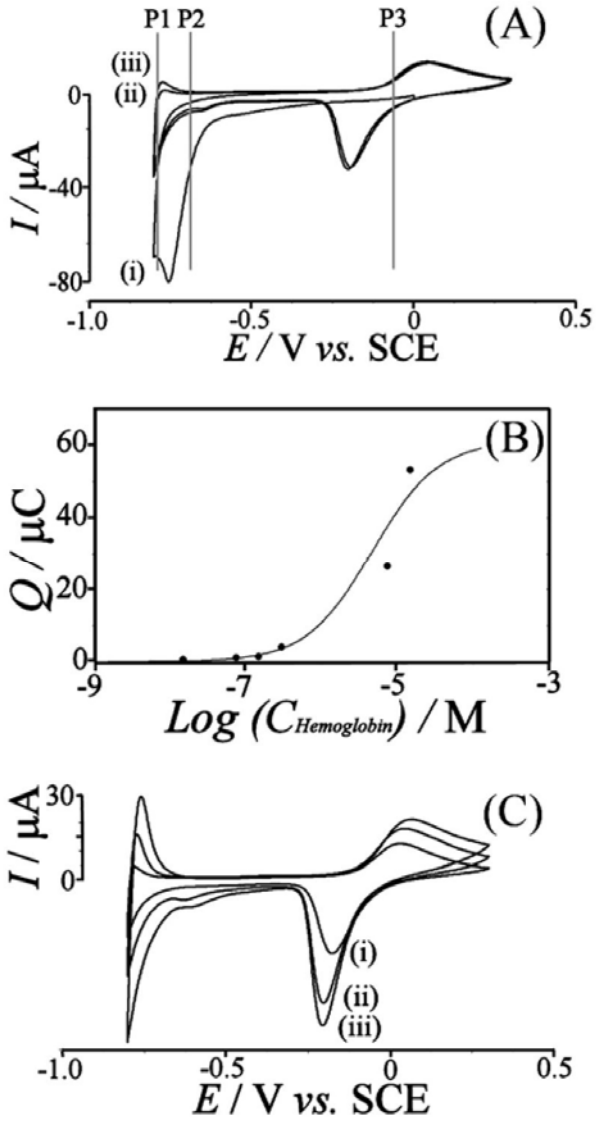

Figure 3.4 (A) **Cyclic voltammograms (scan rate 100 mV s^{-1}) of the (i) 1st scan, (ii) 2nd scan and (iii) 5th scan for a 10 layer TiO_2-cellulose nanocomposite film on ITO immersed in 0.1 M phosphate buffer solution pH5.5 after immobilization of methemoglobin (in 15 µM bovine methemoglobin in 0.1 M phosphate buffer pH 5.5, 72 h).** (B) **Plot of the charge under the reduction peak versus methemoglobin concentration during adsorption into a 10 layer TiO_2-cellulose nanocomposite film. The line shows a Langmuir isotherm with $K_{Hemoglobin}$ = 2 × 10^5 mol^{-1} dm^3.** (C) **Cyclic voltammograms (scan rate 100 mV s^{-1}) of (i) a 5 layer, (ii) a 10 layer, and (iii) a 20 layer TiO_2-cellulose nanocomposite film on ITO immersed in 0.1M phosphate buffer solution pH5.5 after immobilization of methemoglobin (from 15 µM methemoglobin in 0.1M phosphate buffer pH5.5, 72 h).**

Experiments employing different methemoglobin concentrations during the immobilization step (see Figure 3.4B) and different TiO_2-cellulose film thicknesses (see Figure 3.4C) seem to confirm a correlation of the voltammetric process P3 and hemoglobin adsorption into the

TiO_2-cellulose film. However, experiments conducted with an immobilisation solution of 60 μM Fe^{3+} instead of 15 μM methemoglobin give voltammetric responses very similar to those reported above (not shown). Furthermore, the voltammetric features for process P3 are very similar to those reported for the $Fe^{3+/2+}$ redox system at ITO electrodes immersed in phosphate buffer media [33] and therefore this process is tentatively assigned to the simple $Fe^{3+/2+}$ system (Equation 3.2). This assignment will be further confirmed below.

Equation 3.2 P3: $3\ Fe(PO_4)(s) + 3\ e^-(ITO) \rightleftharpoons Fe_3(PO_4)_2(s) + PO_4^{3-}(aq)$

The absence of this process in the first potential cycles (see Figure 3.4A) is explained by the fact that initially Fe^{3+} is adsorbed onto the TiO_2 surface and only after the first reduction (process P2) Fe^{2+} becomes mobile enough (the solubility of $Fe_3(PO_4)_2$ is higher and dissociation into $Fe^{2+}(aq)$ and $PO_4^{3-}(aq)$ more facile) to redistribute directly onto the ITO electrode surface. Process P2 is therefore also associated with the $Fe^{3+/2+}$ redox system (Equation 3.3). Alternatively, process P2 could be assigned to an initial reduction of methemoglobin but this appears less likely based on results from experiments in which methemoglobin is immobilized in the presence of EDTA (vide supra).

Equation 3.3 P2: $3\ Fe(PO_4)(s) + 3\ e^-(TiO_2) \rightleftharpoons Fe_3(PO_4)_2(s) + PO_4^{3-}(aq)$

These results suggest a facile methemoglobin demetallation process in which methemoglobin in contact with the TiO_2-cellulose film is transformed into a metal-free protein. This process may also involve the free hemin metal complex as a reaction intermediate. It has been reported in the literature [34] that demetallation of hemin is possible at pH 5.5 and in the presence of phosphate and ferritin.

3.3.3. Distinguishing Methemoglobin and Fe^{3+} in TiO_2-Cellulose Nanocomposite Films

Next, experiments in the presence of ethylenediamine tetraacetate (EDTA) were conducted in order to remove free Fe^{3+} from the TiO_2-cellulose film and to possibly identify the remaining intact hemoglobin. When the TiO_2-cellulose electrode with hemoglobin immobilized is

transferred into phosphate buffer pH 5.5 containing 3 mM EDTA, the voltammetric responses for processes P2 and P3 disappear rapidly (within three potential cycles, not shown) indicating that under these conditions the demetallation of methemoglobin was virtually complete and all Fe^{3+} is sequestered by EDTA into a water soluble and electrochemically inactive (in this potential range) product. This result confirms that the demetallation process occurs within the TiO_2-cellulose film. Next, experiments were conducted in which 3 mM EDTA was present during the methemoglobin immobilization process (15 μM methemoglobin, 0.1 M phosphate buffer pH 5.5, 3 mM EDTA, 4^oC, 12h) and under these conditions only process P1 is observed. The methemoglobin protein may have been absorbed into the TiO_2-cellulose film but after demetallation and sequestering of Fe^{3+} by EDTA only the metal-free protein seems to reside in the film. The methemoglobin solution did not change colour during the adsorption process which suggests that demetallation occurs only within the TiO_2-cellulose film.

Next, experiments were repeated in 0.1 M acetate buffer pH 5.5 with 3 mM EDTA as both the immobilization medium and the electrolyte. Figure 3.5 shows that under these conditions there is clear evidence for methemoglobin adsorption without demetallation. A new weaker process (P3') is observed at a potential of -0.2 V vs. SCE and this process appears to be independent of the thickness of the TiO_2-cellulose film and sensitive to the presence of trace oxygen. Comparison with literature data [35] suggests that this process may be attributed to the methemoglobin/hemoglobin redox system (Equation 3.4) or a hemin-based redox process.

Equation 3.4 P3': Fe(III)(hemoglobin)(ads) + e^-(ITO) $\rightleftharpoons$ Fe(II)(hemoglobin)(ads)

The magnitude of the current response for P3' and the fact that it is independent of the TiO_2-cellulose film thickness suggests that only a very small amount of methemoglobin close to the ITO electrode surface is reacting. The rates of electron conduction and transfer through TiO_2 are insufficient under these conditions and in this potential range.

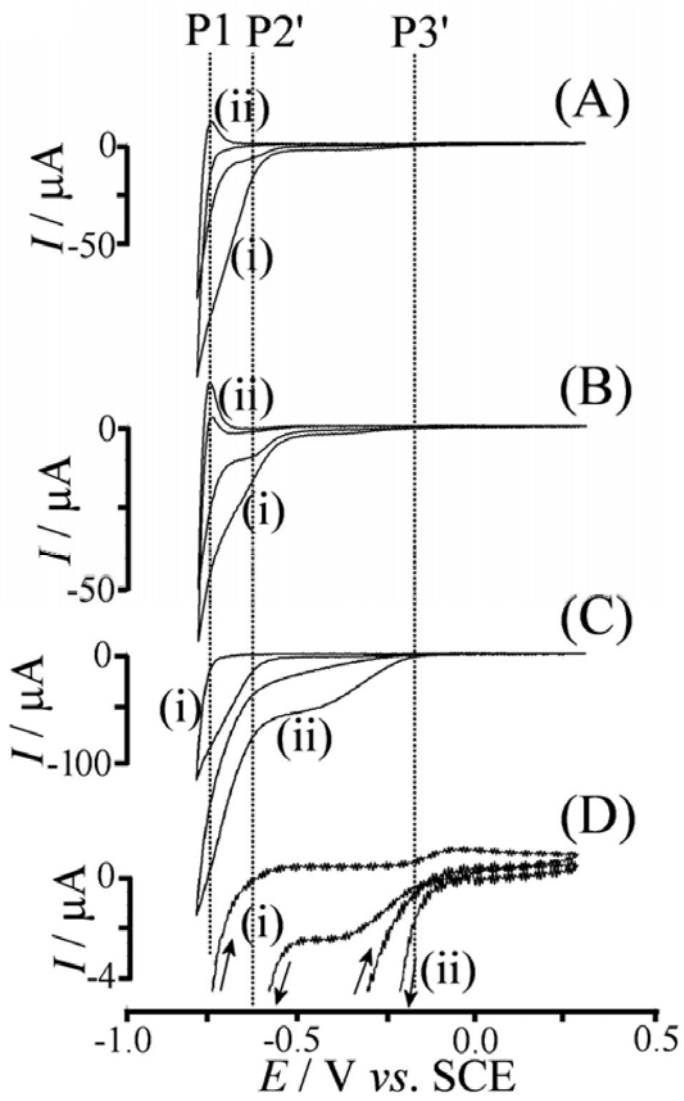

Figure 3.5 Cyclic voltammograms (scan rate 0.1 Vs^{-1}) for the reduction of methemoglobin immobilized into a 10 layer TiO_2-cellulose film (by immersion into 1.5 µM (A) or 0.15 µM (B) methemoglobin in 0.1 M acetate buffer pH 5.5 containing 3 mM EDTA, 4°C, 12h) immersed into 0.1 M acetate buffer pH 5.5 containing 3 mM EDTA. In (A) and (B) the effect of the methemoglobin concentration is shown; (i) and (ii) denote the first and second potential cycle. In (C) and (D) the effect of dioxygen is shown (argon (i), air saturated (ii)).

Process P2' which is observed at ca. -0.7 V vs. SCE is strong during the first potential cycle (see Figure 3.5A). In the second potential cycle this peak is reduced and P1 appears more reversible. After a 5 minute delay this signal recovers (due to slow chemical re-oxidation of hemoglobin) to the original signal and loss of this voltammetric response occurs only very slowly over several hours (presumably due to loss of hemoglobin from the film).

The voltammetric signal for process P2' is changing with TiO_2-cellulose film thickness and this process is also affected by the methemoglobin concentration during the immobilization step (see Figure 3.5B). Therefore this process is attributed to the irreversible hemoglobin reduction within the TiO_2-cellulose film (Equation 3.5).

Equation 3.5 P2': Fe(III)(hemoglobin)(ads) + $e^-(TiO_2)$ $\rightleftharpoons$ Fe(II)(hemoglobin)(ads)

From these experiments it can be concluded that facile demetallation of methemoglobin occurs (i) in the presence of phosphate buffer, (ii) at pH 5.5, (iii) in the presence of a charged surface such as that of TiO_2 nanoparticles, and (iv) probably in the Fe^{3+} redox state (methemoglobin). Demetallation does not occur in the presence of acetate buffer. There remain many questions concerning the structural integrity of the hemoglobin protein within the porous film and about the role of hemin during the electron transfer and demetallation processes.

3.4. Conclusions

It has been shown that redox protein reactivity can be complex and in particular in contact with charged surfaces processes such as structural degradation and demetallation may occur in the case of methemoglobin. The TiO_2-cellulose films offer a novel environment for the immobilization of redox protein and in future in particular cellulose nanofibril building blocks could be very useful in porous electrode and sensor architectures.

3.5. References

[1] K. Oksman, M. Sain, "Cellulose Nanocomposites: Processing, Characterization and Properties", *ACS Symposium Series 938, American Chemical Society, Washington DC,* **2005**.

[2] A.N. Nakagaito, H. Yano, *Applied Physics A - Material Science & Processing* 80, **2005**, 155.

[3] N.L.G. de Rodriguez, W. Thielemans, A. Dufresne, *Cellulose* 13, **2006**, 261.

[4] J. Kim, S. Yun, Z. Ounaies, *Macromolecules* 39, **2006**, 4202.

[5] T. Coradin, J. Allouche, M. Boissiere, J. Livage, Curr. *Nanoscience* 2, **2006**, 219.

[6] G. Decher, J.B. Schlenoff,"Multilayer thin films", *Wiley-VCH, Weinheim*, **2003**.

[7] E. R. Stadtman, H. Arai, B. S. Berlett, *Biochemical and Biophysical Research Communications* 338, **2005**, 432-436.

[8] Z.Q. Lu, Q.D. Huang, J.F. Rusling, *Journal of Electroanalytical Chemistry* 423, **1997**, 59.

[9] X.L. Chen, N.F. Hu, Y.H. Zeng, J.F. Rusling, J. Yang, *Langmuir* 15, **1999**, 7022.

[10] Y.G. Liu, Q. Xu, X.M. Feng, J.J. Zhu, W.H. Hou, *Analytical & Bioanalytical Chemistry* 387, **2007,** 1553.

[11] S.Z. Zong, Y. Cao, Y.M. Zhou, H.X. Ju, *Analytical Chimica Acta* 582, **2007**, 361.

[12] G.F. Wang, X.H. Deng, W.Z. Zhang, B. Fang, *Analytical Chimica* 96, **2006**, 247.

[13] D.F. Cao, N.F. Hu, *Biophysical Chemistry* 121, **2006**, 209.

[14] E. Topoglidis, C.J. Campbell, A.E.G. Cass, J.R. Durrant, *Electroanalytics* 18, **2006**, 882.

[15] X.J. Liu, T. Chen, L.F. Liu, G.X. Li, *Sensors & Actuators B - Chemistry* 113, **2006**, 106.

[16] P.L. He, N.F. Hu, *Electroanalytics* 16, **2004**, 1122.

[17] S.Z. Zong, Y. Cao, Y.M. Zhou, H.X. Ju, *Langmuir* 22, **2006**, 8915.

[18] Y.L. Zhou, Z. Li, N.F. Hu, Y.H. Zeng, J.F. Rusling, *Langmuir* 18, **2002**, 8573.

[19] E. Topoglidis, Y. Astuti, F. Duriaux, M. Grätzel, J.R. Durrant, *Langmuir* 19, **2003**, 6894.

[20] H.H. Liu, G.L. Zou, *Journal of Biochemical & Biophysical Methods* 68 **2006**, 87.

[21] M.S. Hargrove, T. Whitaker, J.S. Olson, R.J. Vali, A.J. Mathews, *Journal of Biological Chemistry* 272, **1997**, 17385.

[22] See for example D.R. Wilson, A.H. Burr, *Biochimica & Biophysica Acta* 830 **1985**, 86.

[23] See for example M.T. de Groot, M. Merkx, M.T.M. Koper, *Electrochemical Communications* 8, **2006**, 999.

[24] N. Carette, W. Hagen, L. Bertrand, N. de Val, D. Vertommen, F. Roland, L. Hue, R.R. Crichton, *Journal of Inorganic Biochemistry* 100, **2006**, 1426.

[25] B. Venkatesh, P.T. Manoharan, J.M. Rifkind, *Progress in Inorganic Chemistry* 47, **1998**, 563.

[26] B. Venkatesh, S. Venkatesh, S. Jayadevan, J.M. Rifkind, P.T. Manoharan, *Biopolymers*

80, **2005**, 18.

[27] Z. Brusova, L. Gorton, E. Magner, *Langmuir* 22, **2006**, 11453.

[28] S.J. Stott, R.J. Mortimer, S.E. Dann, M. Oyama, F. Marken, *Physical Chemistry & Chemical Physics* 8, **2006**, 5437.

[29] E.V. Milsom, H.R. Perrott, L.M. Peter, F. Marken, *Langmuir* 21, **2005**, 9482.

[30] F. Fabregat-Santiago, I. Mora-Sero, G. Garcia-Belmonte, J. Bisquert, *Journal of Physical Chemistry B* 107, **2003**, 758.

[31] C.R. Ottermann, K. Bange, *Thin Solid Films* 286, **1996**, 32.

[32] A. Sarko, R. Muggli, *Macromolecules* 7, **1974**, 486.

[33] F. Marken, D. Patel, C.E. Madden, R.C. Millward, S. Fletcher, *New Journal of Chemistry* 26, **2002**, 259.

[34] R.R. Crichton, J.A. Soruco, F. Roland, M.A. Michaux, B. Gallois, G. Precigoux, J.P. Mahy, D. Mansuy, *Biochemistry* 36, **1997**, 15049.

[35] K.M. Faulkner, C. Bonaventura, A.L. Crumbliss, *Journal of Biological Chemistry* 270, **1995**, 13604.

Chapter 4: Nanocellulose Composite Electrodes II

PDDAC-Nanocellulose Composite Electrodes

4.1. Introduction

The self-assembly of cellulose nanofibrils into new structures has been highlighted as an important development [1]. In the previous chapter it was demonstrated that negatively charged cellulose nanofibril building blocks in aqueous solution are readily combined (in a layer-by-layer assembly process) with positively charged titania nanoparticles [2]. These extremely thin mesoporous films had interesting electrical properties and enabled the absorption and electrochemical study of redox proteins. In this chapter, attention is turned to the use of cellulose nano-architectures in the absorption and detection of environmental analytes. Further to the previous chapter, the cellulose nanofibrils are characterized using a range of experimental techniques including scanning electron microscopy (SEM), Raman and FT-IR spectroscopy and small and wide angle X-ray scattering (SAXS/WAXS).

The selective absorption and release of analytes at modified electrode surfaces is important for sensing applications and in particular for the direct determination of low concentration targets in complex matrices [3]. Modified electrodes have been commonly used for example for the determination of trace mercury [4], dopamine [5], glucose [6] and DNA [7]. Here, the application of cellulose composite films re-constituted onto the electrode surface is considered as a novel approach to produce selective and potentially bio-compatible sensor films with high selectivity. The re-constitution of a cellulose “backbone” together with suitable “receptor” molecules introduces selectivity towards anions and in particular towards hydrophobic anions. These anions can be effectively extracted from aqueous solution into cationic binding sites and then determined with a voltammetric technique. Poly-(diallyldimethylammonium chloride) (PDDAC) is a common and harmless polymeric substance. Here it has been used as an additive to demonstrate the formation of a permselective cellulose film on an electrode surface.

In this chapter both re-constituted cellulose and cellulose-PDDAC film electrodes are characterized and redox processes within these films are investigated. The principle of embedding the "receptor" into the cellulose "backbone" is demonstrated and model redox systems such as $Fe(CN)_6^{3-/4-}$ are employed to investigate the binding ability, film composition effects, and diffusion effects. Triclosan [8] is an important environmental target analyte due to its prevalent use as a biocide and it subsequent release into eco-systems via water ways. Triclosan is an electrochemically active molecule [9] making it an ideal candidate for examining the potential benefits of cellulose nanocomposite films in analytical processes.

4.2. Experimental

4.2.1. Reagents

KCl, $K_3Fe(CN)_6$, $K_4Fe(CN)_6$, poly-(diallyldimethylammonium chloride) (PDDAC, very low molecular weight, 35 wt.% in water), and potassium phosphate (monobasic) were obtained from Aldrich and used without further purification. Triclosan (2,4,4'-trichloro-2'-hydroxydiphenyl ether or Irgasan) was obtained from Fluka. Cellulose nanofibrils (0.69 wt% solutions in water) were prepared from sisal following a literature procedure [10]. Demineralised and filtered water was taken from an Elgastat water purification system (Elga, High Wycombe, Bucks) with a resistivity of not less than 18 MOhm cm.

4.2.2. Instrumentation

For voltammetric studies a microAutolab II potentiostat system (EcoChemie, NL) was employed with a Pt gauze counter electrode and a saturated Calomel (SCE) reference electrode (REF401, Radiometer, Copenhagen). The working electrode was a 3 mm diameter glassy carbon electrode (BAS, US). Experiments were conducted after de-aerating with high purity argon (BOC) for at least 15 minutes prior to recording voltammograms. The temperature during experiments was 20 ± 2 ^oC.

Raman spectroscopy studies were carried out with a Renishaw Raman microscope system with a resolution of ca. 2 cm^{-1} and using an excitation energy of 5.08 eV (244nm) provided by a frequency-doubled continuous-wave argon ion laser. FTIR spectra were obtained with Nicolet Protégé 460 FTIR spectrometer employing KBr pellets. For surface topography imaging an atomic force microscope (Digital Instruments Nanoscope III, used in contact mode) was employed. Field emission gun scanning electron microscopy (FEGSEM) images were obtained using a Leo 1530 system. Samples were gold sputter coated to improve the image quality. A SAXS/WAXS (simultaneous small-angle X-ray scattering and wide-angle X-ray scattering) pattern of cellulose films was obtained on a SAXSess system using a PW3830 X-ray generator. The X-ray image plates were observed using a Perkin Elmer Cyclone Storage Phosphor System. The wide angle patterns were recorded with Cu Kα radiation (λ = 1.5406

Å) at 40 kV and 50 mA in the region of 2θ from 5° to 25° with an exposure time of 45 minutes whilst simultaneous recording small angle patterns in the region of 0.2Å to 100Å. Elemental C, H, N, Cl microanalysis was carried out at the Department of Chemistry Services at Bristol University. Fe elemental microanalysis was carried out in house by digestion in nitric acid and AAS detection.

4.2.3. Reconstitution of Cellulose and Cellulose Nanocomposite Films

For re-constitution of a plain cellulose film a 5 μL solution of 0.69 wt.% cellulose nanofibrils was deposited onto a 3 mm diameter glassy carbon electrode (BAS), placed upright in a holder, and kept in an oven at 60°C for 20 minutes. The resulting 30 μg film deposit was approximately 1.5 to 2.0 μm thick (*vide infra*) and remained intact upon immersion in aqueous electrolyte media. In order to form cellulose-PDDAC composite films, an appropriate amount of poly-(diallyldimethylammonium chloride) (PDDAC) solution was added in the cellulose solution, vigorous stirring (ultrasonication) was applied, and the resulting mixture was then used for deposition processes. The same evaporation conditions were employed. Typically, a solution of 0.46 wt.% cellulose nanofibrils and 0.12 wt.% PDDAC was used to create cellulose-PDDAC composite films with ca. 80 wt.% cellulose and ca. 20 wt.% PDDAC.

Free standing films were required for SAXS/WAXS and elemental microanalysis. These films were prepared from 1 mL of deposition solution on a flat Teflon substrate (area ca. 2 cm^2), placed in an oven at 60°C for 1 hour, and peeled off the Teflon surface with a pair of tweezers. The films were then left to equilibrate at ambient temperature and humidity.

4.3. Results and Discussion

4.3.1. Reconstitution of Cellulose and Cellulose – PDDAC Films at Electrode Surfaces

In order to form thin cellulose films a solvent evaporation technique was employed (see experimental). Evaporation of an aqueous 0.69 wt.% solution of cellulose nanofibrils (5 μL) onto glass or glassy carbon electrode surfaces (ca. 7×10^{-6} m^2 area) resulted in a uniform and stable film coating. During the drying process, bonds (predominantly hydrogen bonds) between randomly packed cellulose nanofibrils developed and the resulting structure remained intact even when re-immersed into aqueous electrolyte solutions. An AFM image of a typical cellulose film (with a scratch revealing the bare substrate on the right) is shown in Figure 4.1A. Individual cellulose nanofibrils can be seen to pack densely. From the topography height information (not shown), the approximate thickness of this kind of film can be estimated as ca. 1.5 to 2.0 μm.

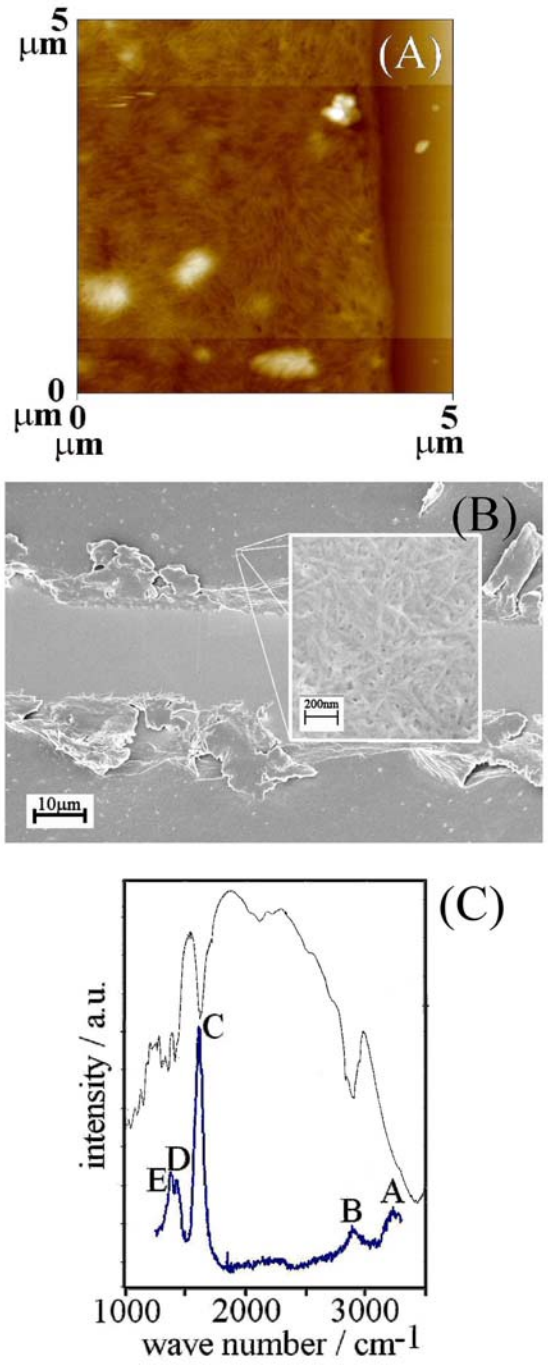

Figure 4.1 (A) AFM image for a cellulose nanofibril film showing individual nanofibrils packed into a dense layer of approximately 1.5 to 2.0 μm thickness. A scratch on the right reveals the substrate. (B) Field emission gun scanning electron microscopy (FEGSEM) images for a co-deposited film of cellulose nanofibril (80 wt.%) and PDDAC (20 wt.%) on a glass surface. A scratch was applied to investigate the mechanical properties of the film. The inset shows a magnified region with individual cellulose nanofibrils and pores. Gold sputter coating was applied prior to imaging. (C) FTIR absorption (obtained with KBr pellet, top) and confocal Raman (bottom, λ=244 nm) obtained for a cellulose nanofibril film.

The properties of the re-constituted cellulose film can be controlled by nano-composite formation for example with poly-electrolytes. Here, poly-(diallyldimethylammonium chloride) (or PDDAC) poly-cationomer is mixed into the cellulose nanofibril sol and evaporation of the mixture then leads to modified cellulose films. A typical SEM image of this kind of film is shown in Figure 4.1B. It can be seen that a highly uniform deposit composed predominantly of nanofibrils is formed. At high magnification again individual nanofibrils and pores are visible typically with up to 10 nm diameter.

Raman spectroscopy, when obtained with a short wave length UV-laser in particular, is a powerful tool for the investigation of the cellulose structures [11]. A Raman spectrum obtained with a confocal microscopy system (excitation wavelength 244 nm) for a cellulose nanofibril film deposit and a FTIR spectrum for a KBr pellet (see Figure 4.1C, bottom and top, respectively) reveal characteristic absorption bands for the cellulose-I structures. The absorption band A at 3250 cm^{-1} can be attributed to OH-stretching of hydroxyl groups in the cellulose chain [12], whilst the absorption bands at B and D,E are due to CH-stretching [13] and -bending modes, respectively, in the cellulose chain. The strong additional band C at 1640 cm^{-1} is believed to be inherently linked to the cellulose backbone interaction with absorbed water molecules in the structure and has also been observed for other polysaccharides [14].

In order to obtain elemental analyses for cellulose and cellulose-PDDAC films, free-standing films were required. When cast onto Teflon coated surfaces and dried at 60 ^{o}C, the cellulose sol allows thicker free-standing cellulose films to be formed and peeled-off intact. Similar films can be readily formed for cellulose-PDDAC and post-treated for example by soaking in aqueous solution. A plain free-standing cellulose film is optically almost transparent. However, upon the incorporation of PDDAC, films become more opaque probably due to more heterogeneity within the structure. Next, the elemental composition of the cellulose films was studied using microanalysis. For a plain free-standing cellulose film (formed by the deposition of 0.69 wt.% cellulose nanofibril solution) the elemental composition was determined as 41.55% C (theoretical 44.44% without H_2O) and 6.09% H (theoretical 6.22% without H_2O) with zero nitrogen content. A good match for C and H was observed when taking into account the presence of ca. 0.6 equivalent H_2O per cellulose monomer. Upon

modification of the film (by changing the deposition solution composition) to 80 wt.% cellulose nanofibrils and 20 wt.% PDDAC (equilibrated in 0.1 M phosphate buffer pH 9.5 for 10 minutes) the film elemental composition changed to 41.2% C, 6.5% H, 1.5% N, and 3.7%Cl. The theoretical elemental composition assuming 1.3 H_2O per formula weight is 41.5% C, 7.5% H, 1.5% N, and 3.8% Cl and is agreement with the measured values. The increase in water content is likely to result from the more hydrophilic nature of PDDAC poly-electrolyte.

The elemental analysis for nitrogen provides a convenient measure for cationic binding sites in the cellulose-PDDAC film deposits on electrode surfaces. A content of 1.5% N in approximately 30 μg film corresponds to ca. 30 nmol cationic binding sites (or formally a concentration of ca. 2 mol dm^{-3} within the film). Some of these cationic sites are responsible for binding to the sulfate half-ester groups on the cellulose surface (vide infra).

4.3.2. Small and Wide Angle X-ray Scattering Studies of Reconstituted Cellulose and Cellulose – PDDAC Films

X-ray scattering techniques offer a powerful probe into both atomic and nano-structure of composite materials [15]. Previous studies of cellulose nanofibril materials have shown that the nanofibrils usually have a ribbon-like morphology [16]. Here, the morphologies of both cellulose and cellulose-PDDAC composite films were investigated with wide and small angle X-ray scattering techniques and the ribbon morphology is confirmed.

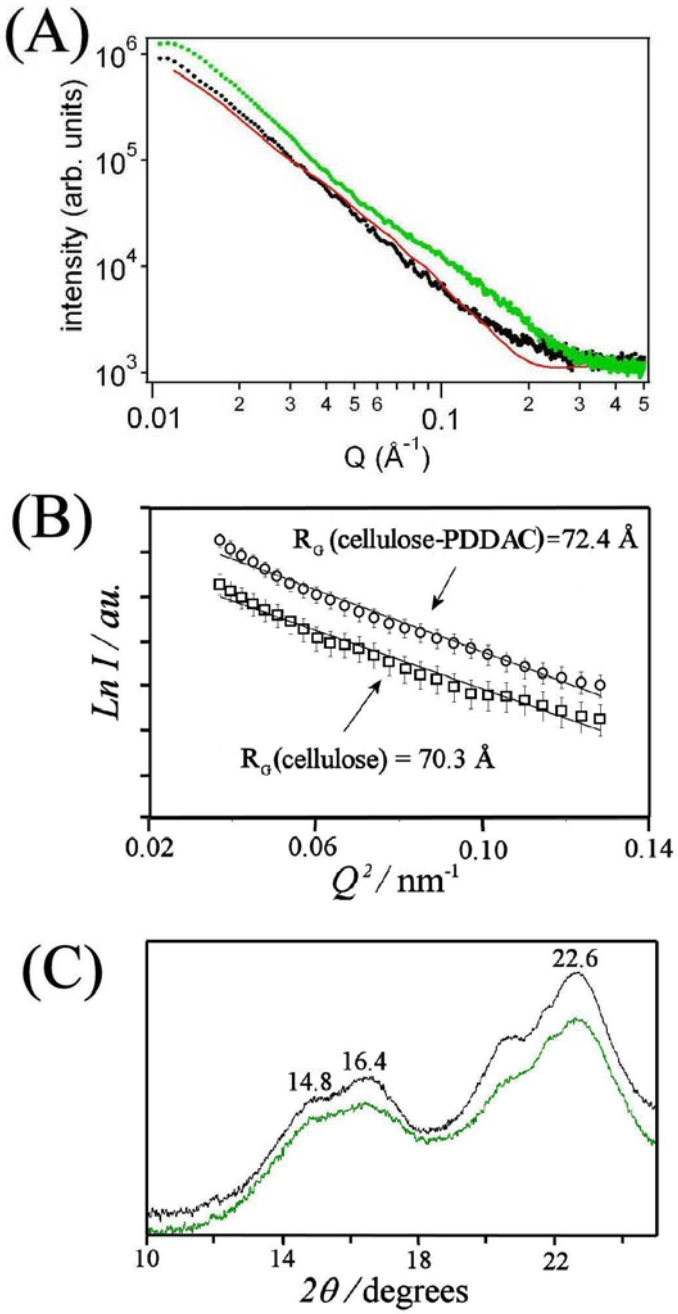

Figure 4.2 (A) **Small angle X-ray scattering pattern for nanocellulose films re-constituted from an aqueous 0.69 wt.% cellulose nanofibril solution (black dots) and reconstituted from aqueous 0.46 wt.% cellulose nanofibrils and 0.12 wt.% PDDAC (green dots). The red line is a simulated fit of a parallelepiped or ribbon-based scattering pattern with 24 ± 0.2 Å x 233 ± 18 Å nm x 1300 ± 70 Å ribbon dimensions (assuming monodispersity, see text).** (B) **A Guinier plot of the natural logarithm of intensity, ln(*I*), versus the momentum transfer squared, Q^2, measured for nanocellulose films re-constituted from aqueous 0.69 wt.% cellulose nanofibril solution (squares) and from 0.46 wt.% cellulose nanofibrils and 0.12 wt.% PDDAC (circles) both with a similar radius of gyration, $R_G \approx 7$ nm.** (C) **Wide-angle X-ray scattering pattern for nanocellulose films reconstituted from aqueous 0.69 wt.% cellulose nanofibril solution (black-line) and from 0.46 wt.% cellulose nanofibrils and 0.12 wt.% PDDAC (green-line). Numbers indicate characteristics lines for the cellulose–I structure.**

In Figure 4.2A the small angle X-ray scattering pattern for a nanocellulose film and a nanocellulose-PDDAC modified film (80 wt.% cellulose and 20 wt.% PDDAC) are shown. A direct relationship between the scattering intensity, *I*, and the value of the momentum transfer, *Q* (which is given by $Q = 4\pi/\lambda \sin(\theta)$ where θ is half the scattering angle) is observed. A high degree of poly-dispersity is manifest by the lack of any well defined peaks in the scattering pattern. The small angle scattering analysis package written by 'The SANS Group' at NIST for the Igor Pro platform was used to determine the geometry and consequent dimensions of the particles in the plain nanocellulose film. When testing different models, it was found that a theoretical ribbon (parallelepiped) scattering pattern gave the best match between experiment and simulation (red-line, Figure 4.2A). This result is consistent with recent work by Celine Bonini et al. [17] on similar cellulose nanofibril structures. For the best fitting model using a mono-disperse parallelepiped, the rectangular cross-section of the ribbon had average dimensions of approximately 2.4 nm × 23 nm (fig. 4.2A). In this case, not considering poly-dispersity severely limits the accuracy of the fit of experimental data and the published TEM data (3 nm to 5 nm ribbon diameter and ca. 250 nm length [17]) are believed to be more accurate. Other factors used in the simulation were a background of 1110 au, a contrast setting of 1.46×10^{-5} Å^{-2} (calculated from the monomeric formula of cellulose, $C_6H_{10}O_5$, and a crystal density of 1.62 kg m^{-3}), and scale factor of 29.0197. The poly-disperse ribbon structure is consistent with the appearance of AFM and SEM images (see Figure 4.1) and likely to result from the hydrogen bonding in crystalline cellulose-I.

Upon the introduction of PDDAC into the cellulose film, an additional feature is observed in the scattering pattern (see green dots in Figure 4.2A) at ca. 1.2 nm^{-1}. This feature suggests an interaction of the polymer with the cellulose. Using the relationship $d = 2\pi/Q$ this feature corresponds to a repeat distance of approximately 5.2 nm – slightly more than the width of the ribbons in the plain cellulose samples. This indicates that a thin polymer layer is present between two cellulose ribbons (very much like a "sandwich" structure). It was not possible to fit this pattern using the same ribbon model as used for plain cellulose, suggesting that a higher order structure exists in this sample.

Next, Guinier analysis was applied to the experimental curves of both films. A good linearity (see Figure 4.2B) is observed in the range 4 x 10^{-2} nm^{-2} < Q^2 < 1.2 x 10^{-1} nm^{-2} (the Guinier condition, $QR_G < 1$ applies in this range). The measured slope can be used to extract particle size information based on Equation 4.1 [18].

Equation 4.1

$$\ln(I) = \ln(I_0) - \left(\frac{R_G^{\,2}}{3}\right) \times Q^2$$

In this expression R_G is the radius of gyration. The addition of the polymer increased the radius of gyration slightly. The measured values are for the plain nanocellulose film, R_G = 70.3 Å and for the cellulose-PDDAC film, R_G = 72.4 Å. The magnitude of R_G when compared to the aspect ratio predicted by the simulation suggests that the ribbon structure is bundled and only slightly expanded. The slight R_G increase for the cellulose-PDDAC film seems reasonable in the context of the ribbon morphology.

In the wide-angle X-ray scattering pattern (see Figure 4.2C), a classic cellulose pattern is observed for both the plain cellulose and the cellulose-PDDAC films. The data are consistent with scattering by the cellulose-I polymorph [19], where the intensity peak at 14.8° is caused by scattering from the $1\bar{1}0$ diffraction plane, 16.4° the 110 diffraction plane, and 22.6° by the 020 diffraction plane. The additional peak found in the pattern at 20.6° (shoulder) could be due to a small amount of the polymorphic variation cellulose-III structure, which is commonly seen in reconstituted forms of cellulose.

The structural characterization of the cellulose-PDDAC film clearly suggests a highly distributed PDDAC poly-cation in a cellulose backbone. The "sandwich" structure should open up an extended network of nanopores where anions can penetrate the film and accumulation of anions (by ion exchange) as well as propagation (by diffusion) throughout the film are anticipated. In order to explore the properties and reactivity of cellulose-PDDAC films electrochemical studies are reported next.

4.3.3. Electrochemical Processes in Re-constituted Cellulose and Cellulose – PDDAC Films I.: The $Fe(CN)_6^{3-/4-}$ Redox System

Electrochemical experiments at electrodes modified with thin films give access to quantitative data on ion permeability and absorption effects. Here, both cellulose and cellulose-PDDAC films were investigated in aqueous 0.1 M KCl employing the $Fe(CN)_6^{3-/4-}$ redox system. A film of cellulose nanofibrils (from 5 μL 0.69 wt.% solution deposited onto a 3 mm diameter glassy carbon electrode) has a strong effect on the appearance of voltammograms for the oxidation of $Fe(CN)_6^{4-}$ (see Figure 4.3A). In the absence of the cellulose film a well-defined voltammetric response (curve ii) is observed with a reversible potential of ca. 0.21 V vs. SCE. This process is consistent with the one electron redox system $Fe(CN)_6^{4-/3-}$ (Equation 4.2).

Equation 4.2 $$Fe(CN)_6^{4-}(aq) \rightleftharpoons Fe(CN)_6^{3-}(aq) + e^-$$

The cellulose nanofibril film without PDDAC has a very strong blocking effect which reduces the peak current by ca. 95% (see curve i). The remaining current response appears at the same potential and is believed to be due to a pinhole effect where bigger pores (see Figure 4.1) allow some $Fe(CN)_6^{4-}$ to diffuse into the film and to the electrode surface.

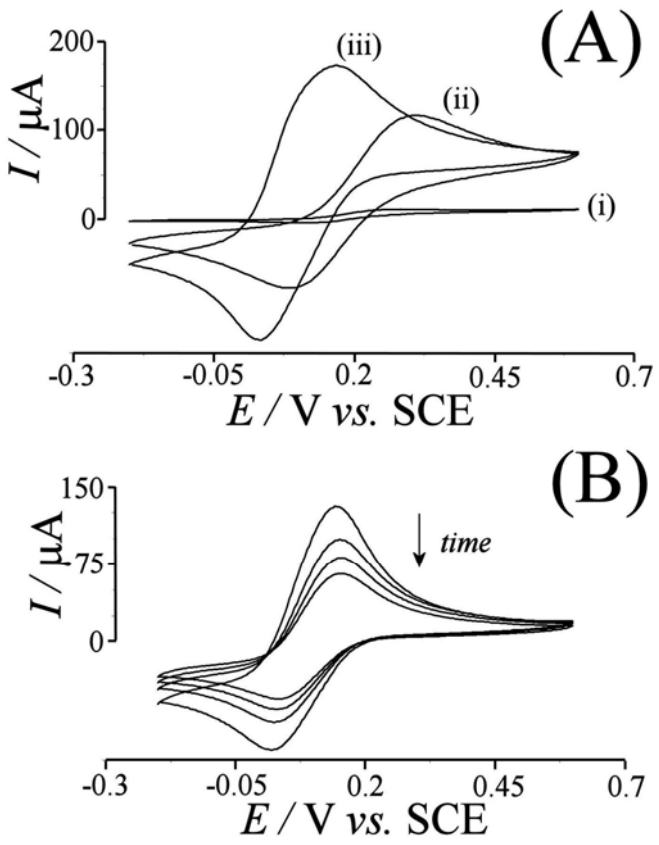

Figure 4.3 (A) **Cyclic voltammograms (2nd scan shown, scan rate 100 mV s^{-1}) for the oxidation and re-reduction of 1 mM ferrocyanide in aqueous 0.1 M KCl at (i) a cellulose nanofibril modified electrode, (ii) a bare glassy carbon electrode, and (iii) a cellulose-PPDAC film (80 wt.% cellulose, 20 wt.% PDDAC) modified glassy carbon electrode (3 mm diameter).** (B) **Cyclic voltammograms (2nd scan shown, scan rate 100 mV s^{-1}) for the oxidation and re-reduction of $Fe(CN)_6^{4-}$ (immobilized in a cellulose-PPDAC film with 80 wt.% cellulose and 20 wt.% PDDAC at a glassy carbon electrode after soaking in 1 mM $Fe(CN)_6^{4-}$ in 0.1 M KCl for 15 minutes) immersed into 0.1 M KCl and measured periodically (data shown for 5 minute, 10 minute, 15 minute, and 20 minute immersion).**

Next, poly-(diallyldimethylammonium chloride) or PDDAC embedded into the cellulose film was investigated. Curve iii in Figure 4.3A shows that in the presence of a film of 80 wt.% cellulose and 20 wt.% PDDAC the peak current for the oxidation of $Fe(CN)_6^{4-}$ is substantially increased and the reversible potential is shifted negative to ca. 0.11 V vs. SCE. The potential shift [20] and appearance of the peak are consistent with a one electron transfer within the cellulose-PDDAC membrane (Equation 4.3).

Equation 4.3 $$Fe(CN)_6^{4-}(mem) \rightleftharpoons Fe(CN)_6^{3-}(mem) + e^-$$

In order to explore the accumulation and reactivity of $Fe(CN)_6^{4-}$ in a cellulose-PDDAC film in more detail, the modified glassy carbon electrode was pre-treated by immersion into a solution of 1 mM $Fe(CN)_6^{4-}$ in 0.1 M KCl and then rinsed and transferred into clean aqueous 0.1 M KCl. Figure 4.3B shows that under these conditions a similar response was obtained and that only a very slow loss of the voltammetric signal occurs (ca. 50% over 30 minutes) consistent with a high partitioning coefficient and strong binding of the $Fe(CN)_6^{4-}$ anion into the film and/or slow diffusion (vide infra).

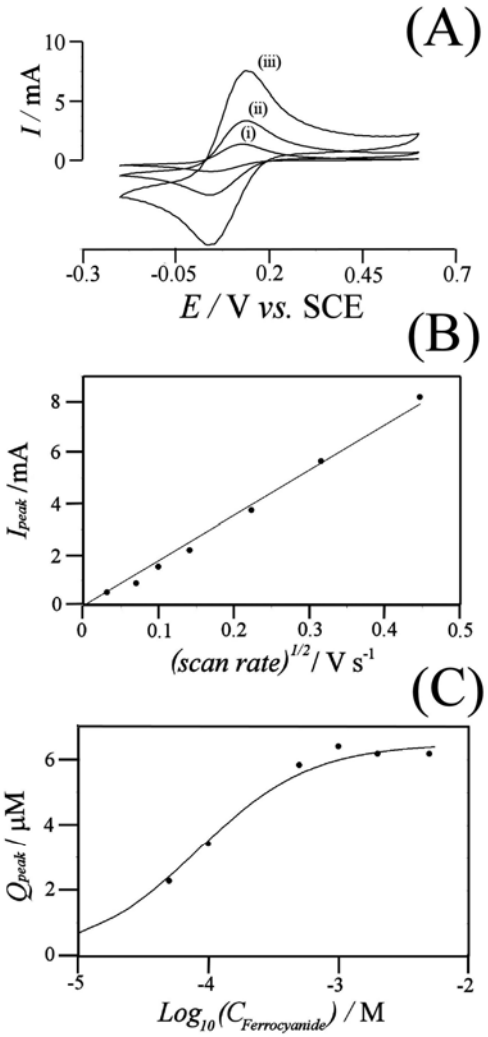

Figure 4.4 (A) **Cyclic voltammograms (2nd scan shown) for the oxidation and re-reduction of $Fe(CN)_6^{4-}$ (immobilized by soaking in a 1 mM $Fe(CN)_6^{4-}$ in 0.1 M KCl for 15 minutes) at a cellulose-PDDAC modified electrode (80 wt.% cellulose and 20 wt.% PDDAC) immersed in 0.1 M KCl at scan rates of (i) 0.1 (ii) 0.05 and (iii) 0.01 V s^{-1}.** (B) **Plot of the change of peak current (I_{peak}) versus the square root of the scan rate for the oxidation of ferrocyanide in a cellulose-PDDAC film modified electrode (80 wt.% cellulose and 20 wt.% PDDAC) immersed in 0.1 M KCl.** (C) **Langmuir isotherm plot for the immobilization of varying amounts of $Fe(CN)_6^{4-}$ (from a 0.1 M KCl solution) into a cellulose-PDDAC film. The approximate binding constant is K = 12000 mol^{-1} dm^3.**

The effect of the scan rate on the voltammetric response is shown in Figure 4.4A and Figure 4.4B. The process, although complex in peak shape, follows the trend expected for a diffusion controlled process over a range of scan rates from 200 to 10 mV s^{-1}. Therefore diffusion within the cellulose-PDDAC film is dominating the transport process (probably associated with both diffusion of anions along poly-cationomer "sandwich" domains and charge transport via electron hopping). The binding of $Fe(CN)_6^{4-}$ into cellulose-PDDAC film is concentration dependent with an isotherm at least approximately consistent with Langmuirian characteristics (see Figure 4.4C, note that diffusion effects may cause deviations from ideal behaviour). The approximate binding constant K = 12000 mol^{-1} dm^3 is observed in aqueous 0.1 M KCl.

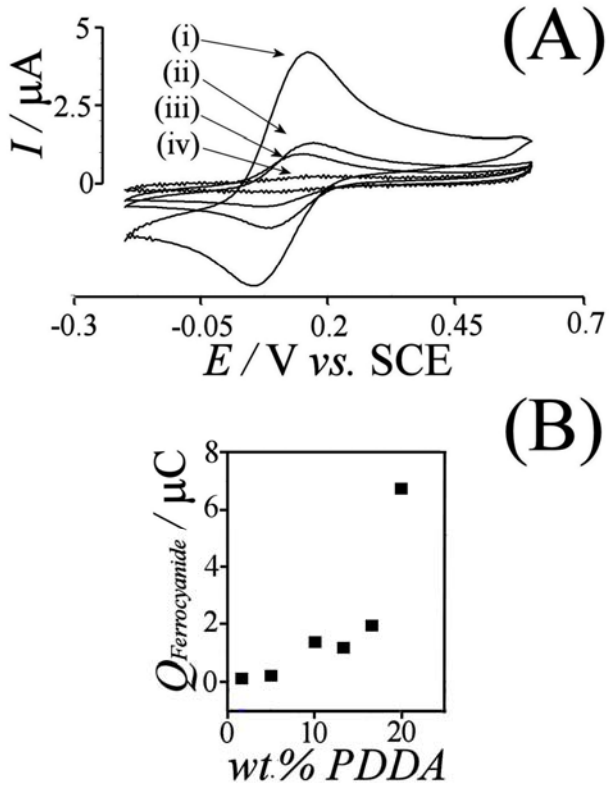

Figure 4.5 (A) Cyclic voltammograms (2nd scan, scan rate 100 mV s^{-1}) for the oxidation and re-reduction of $Fe(CN)_6^{4-}$ immobilized (soaked in 1 mM $Fe(CN)_6^{4-}$ in 0.1 M KCl for 15 minutes) into cellulose-PDDAC films with varying compositions ((i) 20, (ii) 18, (iii) 15, and (iv) 6 wt.% PDDAC) at a 3 mm diameter glassy carbon electrode immersed in 0.1 M KCl. (B) Plot of the change in charge under the oxidative peak ($Q_{Ferrocyanide}$) versus wt.% content of PDDAC in the film at the electrode surface.

The effect of PDDAC content on the film behaviour can be monitored electrochemically (Figure 4.5). As the amount of PDDAC increases, so does the current response seen in the

cyclic voltammetry (Figure 4.5A). This can in turn be correlated to the number of ferrocyanide anions present in the film at the electrode surface, by integrating the anodic peak current. The corresponding plot (see Figure 4.5B) shows a monotonic but non-linear increase which is believed to be associated with the concomitant increase in both the bound $Fe(CN)_6^{4-}$ concentration and mobility (or diffusivity).

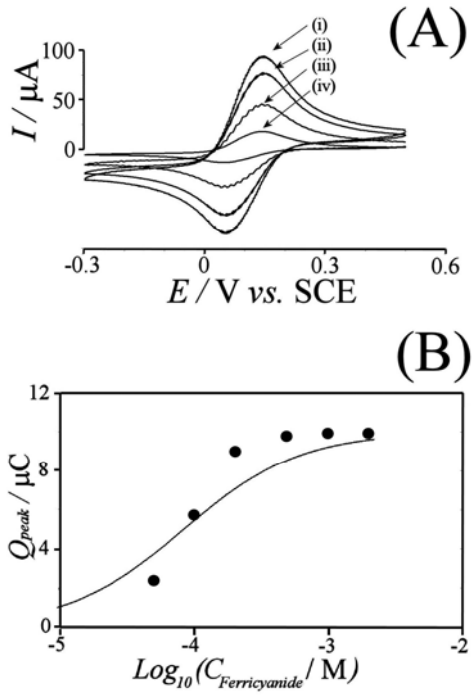

Figure 4.6 (A) **Cyclic voltammograms (2nd scan shown) for the reduction and re-oxidation of $Fe(CN)_6^{3-}$ (immobilized from 1 mM $Fe(CN)_6^{3-}$ in 0.1 M KCl for 15 minutes) in a cellulose-PDDAC film (80 wt.% cellulose 20 wt.% PDDAC) immersed in 0.1 M KCl with varying scan rates of (i) 200, (ii) 100, (iii) 50, and (iv) 10 mV s^{-1}.** (B) **Langmuir isotherm plot for the charge under the reduction signal versus the concentration of $Fe(CN)_6^{3-}$ during immobilization. The line show the expected behaviour for a binding constant K = 12000 mol^{-1} dm^3.**

Next, the characteristics for accumulation and reactivity of $Fe(CN)_6^{3-}$ are contrasted with those observed for $Fe(CN)_6^{4-}$ (see Figure 4.6). Due to the lower charge of $Fe(CN)_6^{3-}$ compared to that of $Fe(CN)_6^{4-}$ the initial peak currents (and charge under the voltammetric response) are increased by approximately 25% (assuming the same number of cationic binding sites in the cellulose-PDDAC film).

The total number of binding sites within the cellulose-PDDAC film has been investigated by elemental analysis. Based on the nitrogen content (*vide supra*) in a film composed of 80 wt.%

cellulose and 20 wt.% PDDAC approximately 30×10^{-9} mol binding sites should be available within the film deposit. The iron content in cellulose-PDDAC films soaked in $Fe(CN)_6^{4-}$ was investigated by elemental analysis for 1 mM, 5 mM and 10 mM solutions (all corresponding to fully saturated binding sites, see Figure 4.4C). Consistently a constant iron content of ca. 0.5 % was determined which is indicating that in total ca. 2.7×10^{-9} mol $Fe(CN)_6^{4-}$ are present at the cellulose-PDDAC modified electrode. Taking into account the 4-fold negatively charged nature of the anion, this result suggests that approximately 30% of the available anion binding sites are occupied by $Fe(CN)_6^{4-}$. This result appears very realistic given that some of the cationic sites are required to bind to or compensate the negative surface charges of the cellulose nanofibrils. It is interesting to compare the total iron content of 2.7×10^{-9} mol (or 260 μC charge) with the charge under voltammetric experiments with immobilized $Fe(CN)_6^{3-/4-}$ (typically 10 μC). It is obvious that only a very thin layer of the film (ca. 5% or 75 nm to 100 nm) adjacent to the electrode is active. Accordingly, the apparent diffusion coefficient for the $Fe(CN)_6^{3-/4-}$ redox system (which includes actual diffusion as well as electron hopping transport contributions) is in the order of 10^{-15} m^2s^{-1} (or 6 orders of magnitude lower in the cellulose-PDDAC membrane than in aqueous solution [21]). This is only a crude estimate and it is likely that under these conditions, the diffusion coefficients for $Fe(CN)_6^{4-}$ and $Fe(CN)_6^{3-}$ are not equal and concentration dependent.

4.3.4. Electrochemical Processes in Re-constituted Cellulose and Cellulose – PDDAC Films II.: The Accumulation and Oxidation of Triclosan

Triclosan (or 2,4,4'-trichloro-2'-hydroxydiphenyl ether) is a poly-chlorinated aromatic phenol which is poorly water soluble (in neutral media) and widely used as biocide. As a phenol it is readily oxidized and the anodic peak current observed in voltammetric measurements has been employed for the quantitative determination at mercury electrodes [22], at carbon microfibers [23], and at screen-printed electrodes [24]. The hydrophobic nature of the triclosan anion has been exploited recently for the accumulation and detection in carbon-PDDAC thin-film electrodes [25].

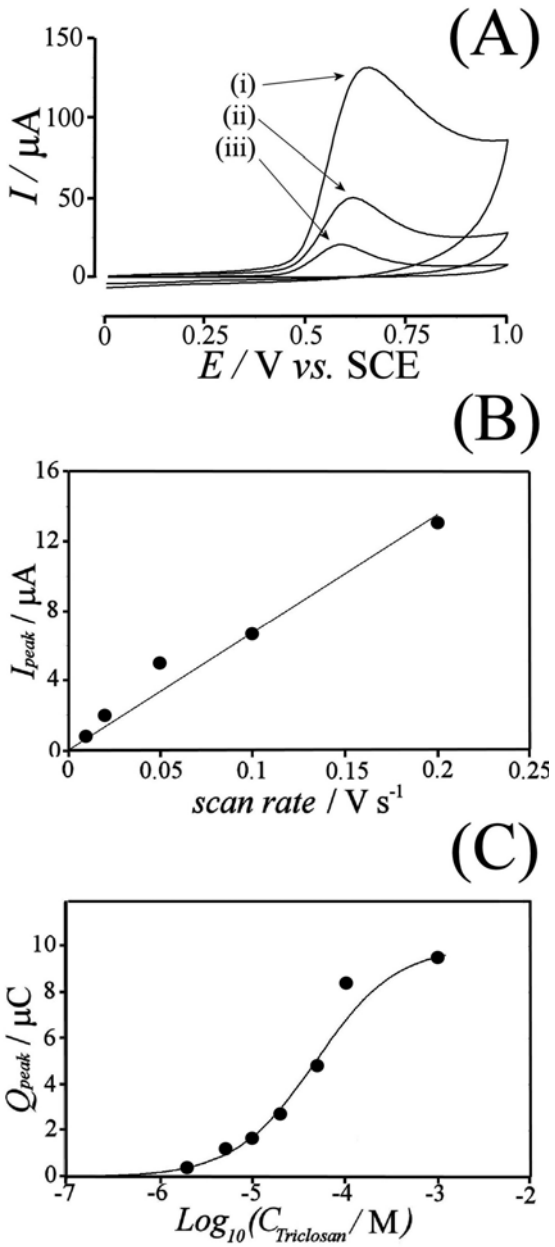

Figure 4.7 (A) **Cyclic voltammograms (1st scan shown) for the oxidation of triclosan (immobilized into a 80 wt.%-20 wt.% cellulose-PPDAC film at a 3 mm diameter glassy carbon electrode by soaking in a 1 mM triclosan in 0.1 M phosphate buffer pH 9.5 for 15 minutes) immersed in 0.1 M phosphate buffer pH 9.5 with a scan rate of (i) 200 (ii) 50 and (iii) 10 mV s^{-1}.** (B) **Plot of the peak current (I_{peak}) versus the scan rate for the oxidation of triclosan (immobilized as in A) in a cellulose-PDDAC film immersed in 0.1 M phosphate buffer pH 9.5.** (C) **Langmuir isotherm plot for the immobilization of varying amounts of triclosan (immobilized as in A) in a cellulose-PDDAC film. The line indicates the theoretical curve for the binding constant K = 21000 mol^{-1} dm^3.**

Figure 4.7 shows typical voltammetric data for the oxidation of triclosan immobilized (from a solution in 0.1 phosphate buffer pH 9.5) into a cellulose-PDDAC film (80 wt.% cellulose 20

wt.% PDDAC). In the absence of PDDAC no oxidation of triclosan occurs and therefore the positive binding sites in the PDDAC component are crucial. The oxidation of triclosan is chemically irreversible and believed to lead to radical intermediates and oligomeric products [26] similar to poly-oxyphenylenes formed during phenol oxidation (Equation 4.4).

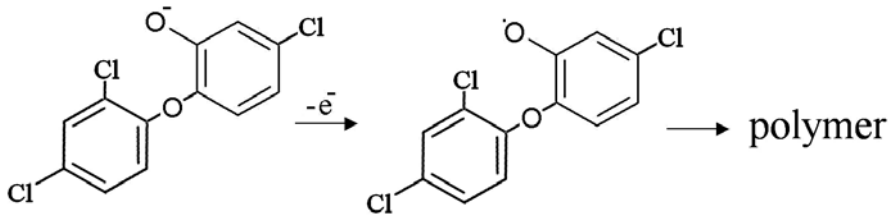

Equation 4.4

The voltammetric response for the oxidation is dependent on the scan rate (see Figure 4.7A and B) and the peak current appears to be increasing approximately linear with scan rate. The reason for the linear dependence (in contrast to the characteristics observed for $Fe(CN)_6^{3-/4-}$ in Figure 4.4) is likely to be the irreversible formation of products which is limiting the diffusion of more reagent from the bulk of the cellulose-PDDAC film towards the electrode and suppressing any contributions from electron hopping transport. The detection of varying concentrations of triclosan is demonstrated in Figure 4.7C. Lower concentrations down into the micromolar level are easily detected and the binding of triclosan can be well approximated by a Langmuirian relationship with a binding constant K = 21000 mol^{-1} dm^3.

4.4. Conclusions

It has been shown that reconstituted cellulose and cellulose-PDDAC films exhibit an interesting ribbon structure where "receptors" such as poly-cationic PDDAC can be embedded in a "sandwich" structure to provide selective binding sites for the accumulation and transport of multiply charged or hydrophobic anions such as $Fe(CN)_6^{3-/4-}$ or triclosan. Voltammetric studies show that although diffusion within the cellulose-PDDAC structure is slow (ca. 6 orders of magnitude slower than in aqueous solution) good analytical signals are obtained and hydrophobic anionic impurities such as triclosan can be accumulated and detected down to a 10^{-6} mol dm^{-3} level. The versatility of cellulose and the facile incorporation of "receptor"

components into nanocellulose films will be of interest in many areas of sensor development, membrane technology, and drug release applications.

4.5. References

[1] K. Oksman, M. Sain, "Cellulose Nanocomposites, Processing, Characterization and Properties", *ACS Symposium Series 938, American Chemical Society, Washington DC,* **2005**.

[2] M.J. Bonné, E.V. Milsom, M. Helton, W. Thielemans, S. Wilkins, F. Marken, *Electrochemical Communications* 9, **2007**, 1985.

[3] A. Logrieco, D.W.M. Arrigan, K. Brengel-Pesce, P. Siciliano, I. Tothill, *Food Additives & Contaminants* 22, **2005**, 335.

[4] N.L. Dias, L. Caetano, D.R. do Carmo, A.H. Rosa, *Journal of the Brazilian Chemical Society* 17, **2006**, 473.

[5] M. Amiri, S. Shahrokhian, F. Marken, *Electroanalysis* 19, **2007**, 1032.

[6] Y.H. Wu, S.S. Hu, *Microchimica Acta* 159, **2007**, 1.

[7] P.A. He, Y. Xu, Y.Z. Fang, *Analytical Letters* 38, **2005**, 2597.

[8] H. P. Schweizer, *Fems Microbiology Letters* 202, **2001**, 1-7.

[9] J. Farrell, J. K. Wang, R. LeBlanc, In "Pesticide Decontamination and Detoxification", *Amer Chemical Soc: Washington,* **2004**; Vol. 863, p 99-112.

[10] N.L.G. de Rodriguez, W. Thielemans, A. Dufresne, *Cellulose* 13, **2006**, 261.

[11] M. Österberg, U. Schmidt, A.A. Jääskeläinen, *Colloids and Surfaces A* 291, **2006**, 197.

[12] A. J. Michell, *Carbohydrate Research* 173, **1988**, 185.

[13] A. J. Michell, *Carbohydrate Research 241*, **1993**, 47.

[14] S. A. Barker, in "Methods in Carbohydrate Chemistry vol. III: Cellulose", R.L. Whistler, M.L. Wolfrom, (eds.), *Academic Press, New York*, **1962**, p.104.

[15] O. Glatter, O. Kratky, (eds.) "Small Angle X-ray Scattering". *Academic Press, New York*, **1982**.

[16] P. Terech, L. Chazeau, J.Y. Cavaille, *Macromolecules* 32, **1999**, 1872.

[17] C. Bonini, L. Heux, J. Y. Cavaille, P. Lindner, C. Dewhurst, P. Terech, *Langmuir* 18, **2002**, 3311-3314.

[18] R. Hosemann, S.N. Bagchi,"Direct Analysis of Diffraction by Matter". *North Holland Publishing Co., Amsterdam, The Netherlands*, **1962**, 734 pp.

[19] A. Isogai, M. Usuda,; T. Kato, T. Uryu, R.H. Atalla, *Macromolecules* 22, **1989**, 3168.

[20] K.J. McKenzie, P.M. King, F. Marken, C.E. Gardner, J.V. Macpherson, *Journal of Electroanalytical Chemistry* 579, **2005**, 267.

[21] R.N. Adams, "Electrochemistry at solid electrodes", *Marcel Dekker, New York,* **1969**, p.220.

[22] A. Safavi, N. Maleki, H.R. Shahbaazi, *Analytical Chimica Acta* 494, **2003**, 225.

[23] L.H. Wang, S.C. Chu, C.Y. Chin, *Bulletin of Electrochemistry 494*, **2004**, 225.

[24] R.M. Pemberton, J.P. Hart, *Analytical Chimica Acta* 390, **1999**, 107.

[25] M. Amiri, S. Shahrokhian, E. Psillakis, F. Marken, *Analytical Chimica Acta 593*, **2007**, 117.

[26] M.A. Ghanem, R.G. Compton, B.A. Coles, E. Psillakis, M.A. Kulandainathan, F. Marken, *Electrochimica Acta*, **2007**, doi:10.1016/j.electacta.2007.01.065.

Chapter 5: Nanocellulose Composite Electrodes III

Nanocellulose-Chitosan Composite Electrodes

5.1. Introduction

It has now been demonstrated that cellulose architectures can be formed on the nano-scale and that the chemical behaviour of these architectures may be altered by the inclusion of additional components. Chitosan is a natural polymer with a linear stereoregular structure (poly-D-glucosamine [1]) derived in industrial scale from chitin (mainly from crustacean exoskeletons) by deacetylation. Chitosan is an important additive to thicken or stabilise foods or pharamceuticals [2], for drug release systems [3], it is used to purify water [4], in textiles and synthetic polymers [5] or composites [6], and in technical membranes [7]. Chitosan has been used in chemical analysis for example as imprinted solid phase extraction substrate [8], for metal complexation [9], and for metal detection [10]. Chitosan has been reported to exhibit a $pK_A \approx 6$ to 7 [11,12,13,14] and is therefore a poly-electrolyte only under acidic conditions. Chitosan can be dissolved in acidic aqueous media and sensor films on electrode surfaces have been prepared for example by layer-by-layer deposition [15,16], chitosan hydrogel deposition [17], electro-deposition [18,19], and crosslinked composite deposition [20]. In this chapter chitosan is employed as a "binder" for cellulose nanofibrils (from sisal, ca. 4 nm diameter and 250 nm length [21]) in order to form thin and stable cellulose-chitosan composite membranes.

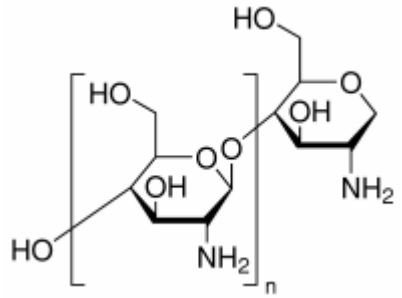

Chemical Structure of Chitosan from crab shells, Deacetylated chitin, Poly(D-glucosamine)

In electroanalysis, chitosan has been used to prepare protein-sensor films [22], and composite sensor films [23]. An electro-spinning method has been employed to deposit chitosan nanofibers onto ITO substrates [24] and surfactant modified chitosan films have been reported for dopamine and ascorbate electroanalysis [25]. A gold-chitosan glucose sensor [26] and a gold-horseradish-peroxidase-chitosan based peroxide sensor [27] were proposed. In most electrochemical applications chitosan is a binder and matrix for nanocarbon [28] and other active components [29]. There are no previous reports on the formation of cellulose-chitosan nanocomposite films and their electrochemical properties.

The re-constitution of a cellulose "backbone" together with suitable poly-electrolyte "receptor" molecules such as chitosan is introducing selectivity towards anionic analytical targets and in particular towards hydrophobic anions. In chapter 4 we have shown that a similar membrane material can be obtained from cellulose nanofibrils and poly-(diallyldimethylammonium chloride) or PDDAC and that the binding sites introduced by PDDAC are accumulating anions from dilute aqueous solutions, such as $Fe(CN)_6^{4-}$. These tetra-valent anions can be effectively extracted from aqueous solution into cationic binding sites and then determined for example with a voltammetric technique [30].

In this study, both re-constituted cellulose film- and re-constituted cellulose-chitosan film-modified electrodes are characterized and redox processes within these films are investigated. The principle of embedding the chitosan "receptor" into the cellulose "backbone" is demonstrated and model redox systems such as $Fe(CN)_6^{3-/4-}$ and triclosan are employed to investigate the binding ability, film composition effects, and diffusion effects.

The anionic surfactant dodecylsulfate, found commonly in cleaning agents and household products, is shown to accumulate and strongly bind into cellulose-chitosan membranes. A competitive binding assay based on dodecylsulfate replacing $Fe(CN)_6^{4-}$ from the electrochemically active film is proposed as a potential model for surfactant detection.

5.2. Experimental

5.2.1. Chemical Reagents

KCl, $K_3Fe(CN)_6$, $K_4Fe(CN)_6$, sodium dodecylsulfate (SDS), sodium acetate, acetic acid, sodium hydroxide, chitosan (poly-D-glucosamine, low molecular weight, 75-85% deacetylated) and potassium phosphate (monobasic) were obtained from Aldrich and used without further purification. Triclosan (2,4,4'-trichloro-2'-hydroxydiphenylether or Irgasan) was obtained from Fluka. Cellulose nanofibrils 0.69 wt% solutions in water were prepared from sisal following a literature procedure [31]. Demineralised and filtered water was taken from an Elgastat water purification system (Elga, High Wycombe, Bucks) with a resistivity of not less than 18 MOhm cm.

5.2.2. Instrumentation

For voltammetric studies a microAutolab II potentiostat system (EcoChemie, NL) was employed with a Pt gauze counter electrode and a saturated Calomel (SCE) reference electrode (REF401, Radiometer, Copenhagen). The working electrode was a 3 mm diameter glassy carbon electrode (BAS, US). Experiments were conducted after de-aerating with high purity argon (BOC) for at least 15 minutes prior to recording voltammograms. For surface topography imaging an atomic force microscope (AFM, Digital Instruments Nanoscope III, used in tapping mode) was employed and Fe elemental microanalysis was carried out in house by digestion in nitric acid and AAS detection. The temperature during experiments was 20 ± 2 ^oC.

5.2.3. Reconstitution of Cellulose-Chitosan Films

Co-deposition of cellulose and chitosan on glassy carbon electrodes was achieved by a solvent evaporation approach. The colloidal cellulose suspension was diluted with water (to 0.35 wt.%). Chitosan (0.35 g) was first dissolved in 6 cm^3 concentrated acetic acid then 70 cm^3 water was added to dilute. The pH was increased to ca. pH 5 using concentrated sodium

hydroxide and the solution volume was then adjusted to 100 cm^3 with water to give a concentration of 0.35 wt.% chitosan. The deposition solution was produced by mixing the cellulose and chitosan components (typically 1:1) in a sonic bath. The combined solution was then deposited (typically 5 μL volume) on a 3 mm diameter glassy carbon electrode (Bioanalytical Systems Inc., US), placed upright in an oven at 60 °C for 30 minutes, and re-equilibrated to room temperature before use. Films with varying chitosan content were prepared simply by changing the ratio of the two components.

5.3. Results and Discussion

5.3.1. Deposition of Cellulose-Chitosan Composite Films at Glassy Carbon Electrode Surfaces

In order to form thin cellulose-chitosan films a solvent evaporation technique is employed (see experimental). Evaporation of an aqueous 0.17 wt.% solution of cellulose nanofibrils and 0.17 wt.% solution of low molecular weight chitosan (5 μL in acetate buffer) onto glass, Teflon, or a 3 mm diameter glassy carbon electrode surface (ca. 7×10^{-6} m^2 area) followed by 30 minute 60^{o}C heat treatment results in an apparently uniform and stable film coating. During the drying process, bonds (predominantly hydrogen bonds) between randomly packed cellulose nanofibrils (with ca. 4 nm diameter and ca. 250 nm length) and chitosan develop and the resulting film remains intact when re-immersed into aqueous electrolyte solutions.

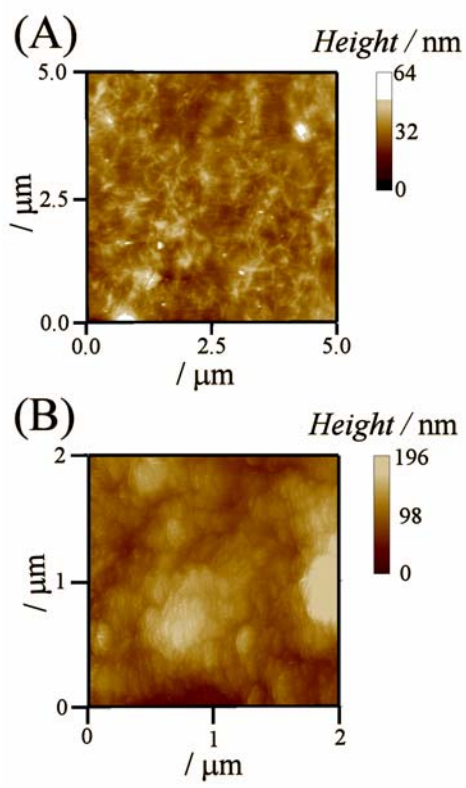

Figure 5.1AFM images of (A) **a newly formed cellulose-chitosan film still containing acetate and** (B) **a cellulose-chitosan film after immersion into water. Films were deposited on ITO substrates and the typical thickness estimated from cross sectional scans (not shown) as 0.8 μm.**

Atomic force microscopy (AFM) images of typical cellulose-chitosan films are shown in Figure 5.1 The initial film containing cellulose-chitosan and acetate seems rough on a micron scale but after immersion into water, the excess of acetate salt is removed and a more smooth surface topography is observed (see Figure 5.1B). The average thickness of these films is estimated as 0.8 μm (cross sectional AFM scans not shown) in good agreement with a recent study of cellulose nanocomposite film electrodes [21].

Chitosan is providing binding sites and pH-dependent film characteristics whereas the cellulose nanofibrils are believed to provide a structural "backbone" within the nanocomposite. In order to explore the binding and transport properties within the film, three types of systems are investigated: (i) the adsorption and mobility of the $Fe(CN)_6^{3-/4-}$ redox system, (ii) the adsorption and reactivity of triclosan, and (iii) the replacement of $Fe(CN)_6^{3-/4-}$ by the surfactant SDS.

5.3.2. Electrochemical Processes in Cellulose-Chitosan Composite Films I.: The $Fe(CN)_6^{3-/4-}$ Redox System

Cellulose-chitosan films are investigated in aqueous 0.1 M KCl employing the $Fe(CN)_6^{3-/4-}$ redox system. Typical cyclic voltammograms obtained without cellulose-chitosan film (ii), with a pure cellulose film (i), and with a cellulose-chitosan film (iii) are shown in Figure 5.2A. In the absence of the cellulose film, a well-defined voltammetric response is observed with a reversible potential of ca. 0.21 V vs. SCE. This process is consistent with the one electron redox system $Fe(CN)_6^{4-/3-}$ (Equation 5.1).

Equation 5.1 $$Fe(CN)_6^{4-}(aq) \rightleftharpoons Fe(CN)_6^{3-}(aq) + e^-$$

The cellulose nanofibril film without chitosan has a predominantly blocking effect which is reducing the peak current by ca. 95% (see curve i). The remaining current response appears at the same reversible potential and is believed to be due to a pinhole effect [21] where bigger pores allow some $Fe(CN)_6^{4-}$ diffusion into the film and to the electrode surface.

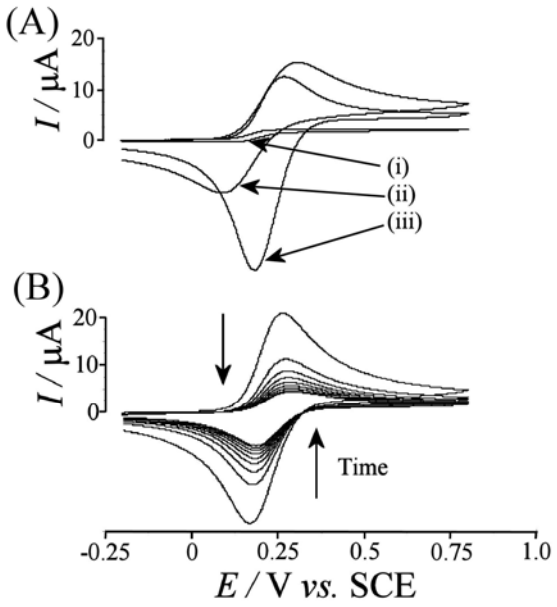

Figure 5.2 (A) **Cyclic voltammograms (scan rate 50 mV s^{-1}) for the oxidation and re-reduction of 2 mM $Fe(CN)_6^{4-}$ in aqueous 0.1 M KCl at (i) a cellulose nanofibril modified electrode without chitosan, (ii) a bare glassy carbon electrode, and (iii) a cellulose-chitosan (50 wt.% cellulose, 50 wt.% chitosan) film modified glassy carbon electrode (3 mm diameter).** (B) **Cyclic voltammograms (1nd scan shown, scan rate 50 mV s^{-1}) for the oxidation and re-reduction of $Fe(CN)_6^{4-}$ (immobilized in a cellulose-chitosan film with 50 wt.% cellulose and 50 wt.% chitosan after pretreatment in 2 mM $Fe(CN)_6^{4-}$ in 0.1 M KCl for 15 minutes) at a glassy carbon electrode immersed into 0.1 M KCl and measured periodically (data shown for 40 minute immersion).**

Figure 5.2A(iii) shows that in the presence of a composite film of 50 wt.% cellulose and 50 wt.% chitosan the peak current for the reduction of $Fe(CN)_6^{4-}$ is substantially increased when compared to the plain cellulose electrode and increased even when compared to a plain glassy carbon electrode (see Figure 5.2A(ii)). The process occurs at a slightly more positive potential and is consistent with a one electron transfer within the cellulose-chitosan membrane (Equation 5.2).

Equation 5.2 $$Fe(CN)_6^{4-}(mem) \rightleftharpoons Fe(CN)_6^{3-}(mem) + e^-$$

In order to explore the accumulation and reactivity of $Fe(CN)_6^{4-}$ in a cellulose-chitosan film in more detail, the modified glassy carbon electrode was initially pre-treated by immersion into a solution of 2 mM $Fe(CN)_6^{4-}$ in 0.1 M KCl and then rinsed and transferred into clean aqueous

0.1 M KCl. Figure 5.2B shows that under these conditions a similar response is obtained and that a slow loss of the voltammetric signal occurs with time. Over a period of 40 minutes, the electrochemical signal is reduced by ca. 75 % but it is still visible and quantifiable. The experimental observations are consistent with adsorption of $Fe(CN)_6^{4-}$ into the cellulose-chitosan film (via exchange with acetate and electrostatic binding to the protonated chitosan). Once adsorbed, the $Fe(CN)_6^{4-}$ is only slowly released into a 0.1 M KCl solution. The release process is an anion exchange process which is governed by the partitioning coefficient and binding of the $Fe(CN)_6^{4-}$ anion into the film and/or slow diffusion of the $Fe(CN)_6^{4-}$ anion.

The effect of the scan rate on the voltammetric response for the oxidation of $Fe(CN)_6^{4-}$ within the cellulose-chitosan film is investigated in Figure 5.3A and Figure 5.3B. The process (although complex in peak shape) follows the trend expected for a diffusion controlled process over a range of scan rates from 500 to 5 mV s^{-1}. Therefore diffusion within the cellulose-chitosan film is dominating the transport process (probably associated with both diffusion of anions along poly-cationomer domains as well as electron exchange hopping [32]).

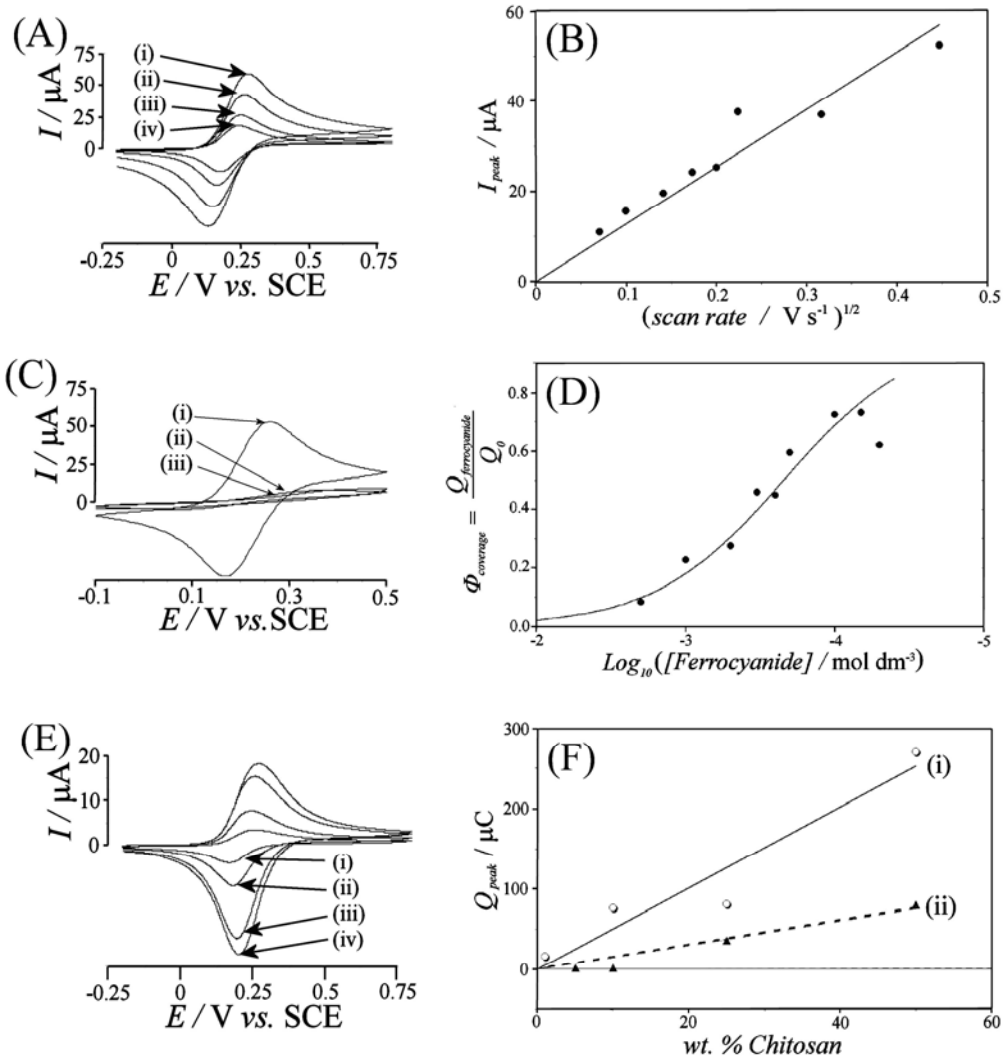

Figure 5.3 (A) **Cyclic voltammograms (1st scan shown) for the oxidation and re-reduction of $Fe(CN)_6^{4-}$ (immobilized by pretreatment in a 2 mM $Fe(CN)_6^{4-}$ in 0.1 M KCl for 15 minutes) at a cellulose-chitosan modified electrode (50 wt.% cellulose and 50 wt.% chitosan) immersed in 0.1 M KCl with varying scan rates of (i) 100, (ii) 50, (iii) 20 and (iv) 10 mV s^{-1}.** (B) **Plot of the change of peak current (I_{peak}) versus the square root of the scan rate for the oxidation of $Fe(CN)_6^{4-}$ in a cellulose-chitosan film modified electrode (50 wt.% cellulose and 50 wt.% chitosan) immersed in 0.1 M KCl. (C) Cyclic voltammograms (1st scan shown; scan rate 50 mV s^{-1}) for the oxidation and re-reduction of 1mM $Fe(CN)_6^{4-}$ immobilised at a 50 wt.% cellulose 50 wt.% chitosan film modified 3mm diameter glassy carbon electrode immersed in 0.1 M phosphate buffer with (i) pH 6, (ii) pH 8 and (iii) pH 10.** (D) **Langmuir isotherm plot for the immobilization of varying amounts of $Fe(CN)_6^{4-}$ (from a 0.1 M phosphate buffer pH 6 solution) into a cellulose-chitosan film. The line indicates the behaviour for a binding constant $K_{Ferrocyanide}$ = 2.2 x 10^3 mol^{-1} dm^3.** (E) **Cyclic voltammograms (1st scan, scan rate 50 mV s^{-1}) for the oxidation and re-reduction of $Fe(CN)_6^{4-}$ immobilized (pretreatment in 2 mM $Fe(CN)_6^{4-}$ in 0.1 M KCl for 15 minutes) into cellulose-chitosan films with varying composition (with (i) 5, (ii) 10, (iii) 25, and (iv) 50 wt.% chitosan) at a 3 mm diameter glassy carbon electrode immersed in 0.1 M KCl.** (F) **The charge (experimental under the peak or calculated) for the oxidation and re-reduction of $Fe(CN)_6^{4-}$ immobilized (pretreatment in 1 mM $Fe(CN)_6^{4-}$ in 0.1 M phosphate buffer pH 6 for 20 minutes) into cellulose-chitosan films with varying composition (between 50 and 1 wt.% chitosan) for (i) free standing films when (converted into charge from elemental analysis of iron and assuming a one electron process) and for (ii) the electrochemically detected charge at a 3 mm diameter glassy carbon electrode immersed in 0.1 M phosphate buffer pH 6.**

The binding of $Fe(CN)_6^{4-}$ into the cellulose-chitosan film is pH and concentration dependent. It has been observed previously that chitosan exhibits strong pH effects when binding species and for pure chitosan the pK_A has been reported at 6-7 [33,34]. For $Fe(CN)_6^{4-}$, at about pH 7 the binding effect of the cellulose-chitosan films is greatly reduced (see Figure 5.3C) consistent with the deprotonation of the ammonium functionality in the film. Therefore, the pH during experiments has to be controlled at about pH 6. Next, the $Fe(CN)_6^{4-}$ binding is monitored with respect to concentration. By reducing the pretreatment concentration systematically, the voltammetric response can be seen to decrease characteristically. The charge under the oxidation peak can be determined and used as an approximate measure of the amount of $Fe(CN)_6^{4-}$ within the film. In first approximation, behaviour consistent with Langmuirian-type binding is observed with an approximate binding constant $K_{Ferrocyanide} = 2.2 \times 10^3$ $mol^{-1}dm^3$ (in aqueous 0.1 M phosphate buffer pH 6). Using the Langmuir isotherm model under these conditions is highly oversimplified (*vide infra*) but does help quantifying the observed processes.

Next, the effect of chitosan content in the film is investigated. Figure 5.3E shows typical voltammetric responses obtained as a function of chitosan content. As the amount of chitosan within the composite film increases, so does the current response seen in the cyclic voltammetry. It is possible to integrate the anodic peak current in order to determine a relative measure of the number of chitosan binding sites available and Figure 5.3F shows a corresponding plot. The approximately linear correlation suggests that $Fe(CN)_6^{4-}$ indeed is binding to protonated ammonium sites in chitosan. In order to further explore this effect more quantitatively, Fe elemental analysis was employed to determine the maximum binding potential of the cellulose-chitosan films. Free-standing cellulose-chitosan films (see experimental) were prepared formed on a Teflon substrate from 1 mL cellulose-chitosan precursor solution, drying at 60 °C for 40 minutes, re-equilibration to ambient conditions, and pretreatment for 20 minutes in 1 mM $Fe(CN)_6^{4-}$ in 0.1 M phosphate buffer pH 6. The samples were then rinsed, dried ambiently, and submitted for elemental analysis. Data are summarized in Figure 5.3F. As expected, the amount of iron present (expressed here in terms of charge) increased proportionally to the amount of chitosan present in the film. The electrochemically

detected $Fe(CN)_6^{4-}$ is approximately 25% (at a scan rate of 50 mVs^{-1}) of the total content which suggests a diffusion zone of approximately 200nm.

5.3.3. Electrochemical Processes in Cellulose-Chitosan Composite Films II.: The Accumulation and Oxidation of Triclosan

Triclosan (or 2,4,4'-trichloro-2'-hydroxydiphenyl ether) is a poly-chlorinated aromatic phenol which is poorly water soluble (in neutral media) and widely used as a biocide and anti-fungal agent. As a phenol it is readily oxidized and the anodic peak current observed in voltammetric measurements has been employed for the quantitative determination for example at mercury electrodes [35], at carbon microfibers [36], and at screen-printed electrodes [37]. The hydrophobic nature of the triclosan anion has been exploited recently for the accumulation and detection in carbon-chitosan thin-film electrodes [38] and in cellulose-PDDAC films [21]. In this chapter the uptake and reactivity of triclosan is investigated in order to compare the benefits and effects of chitosan relative to those observed for poly-(diallyldimethylammonium chloride) (PDDAC).

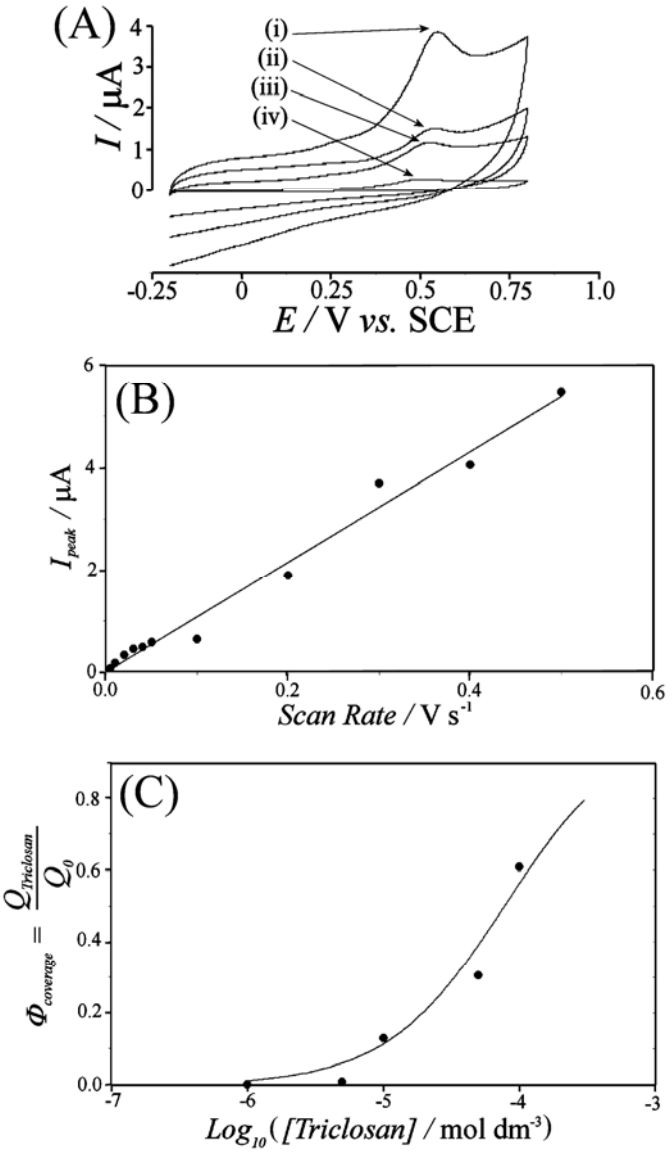

Figure 5.4 (A) **Cyclic voltammograms (1st scan shown) for the oxidation of triclosan immobilized into a 50:50 wt.% cellulose-chitosan film at a 3 mm diameter glassy carbon electrode in a solution of 100 µM triclosan in 0.1 M phosphate buffer pH 9.5 for 15 minutes with a scan rate of (i) 200 mVs^{-1}, (ii) 100 mVs^{-1}, (iii) 40 mVs^{-1}, and (iv) 10 mV s^{-1}.** (B) **Plot of the peak current (I_{peak}) versus the scan rate for the oxidation of triclosan (immobilized as in A) in a cellulose-chitosan film immersed in 0.1 M phosphate buffer pH 9.5.** (C) **Langmuir isotherm plot for the immobilization of varying amounts of triclosan (immobilized as in A) in a cellulose-chitosan film. The line indicates the theoretical curve for the binding constant $K_{Triclosan}$ = 2600 mol^{-1} dm^3.**

Figure 5.4A shows typical voltammetric data for the oxidation of triclosan immobilized (via pretreatment in a solution in 0.1 phosphate buffer pH 9.5) into a cellulose-chitosan film (50

wt.% cellulose 50 wt.% chitosan). In the absence of chitosan (with a pure cellulose film) no oxidation of triclosan occurs and therefore the binding sites in the chitosan composite appear to be crucial.

The oxidation of triclosan is chemically irreversible and believed to lead to radical intermediates and oligomeric products similar to poly-oxyphenylenes formed during phenol oxidation (equation 5.3) [39].

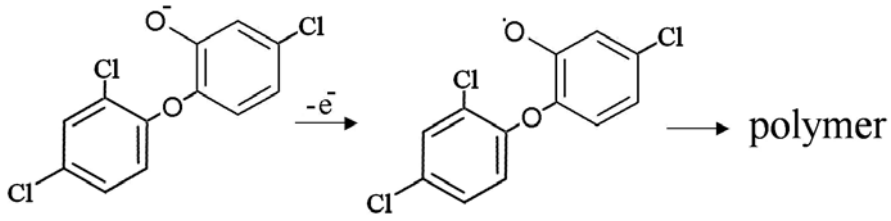

Equation 5.3

The irreversibility of this process leads to a loss of the voltammetric response after the first potential cycle and the need to renew electrodes for each experiment. The anodic voltammetric response observed for triclosan exhibits a relatively small peak current when compared for example to the oxidation of $Fe(CN)_6^{4-}$. The peak current is linearly dependent on the scan rate (see Figure 5.4B) which is indicative for a lack of diffusion and the oxidation of material only very close to the electrode surface (and/or blocking of the electrode). By varying the concentration of triclosan during the pretreatment process, the binding ability can be assessed. Figure 5.4C shows a plot of data points interpolated with a Langmuir model. The estimate of the binding constant, $K_{Triclosan}$ = 2600 mol^{-1} dm^3 suggests very weak binding of triclosan in cellulose-chitosan composites (compare $K_{Triclosan}$ = ca. 2.1 × 10^4 mol^{-1} dm^3 in cellulose-PDDAC immersed in aqueous 0.1 M phosphate buffer pH 9.5). Binding of triclosan is promoted by electrostatic and hydrophobic interactions and both of these are not strong enough in cellulose-chitosan films at alkaline pH.

5.3.4. Electrochemical Processes in Cellulose-Chitosan Composite Films III.: The Effect of SDS on the $Fe(CN)_6^{3-/4-}$ Redox System

Sodium dodecylsulfate (SDS) is a commonly used surfactant and used here as a model surfactant with negative charge. The interaction of SDS with chitosan has been reported [40] and the effect of ionic strength on the interaction highlighted. Also, a calorimetric titration study of the chitosan – SDS interaction has been reported [41] indicating that dodecylsulfate is readily bound by chitosan.

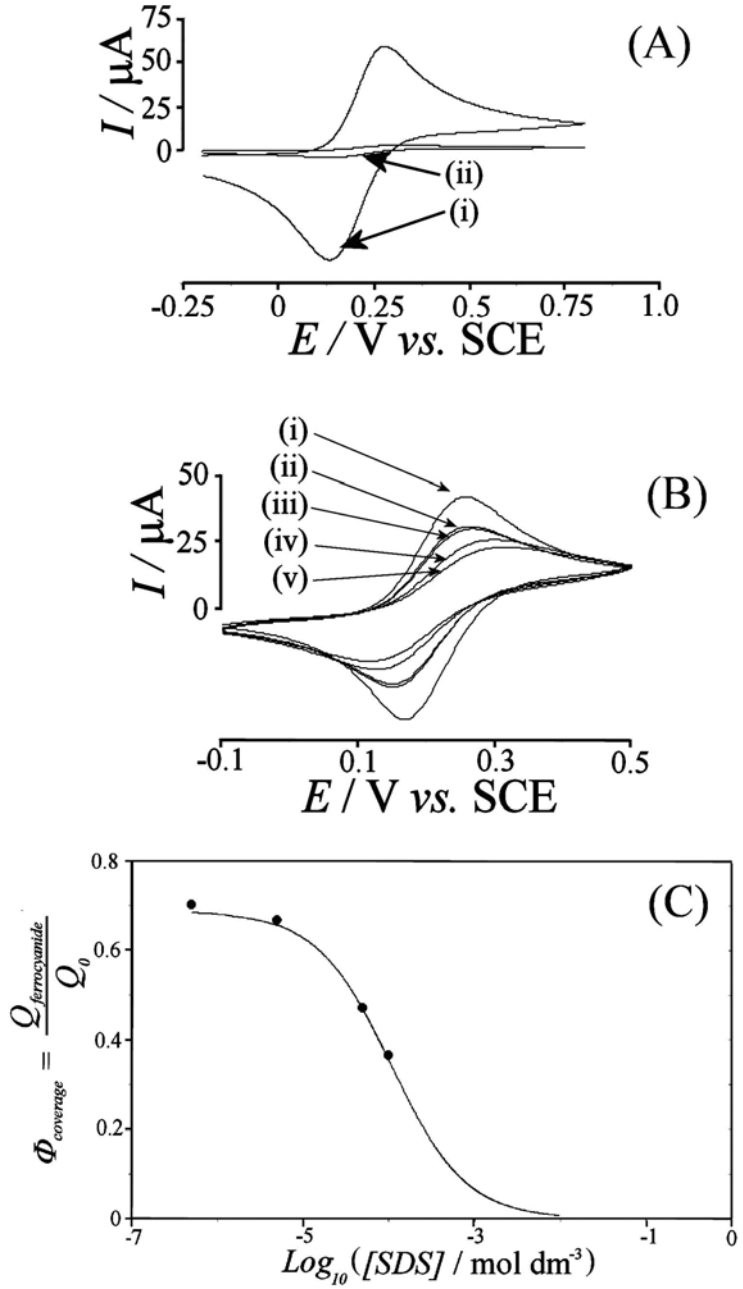

Figure 5.5 (A) **Cyclic voltammograms (1st scan, scan rate 50 mV s^{-1}) for the oxidation and re-reduction of $Fe(CN)_6^{4-}$ immobilized (pretreated in 1 mM $Fe(CN)_6^{4-}$ in 0.1 M phosphate buffer pH 6 for 15 minutes) into 50:50 wt% cellulose-chitosan films (i) without the presence of SDS and (ii) in the presence of 100 μM SDS.** (B) **Cyclic voltammograms (1st scan, scan rate 100 mV s^{-1}) for the oxidation and re-reduction of $Fe(CN)_6^{4-}$ immobilized (pretreated in 1 mM $Fe(CN)_6^{4-}$ in 0.1 M phosphate buffer pH 6 for 20 minutes) into 50:50 wt% cellulose-chitosan film in the presence of (i) 0, (ii) 0.5 μM, (iii) 5 μM, (iv) 50 μM, and (v) 100 μM SDS at a 3 mm diameter glassy carbon electrode immersed in 0.1 M phosphate buffer pH 6.** (C) **Langmuir isotherm plot for the immobilization of varying amounts of SDS when competitively immobilized with 1 mM $Fe(CN)_6^{4-}$ for 20 mins in a 50:50 wt% cellulose-chitosan film. The line indicates the theoretical curve for the binding constants $K_{SDS} = 3 \times 10^4$ mol^{-1} dm^3 and $K_{Ferrocyanide} = 2.2 \times 10^3$ mol^{-1} dm^3 (vide supra).**

SDS is not directly electrochemically active but a method of assessing SDS concentrations would be desirable. Therefore, the effect of SDS on the $Fe(CN)_6^{3-/4-}$ redox system is studied and the competitive binding effect exploited. When a cellulose-chitosan film modified electrode is pretreated in 1 mM $Fe(CN)_6^{4-}$ solution for 15 minutes in a solution of phosphate buffer pH 6 with and without 100 μM SDS present, the voltammetric signal is greatly reduced in the presence of the surfactant (see Figure 5.5A). This observation strongly suggests preferential binding of SDS to the cationic sites of chitosan.

Next, the preferential binding effect of SDS compared to $Fe(CN)_6^{4-}$ is used to indirectly quantify the binding constant of SDS to cellulose-chitosan composite materials. By adhering to an approximate Langmuir binding model (both SDS and ferrocyanide anions are in first approximation assumed to bind to the same type and number of binding sites) the competition between $Fe(CN)_6^{4-}$ binding and SDS binding can be quantified. Only the concentration of $Fe(CN)_6^{4-}$ may be determined electrochemically, but in a series of experiments employing different SDS concentrations, the displacement of $Fe(CN)_6^{4-}$ can be measured. The Langmuir isotherm expression for competitive binding is given in Equation 5.4.

Equation 5.4

$$\Phi_{coverage} = \frac{Q_{Fe(CN)_6^{4-}}}{Q_{0,Fe(CN)_6^{4-}}} = \frac{K_{Fe(CN)_6^{4-}}[Fe(CN)_6^{4-}]}{1 + K_{Fe(CN)_6^{4-}}[Fe(CN)_6^{4-}] + K_{SDS}[SDS]}$$

In this expression, $\Phi_{coverage}$ is the fraction of $Fe(CN)_6^{4-}$ species bound into the film, $Q_{Fe(CN)_6^{4-}}$ is the charge attributed to the oxidation of ferrocyanide in the film (in the presence of SDS), $Q_{0,Fe(CN)_6^{4-}}$ is the charge when all sites are occupied (in the absence of SDS), $K_{Fe(CN)_6^{4-}}$ is the known binding constant for ferrocyanide, *[Fe(CN)$_6^{4-}$]* is the concentration of ferrocyanide in the pretreatment solution, K_{SDS} is the unknown binding constant for SDS, and *[SDS]* is the concentration of SDS in the pretreatment solution. Figure 5.5C shows a plot of data obtained at different SDS concentrations and the line is indicating the expected behaviour based on Equation 5.4. The decrease in $Fe(CN)_6^{4-}$ oxidation response with increasing SDS concentration is consistent with competitive binding and the binding constant for SDS, K_{SDS} = 3×10^4 mol^{-1} dm^3, is obtained. With this binding constant known, it is now possible to use an

appropriate level of ferrocyanide to determine the SDS surfactant concentration. However, other anionic interferents have to be taken into consideration and further experimental work will be required to explore these as well as ionic strength effects.

5.4. Conclusions

The reactivity of cellulose-chitosan films is dominated by the chitosan component. Binding of anions such as $Fe(CN)_6^{4-}$ is effective at a pH lower than the pK_A of chitosan (6-7) and adsorption of $Fe(CN)_6^{4-}$ into cellulose-chitosan films can be described (at least in in first approximation) as Langmuirian with $K_{Ferrocyanide} = 2.2 \times 10^3$ mol^{-1} dm^3. The adsorption of triclosan into cellulose-chitosan films is possible even at alkaline pH, but the magnitude of the current response and the estimated binding constant, $K_{Triclosan} = 2.6 \times 10^3$ mol^{-1} dm^3, suggest a very weak interaction. Finally, competitive binding of surfactants such as dodecylsulfate is observed and the binding constant for SDS, $K_{SDS} = 3 \times 10^4$ mol^{-1} dm^3, has been determined. The relatively high affinity of the cellulose-chitosan composite to the anionic surfactant SDS suggests that cellulose-chitosan composites could be employed in the extraction of surfactants. In future an improved version of the competitive binding assay could be employed for the determination of a wider range of surfactant systems.

5.5. References

[1] S. Dumitriu, "Polysaccharides", *Marcel Dekker, New York,* **1998**.

[2] M. Rinaudo, *Prog. Polym. Sci*. **2006**, *31*, 603.

[3] S.L. Kosaraju, L. D'ath, A. Lawrence, *Carbohydrate Polymers* 64, **2006**, 163.

[4] E. Guibal, M. Van Vooren, B.A. Dempsey, J. Roussy, *Separation Science & Technology* 41, **2006,** 2487.

[5] S.H. Lim, S.M. Hudson, *Journal of Macromolecular Science - Polymer Review* C43, **2003**, 223.

[6] J.D. Schiffman, C.L. Schauer, *Biomacromolecules* 8, **2007**, 594.

[7] B. Krajewska, *Separation &. Purification Technology* 41, **2005**, 305.

[8] E. Birlik, S. Buyuktiryaki, A. Ersoz, A. Denizli, R. Say, *Separation Science & Technology* 41, **2006**, 3109.

[9] A.J. Varma, S.V. Deshpande, J.F. Kennedy, *Carbohydrate Polymers* 55, **2004**, 77.

[10] C.L. Schauer, M.S. Chen, R.R. Price, P.E. Schoen, F.S. Ligler, *Environmental Science & Technology* 38, **2004**, 4409.

[11] H. Sashiwa, Y. Shigemasa, R. Roy, *Chemical Letters 29*, **2000**, 596.

[12] M.M. Beppu, C.C. Santana, *Materials Research* 5, **2002**, 47.

[13] H.S. Kas, *Journal of Microencapsulation* 14, **1997**, 689.

[14] A.K. Singla, M. Chawla, *Journal of Pharmacy & Pharmacology 53*, **2001**, 1047.

[15] C.F. Ou, R. Yuan, Y.Q. Chai, M.Y. Tang, R. Chai, X.L. He, *Analytical Chimica Acta* 603, **2007**, 205.

[16] S.T. Dubas, C. Iamsamai, P. Potiyaraj, *Sensors & Actuators B – Chemistry* 113, **2006**, 370.

[17] Y.H. Bai, Y. Du, J.J. Xu, H.Y. Chen, *Electrochemical Communications* 9, **2007**, 2611.

[18] D. Du, J.W. Ding, J. Cai, A.D. Zhang, *Colloids & Surfaces B - Biointerfaces* 58, **2007**, 145.

[19] Q. Liu, X.H. Xu, C.H. Zhang, Q. Chen, *Sensor Letters* 5, **2007**, 459.

[20] A. Schneider, C. Vodouhe, L. Richert, G. Francius, E. Le Guen, P. Schaaf, J.C. Voegel, B. Frisch, C. Picart, *Biomacromolecules* 8, **2007**, 139.

[21] M.J. Bonne, K.J. Edler, J.G. Buchanan, D. Wolverson, E. Psillakis, M. Helton, W. Thielemans, F. Marken, *Journal of Physical Chemistry C* 112, **2008**, 2660.

[22] M.S. Lin, H.J. Len, *Electroanalysis* 17, **2005**, 2068.

[23] Y.H. Bai, Y. Du, J.J. Xu, H.Y. Chen, *Electrochemical Communications 9*, **2007**, 2611.

[24] Y.P. Shan, G.C. Yang, Y.T. Jia, J. Gong, Z.M. Su, L.Y. Qu, *Electrochemical Communications* 9, **2007**, 2224.

[25] X.L. Zou, L.Q. Luo, Y.P. Ding, Q.S. Wu, *Electroanalysis* 19, **2007**, 1840.

[26] Y. Du, X.L. Luo, J.J. Xu, H.Y. Chen, *Bioelectrochemistry* 70, **2007**, 342.

[27] T. Tangkuaram, C. Ponchio, T. Kangkasomboon, P. Katikawong, W. Veerasai, *Biosensors & Bioelectronics* 22, **2007**, 2071.

[28] M.A. Murphy, G.D. Wilcox, R.H. Dahm, F. Marken, *Indian Journal of Chemistry A – Inorganic, Bio-inorganic, Physical Theory & Analytical Chemistry* 44, **2005**, 924.

[29] J. Li, Q. Liu, Y.J. Liu, S.C. Liu, S.Z. Yao, *Analytical Biochemistry* 346, **2005**, 107.

[30] R.G. Compton, C.E. Banks, *Understanding Voltammetry*, World Scientific, London, 2007.

[31] N.L. Garcia de Rodriguez, W. Thielemans, A. Dufresne, *Cellulose* 13, **2006**, 261.

[32] R. Murray, "Molecular Design of Electrode Surfaces", *Wiley, New York*, **1992**.

[33] H. Sashiwa, Y. Shigemasa and R. Roy, *Chemical Letters* 29, **2000**, 596.

[34] L. Rassaei, M.J. Bonné, M. Sillanpää, F. Marken, *New Journal of Chemistry* 32, **2008**, 1253.

[35] A. Safavi, N. Maleki, H.R. Shahbaazi, *Analytical Chimica Acta,* 494, **2003**, 225.

[36] L.H. Wang, S.C. Chu, C.Y. Chin, *Bulletin of Electrochemistry* 20, **2004**, 225.

[37] R.M. Pemberton, J.P. Hart, *Analytical Chimica Acta* 390, **1999**, 107.

[38] M. Amiri, S. Shahrokhian, E. Psillakis, F. Marken, *Analyitcal Chimica Acta 593*, **2007**, 117.

[39] M.A. Ghanem, R.G. Compton, B.A. Coles, E. Psillakis, M.A. Kulandainathan, F. Marken, *Electrochimica Acta* 53, **2007**, 1092.

[40] A. Dedinaite, M. Ernstsson, *Journal of Physical Chemistry B 107*, **2003**, 8181.

[41] R. Barreiro-Iglesias, C. Alvarez-Lorenzo, A. Concheiro, *Journal of Thermal Analytical Calorimetry* 82, **2005**, 499.

Chapter 6: Nanocellulose Composite Electrodes IV

Nanocellulose-Chitosan Composite Electrodes

6.1. Introduction

It has now been demonstrated that cellulose architectures can be formed on the nano-scale and that the chemical behaviour of these architectures may be altered by the inclusion of additional components. Chitosan is a natural polymer with a linear stereoregular structure (poly-D-glucosamine [1]) derived in industrial scale from chitin (mainly from crustacean exoskeletons) by deacetylation. Chitosan is an important additive to thicken or stabilise foods or pharamceuticals [2], for drug release systems [3], it is used to purify water [4], in textiles and synthetic polymers [5] or composites [6], and in technical membranes [7]. Chitosan has been used in chemical analysis for example as imprinted solid phase extraction substrate [8], for metal complexation [9], and for metal detection [10]. Chitosan has been reported to exhibit a $pK_A \approx 6$ to 7 [11,12,13,14] and is therefore a poly-electrolyte only under acidic conditions. Chitosan can be dissolved in acidic aqueous media and sensor films on electrode surfaces have been prepared for example by layer-by-layer deposition [15,16], chitosan hydrogel deposition [17], electro-deposition [18,19], and crosslinked composite deposition [20]. In this chapter chitosan is employed as a "binder" for cellulose nanofibrils (from sisal, ca. 4 nm diameter and 250 nm length [21]) in order to form thin and stable cellulose-chitosan composite membranes.

In electroanalysis, chitosan has been used to prepare protein-sensor films [22], and composite sensor films [23]. An electro-spinning method has been employed to deposit chitosan nanofibers onto ITO substrates [24] and surfactant modified chitosan films have been reported for dopamine and ascorbate electroanalysis [25]. A gold-chitosan glucose sensor [26] and a gold-horseradish-peroxidase-chitosan based peroxide sensor [27] were proposed. In most electrochemical applications chitosan is a binder and matrix for nanocarbon [28] and other active components [29]. There are no previous reports on the formation of cellulose-chitosan nanocomposite films and their electrochemical properties.

The re-constitution of a cellulose "backbone" together with suitable poly-electrolyte "receptor" molecules such as chitosan is introducing selectivity towards anionic analytical targets and in particular towards hydrophobic anions. In chapter 5 we have shown that a similar membrane material can be obtained from cellulose nanofibrils and poly-(diallyldimethylammonium chloride) or PDDAC and that the binding sites introduced by PDDAC are accumulating anions from dilute aqueous solutions, such as $Fe(CN)_6^{4-}$. These tetra-valent anions can be effectively extracted from aqueous solution into cationic binding sites and then determined for example with a voltammetric technique [30].

In this study, both re-constituted cellulose film- and re-constituted cellulose-chitosan film-modified electrodes are characterized and redox processes within these films are investigated. The principle of embedding the chitosan "receptor" into the cellulose "backbone" is demonstrated and model redox systems such as $Fe(CN)_6^{3-/4-}$ and triclosan are employed to investigate the binding ability, film composition effects, and diffusion effects.

The anionic surfactant dodecylsulfate, found commonly in cleaning agents and household products, is shown to accumulate and strongly bind into cellulose-chitosan membranes. A competitive binding assay based on dodecylsulfate replacing $Fe(CN)_6^{4-}$ from the electrochemically active film is proposed as a potential model for surfactant detection.

6.2. Experimental

6.2.1. Chemical Reagents

Acetic acid, sodium acetate trihydrate, and alizarin red S were obtained from Aldrich and used without further purification. A cellulose nanofibril 0.69 wt.% in water solution was prepared from sisal following a literature procedure [10]. Demineralised and filtered water was taken from a Elga water purification system (Vivendi, High Wycombe, Bucks) with a resistivity of not less than 18 MOhm cm.

6.2.2. Instrumentation

For voltammetric studies a microAutolab II potentiostat system (EcoChemie, NL) was employed with a Pt gauze counter electrode and a saturated Calomel (SCE) reference electrode (REF401, Radiometer, Copenhagen). The working electrode was a 3 mm diameter glassy carbon electrode (BAS, US). Experiments were conducted after de-aerating with high purity argon (BOC) for at least 15 minutes prior to recording voltammograms. The temperature during experiments was $20 \pm 2\ ^{o}C$.

UV-visible spectra were obtained using a VISionLite UV-vis spectrometer over a wavelength range of 350 – 800 nm. For surface topography imaging an atomic force microscope (Digital Instruments Nanoscope III, used in contact mode) was employed. A SAXS/WAXS (simultaneous small-angle X-ray scattering and wide-angle X-ray scattering) pattern of cellulose membranes was obtained on a SAXSess system using a PW3830 X-ray generator. The X-ray image plates were observed using a Perkin Elmer Cyclone Storage Phosphor System. The small angle patterns were recorded with Cu Kα radiation ($\lambda = 1.5406$ Å) at 40 kV and 50 mA in the region of 2θ from 5° to 25° with an exposure time of 45 minutes whilst simultaneous recording small angle patterns in the region of 0.2Å to 100Å.

6.2.3. Synthesis of Boronic Acid Dendrimer (by E. Galbraith, University of Bath)

Synthesis of boronic acid appended dendrimer: 200 mg, 0.14 mmol (as 1.0 g of a 20 wt% solution in MeOH) of Generation 1 PAMAM dendrimer (ethylenediamine core, 8 amino surface groups), was diluted in a further 10 mL dry methanol and stirred at 60 ºC in the presence of a 16-fold excess of 2-formylphenylboronic acid (2.24 mmol, 360 mg) for 48 hours under nitrogen gas atmosphere. The solution was then cooled to 0ºC (ice/water bath) and $NaBH_4$ (169 mg, 4.48 mmol) was added portion-wise under a stream of nitrogen to the stirring mixture. The suspension was allowed to warm to room temperature and stirred for a further 8 hours. 2M HCl (aq) was slowly added until no further gas was evolved and the solution was stirred for 2 hours. The resulting crude material was neutralised with NaOH (aq) and diluted further with water (5 mL) and methanol (5 mL) and then passed through an ultrafiltration membrane (MWCO 1000) at 62 psi nitrogen pressure in a Millipore stirred cell. Further concentration with 2 x 5 mL 10% methanol (aq) was performed using the same apparatus. The remaining residue was retrieved by dissolving in methanol and subsequently dried by evaporation at reduced pressure. Isolated yield of colourless gum 287 mg (82%).

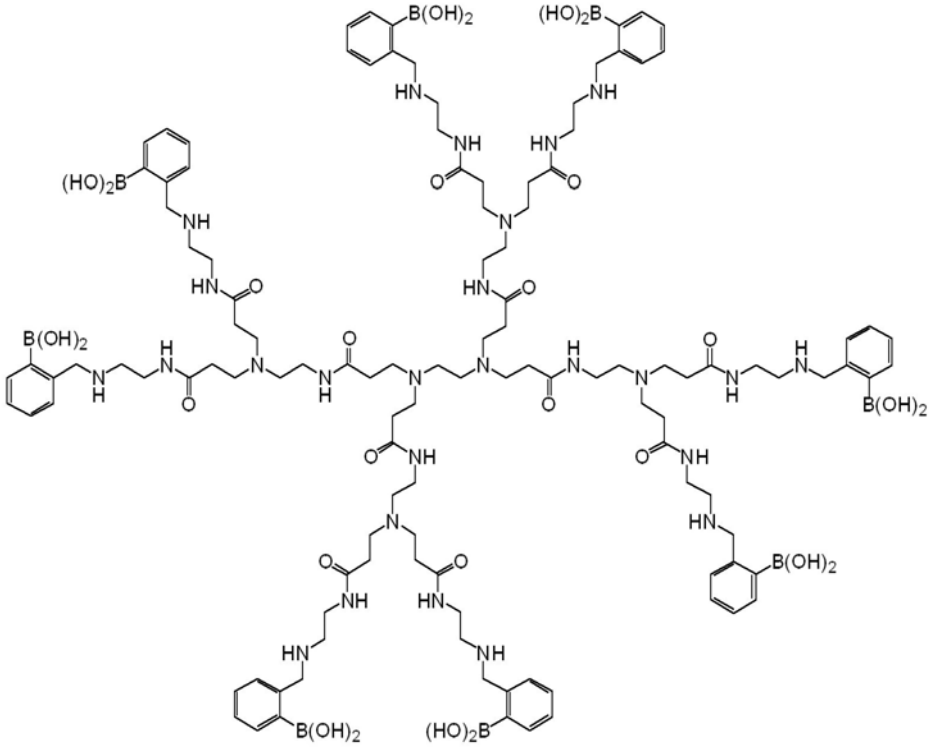

Figure 6.1 Chemical structure of the boronic acid dendrimer 1.

δ_H (300 MHz, d4-MeOD) 7.33-7.31 (8 H, m), 7.12-7.09 (16 H, m), 7.07-7.03 (8 H, m), 3.96 (16 H, s), 3.43 (16 H, t, *J* = 6 Hz), 2.89 (16 H, t, *J* = 6 Hz), 2.71-2.62 (24 H, m), 2.46-2.44 (16 H, m), 2.30-2.21 (28 H, m); δ_C (75.5 MHz, d4-MeOD) 178.5, 177.68, 145.6, 134.4, 131.4, 130.7, 127.0, 58.0, 56.4, 54.0, 41.5, 41.0, 37.7 δ_B NMR (96.3 MHz, d-MeOD**)** 10.3.

6.2.4. Formation of Boronic Acid Dendrimer Crosslinked Nanofibrillar Cellulose Membranes

Nanocomposite membranes of boronic acid dendrimer and cellulose nanofibrils were formed using a solvent casting technique. Boronic acid appended dendrimer was dissolved in 10 mL of methanol to give a 13.9 mg/mL solution. This solution (in appropriate amounts) was directly added to 1 mL aqueous cellulose solution (0.69 wt.% nanofibrils) and thoroughly mixed. For example, 20 µL of the boronic acid dendrimer/methanol solution was added to 1 mL of cellulose solution and then vigorously agitated (by ultrasonication). A 5 µL volume of this solution was placed on the surface of a clean glassy carbon electrode and then dried in an oven at 60°C for 1 hour. This resulted in a film with 4 wt.% boronic acid dendrimer to 96 wt.% cellulose nanofibrils. Free standing membranes were required for SAXS/WAXS experiments. These membranes were prepared by placing 1 mL of deposition solution onto a flat Teflon substrate (area ca. 2 cm^2), drying in an oven at 60°C for 1 hour, and peeling off the resulting membrane from the Teflon surface with a pair of tweezers. The membranes were then left to equilibrate at ambient temperature and humidity before conducting experiments.

6.3. Results and Discussion

6.3.1. Formation and Characterisation of Boronic Acid Dendrimer Crosslinked Nanofibrillar Cellulose Membranes

Membranes of nanofibrillar cellulose are readily obtained by evaporation of a nanocellulose sol in water on suitable substrates [31]. The cellulose nanofibrils are believed to crosslink via hydrogen bridges thereby forming strong and durable network membranes. It is possible to imbed reactive ionomer [32] molecules into these "reconstituted" cellulose membranes. In this study, a dendrimer system with the ability to bind and crosslink cellulose surfaces is used to functionalise cellulose films. Boronic acids are known to bind to poly-ols and carbohydrates [33] and they have been employed to provide functional surfaces in chromatography [34] e.g. for the separation of RNA [35]. Here, boronic acid appended dendrimers (generation 1 PAMAM) are employed to crosslink and modify cellulose membranes. These modified cellulose membranes were formed in a solution evaporation process (see experimental) based on an aqueous sol.

The topography and thickness of membranes were examined by atomic force microscopy (AFM) in tapping mode (see Figure 6.2). Membranes were deposited onto quartz glass substrates from a 5 μL volume of aqueous solution of cellulose nanofibrils (0.69 wt.%) and boronic acid dendrimer (0.03 wt.%) followed by drying for 60 minutes in an oven at 60 °C (giving a film containing 95% cellulose and 4% boronic acid dendrimer, see experimental). Scratches were introduced using a scalpel in order to measure the thickness of membranes (not shown). The profile of the scratch was compared at different locations on the membrane surface yielding an average thickness of approximately 3 μm (for a ca. 5 mm diameter disc-shaped deposit) which suggests a typical membrane volume of 6×10^{-11} m^3 in 5 μL deposition solution (the calculated membrane density is 0.6 g cm^{-3} compared to the crystal density [36] of cellulose 1.582 g cm^{-3}). The membrane topography (see Figure 6.2) clearly reveals cellulose nanofibrils with approximately 250 ± 100 nm length and a 4-5 nm diameter.

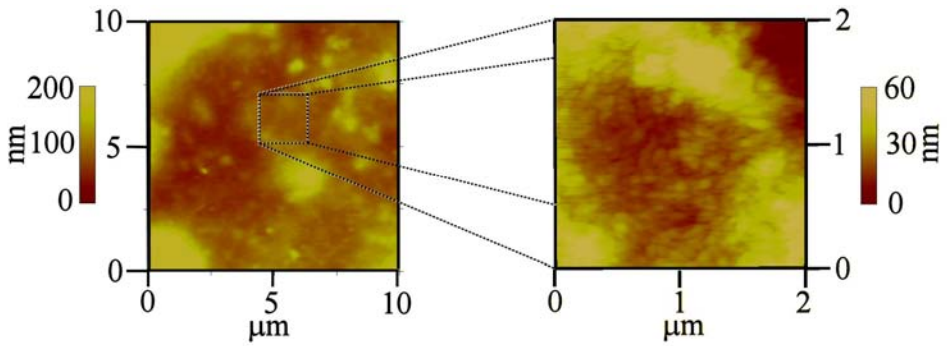

Figure 6.2 AFM images for a 96 wt% cellulose nanofibril – 4 wt% boronic acid dendrimer membrane on a quartz glass substrate showing the topography of individual nanofibrils packed into a dense layer.

X-ray scattering techniques offer a powerful probe into both atomic and nanostructure of composite materials. Previous studies of cellulose nanofibril materials have shown that the nanofibrils have a ribbon morphology [37]. Here, the morphologies of both plain reconstituted cellulose nanofibrils and nanocellulose-boronic acid dendrimer composite membranes are investigated with wide and small angle X-ray scattering techniques.

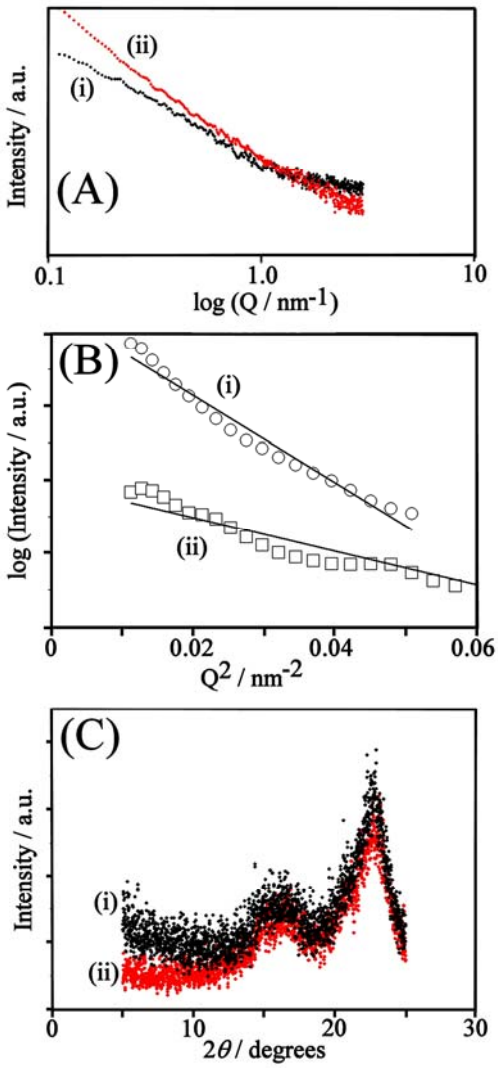

Figure 6.3 X-ray scattering data for (i) nanofibrillar cellulose and (ii) for boronic acid dendrimer crosslinked nanofibrillar cellulose (reconstituted 96 wt.% cellulose nanofibrils and 4 wt.% boronic acid dendrimer). (A) **Small angle scattering data.** (B) **A Guinier plot of the logarithm of intensity versus the momentum transfer squared, Q^2, giving approximate radii of gyration of (i) R_G = 8.3 nm and (ii) R_G = 13.3 nm.** (C) **Wide-angle X-ray scattering data.**

In Figure 6.3A the small angle X-ray scattering pattern are shown for (i) a nanocellulose membrane and (ii) a nanocellulose-boronic acid dendrimer modified membrane (96 wt.% cellulose and 4 wt.% boronic acid dendrimer). An approximately linear relationship between the scattering intensity, I, and the value of the momentum transfer, Q (which is given by $Q = 4\pi/\lambda \sin(\theta)$ where θ is half the scattering angle) is observed. Upon the introduction of boronic acid dendrimer into the cellulose membrane, there is a marked change in the slope of the SAXS pattern. Guinier analysis was applied to the experimental curves for both

membranes. The expression $\ln(I) = \ln(I_0) - \left(\frac{R_G{}^2}{3}\right) \times Q^2$ allows the radius of gyration, R_G, to be estimated as R_g(i) = 8.3 nm (consistent with previous measurements [14]) and R_g(ii) = 13.3 nm. The boronic acid dendrimer is clearly opening up the structure, and consistent with the approximate diameter of the spherical boronic acid dendrimer of 4.4 nm the presence of one dendrimer unit binding the cellulose nanofibrils together is confirmed.

In the wide-angle X-ray scattering pattern (see Figure 6.3C) characteristic cellulose type I crystal structure peaks are observed [38]. The data are consistent with scattering by the cellulose-I polymorph [39], where the peaks occur at 14.8° (scattering from the $1\bar{1}0$ diffraction plane), at 16.4° (110 diffraction plane), and at 22.6° (020 diffraction plane). The additional peak found in the pattern at 20.6° (shoulder) could be due to small amount of the polymorph cellulose-III structure, which is commonly seen in reconstituted forms of cellulose [40].

6.3.2. Spectrophotometric and Voltammetric Study of Alizarin Red S Binding into Boronic Acid Dendrimer Crosslinked Nanofibrillar Cellulose Membranes

Alizarin red S (3,4-dihydroxy-9,10-dioxo-2-anthracenesulfonic acid, sodium salt) is a common fluorescence probe [41] and analytical dye molecule [42]. It is used here to quantify binding to free boronic acids [43] within the cellulose membrane. Alizarin red S is a probe molecule with both spectrophotometric and electrochemical reactivity (in aqueous media a 2-electron 2-proton reversible reduction occurs [44]).

The UV-visible spectrum of alizarin red S was measured to determine the effect of binding into the boronic acid dendrimer crosslinked nanofibrillar cellulose membranes. First, the solution phase absorbance was measured using solutions of 50 μM alizarin red S in 0.1 M acetate buffer at pH 3 and at pH 7 (Figure 6.4A). The pK_a of alizarin red S [45] for the first deprotonation step is ~ 4 (see Equation 6.1) and this leads to a characteristic change in colour from yellow to red. An absorbance peak at a wavelength of ca. 420 nm can be seen for the

solution phase species at pH 3 with the maximum absorption wavelength shifting to ca. 520 nm for alizarin red S at pH 7, consistent with literature reports [46].

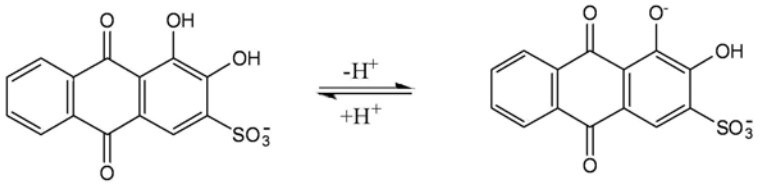

Equation 6.1

Next, alizarin red S was bound into boronic acid dendrimer crosslinked nanofibrillar cellulose membrane. Films without and with crosslinker were formed by drying 0.5 mL of precursor solution on a 1 cm^2 transparent quartz glass substrate. The resulting membrane (thickness ca. 60 μm) was then immersed for 30 minutes in a solution of 500 μM alizarin red S in acetate buffer at pH 3 (or at pH 7). After rinsing and drying the transmission spectrum was recorded (see Figure 6.4A). In the absence of the boronic acid dendrimer no strong binding of alizarin red S occurred. In the presence of the boronic acid dendrimer, a new absorption peak at ~ 455 nm is observed (see Figure 6.4A) for both samples prepared pH 3 and at pH 7. These characteristic absorption peaks are consistent with alizarin red S when bound to phenyl-boronic acids [47]. The minor shift in the wavelength of absorbance peaks for samples obtained at pH 3 and at pH 7 may be due to local changes in the chemical environment of the bound alizarin red S (see Figure 6.4A).

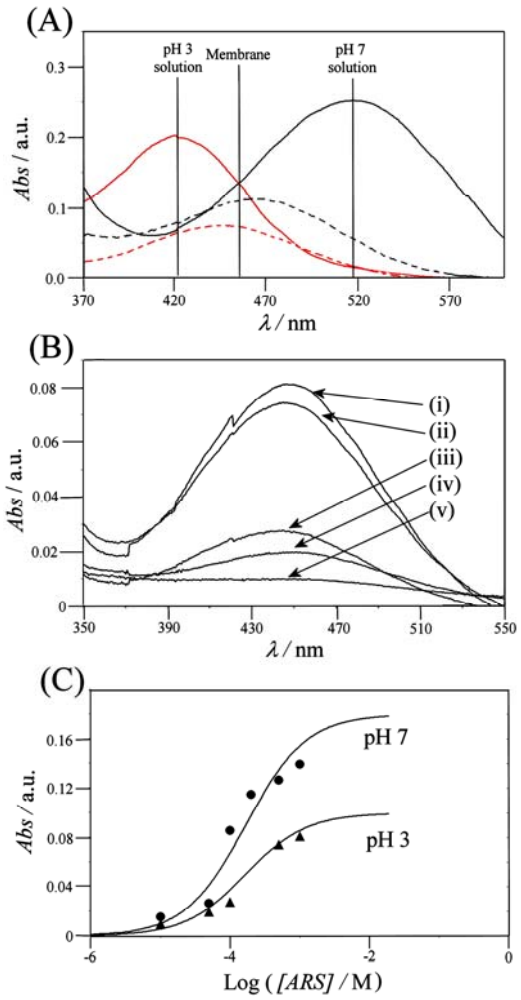

Figure 6.4 (A) **UV-Visible spectra of 50 μM alizarin red S in 0.1 M acetate buffer at pH 3 (red line, λ_{max} ~ 420 nm) and at pH 7 (black line, λ_{max} ~ 520 nm). Also shown are spectra for a boronic acid dendrimer crosslinked nanofibrillar cellulose membrane soaked in 500 μM alizarin red S with 0.1 M acetate buffer at pH 3 (red dashed line) and at pH 7 (black dashed line) both with λ_{max} ca. 455 nm.** (B) **UV-visible spectra for a boronic acid dendrimer crosslinked nanofibrillar cellulose films soaked (i) 1000, (ii) 500, (iii) 100, (iv) 50 and (v) 10 μM alizarin red S in 0.1 M acetate buffer pH 3.** (C) **Langmuir plot of the UV-visible absorption for membrane samples versus the concentration of alizarin red S in the 0.1 M acetate buffer soaking solution for pH 3 and for pH 7. The lines show the expected behaviour for a Langmuirian binding constant K_{obs} = 6000 mol^{-1} dm^3.**

The binding of alizarin red S into the boronic acid dendrimer crosslinked nanofibrillar cellulose membrane was investigated as a function of alizarin concentration (at pH 3 and at pH 7, see Figure 6.4B and C). Analysis based on Langmuirian binding suggested a binding co-efficient for alizarin red S of K_{obs} = 6000 ± 1000 M^{-1} very much consistent with literature reports on solution phase binding [48]. Very similar results are obtained for binding at pH 3

and at pH 7. The binding of alizarin red S to a boronic acid occurs via the catechol moiety [49] (see Equation 6.2).

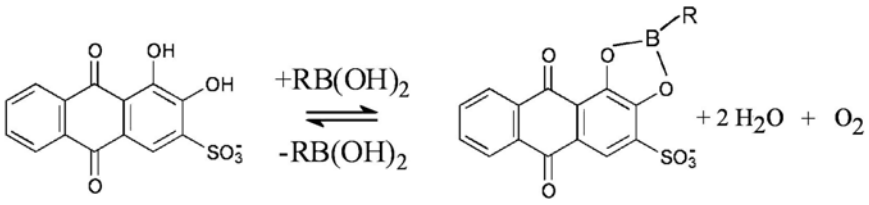

Equation 6.2

Next, voltammetry was used to detect and monitor the diffusion and binding of alizarin red S in the boronic acid dendrimer crosslinked nanofibrillar cellulose membranes. At a bare glassy carbon electrode immersed in 1 mM alizarin red S in aqueous 0.1 M acetate buffer pH 3 a well-defined chemically reversible voltammetric responses is observed with a midpoint potential of ca. -0.37 V vs. SCE (see Figure 6.5A). The reduction of alizarin red S follows a 2-electron 2-proton mechanism [50] (see Equation 6.3).

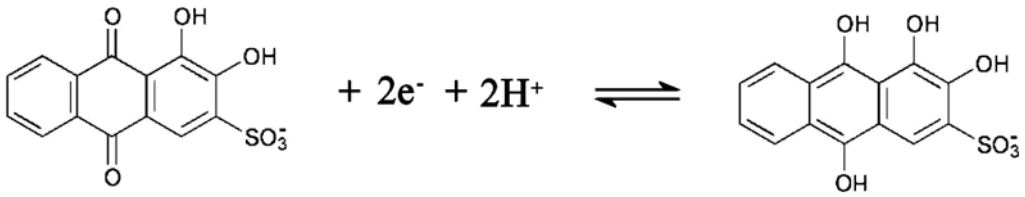

Equation 6.3

Analysis of a plot of the logarithm of peak current versus the logarithm of scan rate (not shown) suggests diffusion characteristics. Next, a film of boronic acid dendrimer crosslinked nanofibrillar cellulose was applied to the glassy carbon electrode (thickness ca. 6 μm, ca. 96 wt.% cellulose and 4 wt.% boronic acid dendrimer) and modified by immersion into 1 mM alizarin red S in 0.1 M acetate buffer (pH 3) for a period of 30 minutes. The electrode was rinsed with deionised water and left to dry in ambient conditions before use in voltammetric experiments.

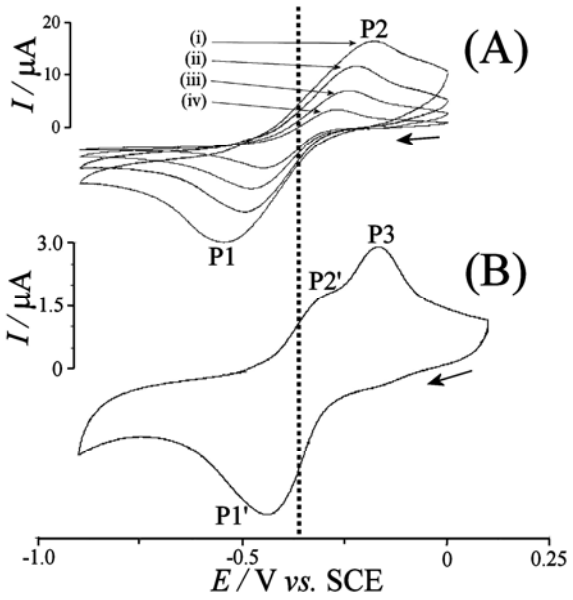

Figure 6.5 (A) **Cyclic voltammograms (2nd scan shown) for the reduction and oxidation of 1 mM alizarin red S (ARS) in 0.1 M acetate buffer pH 3 at a 3mm diameter glassy carbon electrode 3 at scan rates of (i) 500, (ii) 200, (iii) 100 and (iv) 50 mV s^{-1}.** (B) **Cyclic voltammograms (2nd scan shown, 100 mVs^{-1}) for the oxidation and reduction of ARS in a boronic acid dendrimer modified cellulose nanofibril membrane at a glassy carbon surface (immobilized by soaking in a 1 mM ARS in 0.1 M acetate buffer pH 3 for 30 minutes) re-immersed in clean 0.1 M acetate buffer pH 3.**

Figure 6.5B shows typical voltammetric responses for the alizarin red S modified electrode immersed in 0.1 M acetate buffer pH 3. A cathodic peak at -0.47 V vs. SCE (P1') is observed followed by two anodic peaks (P2' and P3) at -0.32 and -0.17 V vs. SCE. When recorded at different scan rates, the peak current (P1') shows an approximately linear dependence on the scan rate consistent with an immobilized redox system. The reduction and re-oxidation process can be assigned to a 2-electron 2-proton process (see Equation 6.4) similar to that observed for alizarin red S in solution. However, the process is confined to a small reaction zone close to the electrode surface.

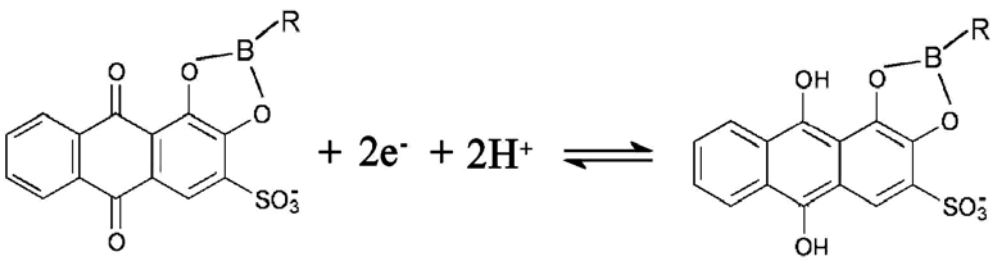

Equation 6.4

The appearance of two oxidation peaks (see Figure 6.5B) suggest that the reduction of the boronic acid bound alizarin red S is causing two distinct forms of alizarin to form. Experiments conducted over a range of scan rates (see Figure 6.6A) confirm that the ratio of the peak currents for both peaks, P2' and P3, remains approximately constant. The peak response P2' is very similar to the corresponding reduction peak for the free alizarin (P2 in Figure 6.5A) and therefore a disproportionation mechanism is proposed. The formation of the reduced form of the boronic acid bound alizarin red S (see Equation 6.4) causes two new phenolic binding sites for boronic acids to form. The rapid re-equilibration will cause more strongly bound alizarin red S to form with 3 or 4 phenolic O-B bonds whereas some alizarin red S molecules will be "freed" from the boronic acid binding. The oxidation of the "free" alizarin red S is assigned to process P2' whereas the oxidation of the more strongly bound alizarin red S is assigned to process P3. Alternatively, structural effects such as a change from 1,2-diol binding to 1,3-diol binding could also explain the observed peak splitting.

The effect of the number of boronic acid binding sites incorporated into the nanofibrillar cellulose membrane may be altered by changing the content of boronic acid dendrimer in the casting solution. In Figure 6.6B, as the amount of boronic acid dendrimer present in the membrane is increased, the current response of the membrane with immobilised alizarin red S also increased. In order to quantify this effect, the charge under the cathodic current response (P2') was plotted versus the weight percentage of boronic acid dendrimer within the membranes (see Figure 6.6D). With no boronic acid dendrimer present, there is a residual voltammetric response due to alizarin red S physically retained in the membrane. Upon the introduction of boronic acid dendrimer the charge under the peak increases steadily until the boronic acid dendrimer content reaches ca. 8 wt.%. In this composition range the voltammetric response is dominated by the boronic acid bound alizarin red S. For a membrane with 4 wt.% boronic acid dendrimer content, a charge of ~ 7 μC was measured which equates to an amount of alizarin red S of ca. 40 pmole detectable in the membrane. This compares to an expected charge of 1 mC calculated based on the available boronic acid binding sites in the 6 μm thick film (for a ca. 3.5 mm diameter disc-shaped deposit). Therefore only about 1% of the cellulose film (ca. 60 nm) is electrochemically active.

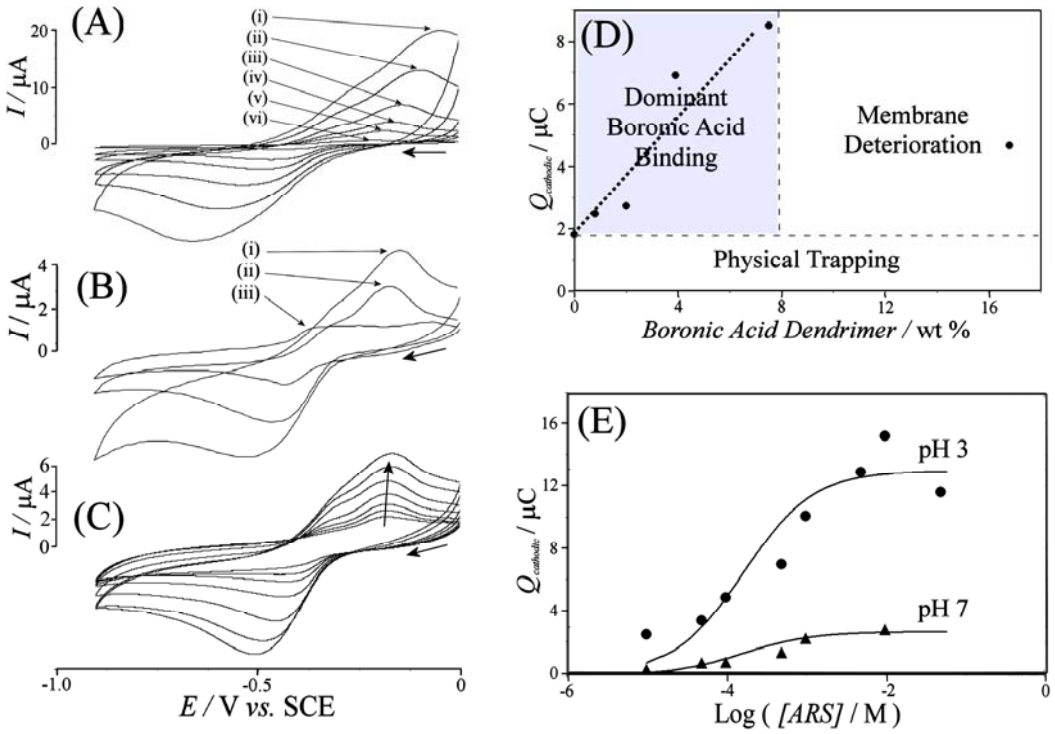

Figure 6.6 (A) **Cyclic voltammograms (scan rate (i) 1000, (ii) 500, (iii) 200, (iv) 100, (v) 50, and 20 mV s^{-1}, 2nd scan shown) for the reduction and re-oxidation of alizarin red S (immobilized by immersion into 1 mM alizarin red S in 0.1 M acetate buffer pH 3 for 30 minutes) at a boronic acid dendrimer crosslined nanofibrillar cellulose film electrode (96 wt.% cellulose and 4 wt.% boronic acid dendrimer) immersed in 0.1 M acetate buffer pH 3.** (B) **Cyclic voltammograms (scan rate 100 mV s^{-1}, 2nd scan shown) for the reduction and re-oxidation alizarin red S (immobilized by immersion into 1 mM alizarin red S in 0.1 M acetate buffer pH 3 for 30 minutes) at boronic acid dendrimer crosslinked nanofibrillar cellulose film electrodes with (i) 8 wt%, (ii) 4 wt% and (iii) 0 wt% boronic acid dendrimer.** (C) **Cyclic voltammograms (scan rate 100 mVs^{-1}, 2nd scan shown) for the reduction and re-oxidation of alizarin red S (immobilized by immersion into alizarin red S with a concentration of 10^{-5} to 5×10^{-2} M in 0.1 M acetate buffer pH 3 for 30 minutes) at a boronic acid dendrimer crosslinked nanofibrillar cellulose film electrode (96 wt.% cellulose and 4 wt.% boronic acid dendrimer) immersed in 0.1 M acetate buffer pH 3.** (D) **Plot of the charge under the reduction of alizarin red S when immobilized into boronic acid dendrimer crosslinked nanofibrillar cellulose versus boronic acid dendrimer content.** (E) **Langmuir isotherm plot for the charge under the alizarin red S reduction peak versus the concentration of alizarin red S during immobilization at pH 3 and at pH 7. The lines indicate the expected behaviour for a binding constant K = 6000 ± 1000 mol^{-1} dm^3.**

For boronic acid dendrimer contents of higher than ~ 8 wt.% the nanocomposite films becomes mechanically unstable and deterioration during voltammetric experiments is observed. Therefore, for all further voltammetric experiments a 4 wt.% boronic acid dendrimer content was employed. The binding constant for the alizarin red S by the

membrane, K_{obs}, was determined in acetate buffer at pH 3 and at pH 7. The concentration of alizarin red S was varied between 10 μM and up 50 mM (reaching the solubility limit). The charge under the reduction peak was plotted versus the alizarin red S concentration used during immobilization (see Figure 6.6E). Assuming Langmuirian binding characteristics, the binding constant for alizarin red S in the membrane was obtained as K_{obs} = 6000 ± 1000 M^{-1} consistent with spectrophotometric measurements (vide supra). The effect of the pH on the binding constant appears to be insignificant. The absence of a pH effect is due to the N-B interaction (see Figure 6.1) suppressing OH^- interaction. The difference in the magnitude of the charge under the reduction peak at pH 3 and at pH 7 can be explained with a different mobility of alizarin red S in protonated and in deprotonated state (see Equation 6.1).

6.4. Conclusions

Boronic acid dendrimer crosslinked nanofibrillar cellulose membranes are stable for less than 8 wt.% boronic acid dendrimer content. The formation of the nanocomposite membrane is believed to be based on the binding ability boronic acids to poly-sacharride interfaces. Excess of boronic acid binding sites introduced into the film allow alizarin red S absorption which was followed both spectrophotometrically and voltammetrically. A Langmuir-type binding isotherm was observed with K = 6000 ± 1000 M^{-1} and with a linear alizarin red S detection range of ca. 10 μM to 1 mM.

6.5. References

[1] S. Dumitriu, "Polysaccharides", *Marcel Dekker, New York,* **1998**.

[2] M. Rinaudo, *Programme in Polymer Science* 31, **2006**, 603.

[3] S.L. Kosaraju, L. D'ath, A. Lawrence, *Carbohydrate Polymers 64*, **2006**, 163.

[4] E. Guibal, M. Van Vooren, B.A. Dempsey, J. Roussy, *Separation Science & Technology* 41, **2006,** 2487.

[5] S.H. Lim, S.M. Hudson, *Journal of Macromolecular Science - Polymer Review C43,* **2003**, 223.

[6] J.D. Schiffman, C.L. Schauer, *Biomacromolecules* 8, **2007**, 594.

[7] B. Krajewska, *Separation & Purification Technology* 41, **2005**, 305.

[8] E. Birlik, S. Buyuktiryaki, A. Ersoz, A. Denizli, R. Say, *Separation Science & Technology* 41, **2006**, 3109.

[9] A.J. Varma, S.V. Deshpande, J.F. Kennedy, *Carbohydrate Polymers* 55, **2004**, 77.

[10] C.L. Schauer, M.S. Chen, R.R. Price, P.E. Schoen, F.S. Ligler, *Environmental Science & Technology* 38, **2004**, 4409.

[11] H. Sashiwa, Y. Shigemasa, R. Roy, *Chemical Letters* 29, **2000**, 596.

[12] M.M. Beppu, C.C. Santana, *Materials Research* 5, **2002**, 47.

[13] H.S. Kas, *Journal of Microencapsulation* 14, **1997**, 689.

[14] A.K. Singla, M. Chawla, *Journal of Pharmacy & Pharmacology* 53, **2001**, 1047.

[15] C.F. Ou, R. Yuan, Y.Q. Chai, M.Y. Tang, R. Chai, X.L. He, *Analytical Chimica Acta* 603, **2007**, 205.

[16] S.T. Dubas, C. Iamsamai, P. Potiyaraj, *Sensors & Actuators B - Chemistry 113,* **2006**, 370.

[17] Y.H. Bai, Y. Du, J.J. Xu, H.Y. Chen, *Electrochemical Communications* 9, **2007**, 2611.

[18] D. Du, J.W. Ding, J. Cai, A.D. Zhang, *Colloids & Surfaces B - Biointerfaces* 58, **2007**, 145.

[19] Q. Liu, X.H. Xu, C.H. Zhang, Q. Chen, *Sensors Letters* 5, **2007**, 459.

[20] A. Schneider, C. Vodouhe, L. Richert, G. Francius, E. Le Guen, P. Schaaf, J.C. Voegel,

B. Frisch, C. Picart, *Biomacromolecules* 8, **2007**, 139.

[21] M.J. Bonne, K.J. Edler, J.G. Buchanan, D. Wolverson, E. Psillakis, M. Helton, W. Thielemans, F. Marken, *Journal of Physical Chemistry C* 112, **2008**, 2660.

[22] M.S. Lin, H.J. Len, *Electroanalysis* 17, **2005**, 2068.

[23] Y.H. Bai, Y. Du, J.J. Xu, H.Y. Chen, *Electrochemical Communications* 9, **2007**, 2611.

[24] Y.P. Shan, G.C. Yang, Y.T. Jia, J. Gong, Z.M. Su, L.Y. Qu, *Electrochemical Communications* 9, **2007**, 2224.

[25] X.L. Zou, L.Q. Luo, Y.P. Ding, Q.S. Wu, *Electroanalysis* 19, **2007**, 1840.

[26] Y. Du, X.L. Luo, J.J. Xu, H.Y. Chen, *Bioelectrochemistry* 70, **2007**, 342.

[27] T. Tangkuaram, C. Ponchio, T. Kangkasomboon, P. Katikawong, W. Veerasai, *Biosensors & Bioelectronics* 22, **2007**, 2071.

[28] M.A. Murphy, G.D. Wilcox, R.H. Dahm, F. Marken, *Indian Journal of Chemistry A – Inorganic, Bio-inorganic, Physical Theory & Analytical Chemsitry* 44, **2005**, 924.

[29] J. Li, Q. Liu, Y.J. Liu, S.C. Liu, S.Z. Yao, *Analytical Biochemistry* 346, **2005**, 107.

[30] R.G. Compton, C.E. Banks, "Understanding Voltammetry", *World Scientific, London,* **2007**.

[31] M.J. Bonne, K.J. Edler, J.G. Buchanan, D. Wolverson, E. Psillakis, M. Helton, W. Thielemans and F. Marken, *Journal of Physical Chemisry C* 112, **2008**, 2660.

[32] K. Tsourounaki, M.J. Bonné, W. Thielemans, E. Psillakis, M. Helton, A. McKenzie and F. Marken, *Electroanalysis*, **2008,** in print.

[33] T.D. James, M.D. Phillips and S. Shinkai, "Boronic acids in saccharide recognition". *The Royal Society of Chemistry, Cambridge,* **2006**.

[34] R. Tuytten, F. Lemiere, W. Van Dongen, E. Witters, E.L. Esmans, R.P. Newton and E. Dudley, *Analytical Chemistry*, 80, **2008**, 1263.

[35] S. Senel, *Colloids & Surfaces A* 219, **2003**, 17.

[36] W. J. Lyons, *J. Chem. Phys*. 1941, **9**, 377

[37] P. Terech, L. Chazeau and J.Y. Cavaille, *Macromolecules* 32, **1999**, 1872.

[38] Y. Nishiyama, J. Sugiyama, H. Chanzy and P. Langan, *Journal of the American Chemical Society* 125, **2003**, 14300.

[39] A. Isogai, M. Usuda, T. Kato, T. Uryu and R.H. Atalla, *Macromolecules* 22, **1989,** 3168.

[40] M. Wada, Y. Nishiyama, H. Chanzy, T. Forsyth and P. Langan, *Powder Diffraction* 23, **2008,** 92.

[41] Y. Kubo, T. Ishida, A. Kobayashi and T.D. James, *Journal of Material Chemistry* 15, **2005**, 2889.

[42] W. Sun and K. Jiao, *Talanta* 56, **2002**, 1073.

[43] S. Arimori, C.J. Ward and T.D. James, *Tetrahedron Letters* 43, **2002**, 303.

[44] V.E. Mouchrek, A.L.B. Marques, J.J. Zhang and G.O. Chierice, *Electroanalysis* 11, **1999**, 1130.

[45] J. Yan, G. Springsteen, S. Deeter and B. Wang, *Tetrahedron*, 2004, **60**, 11205.

[46] S. Murcia-Mascaros, C. Domingo, S. Sanchez-Cortes, M.V. Canamares and J.V. Garcia-Ramos, *Journal of Raman Spectroscopy* 36, **2005**, 420.

[47] G. Springsteen and B.H. Wang, *Tetrahedron* 58, **2002**, 5291.

[48] S. Arimori, C.J. Ward and T.D. James, *Tetrahedron Letters* 43, **2002**, 303.

[49] G. Springsteen and B.H. Wang, *Tetrahedron* 58, **2002,** 5291.

[50] V. Mirceski and M. Lovric, *Electroanalysis* 9, **1997**, 1283.

Chapter 7: Cellulose Material Electrodes I

Absorption & Reactivity of Metal Complexes in Cotton

7.1. Introduction

Presently, this thesis has concentrated upon the micro- and nano-scopic elements of cellulose as an integrated chemical system. Macroscopic cellulose systems are abundant in today's society with a variety of applications, whether it be the clothes we wear or the paper this thesis is written on. Chemical processes that occur in cellulose matrices are numerous and future applications in 'smart materials', for example digital paper, could provide the next revolution in intelligent materials. Many of these potential applications are fundamentally dependent upon the supporting matrix they occur in. In this chapter, the behaviour of metal complexes within cotton cellulose matrices is studied. Potential metal complexes could be chromic for application in dynamic displays on clothes or they could be the catalysts which are used to clean the clothes. By using electrochemical probe molecules we demonstrate the monitoring of the absorption, diffusion and reactivity of metal complexes within common place cellulose matrices.

Cotton consists predominantly (94% [1]) of cellulose and the cellulose structure contains nanocrystalline domains (cellulose-I) as well as amorphous regions [2,3]. "Elementary fibrils" with only 2 to 4 nm diameter are packed into micro- and macro-fibrils which then combine into fibers. The properties of cotton fibers are primarily dependent upon the structure of the cellulose component (which can be modified with appropriate chemical treatments [4]) and to some extent on the macroscopic structure which originates from the growth of the fibers from plant cells. Voltammetry [5,6] is an experimental tool that has never been applied to investigate processes within cotton fibers and which offers a new in situ experimental tool to study absorption and reactivity of redox active systems, for example as a function of external parameters or fiber pre-treatments.

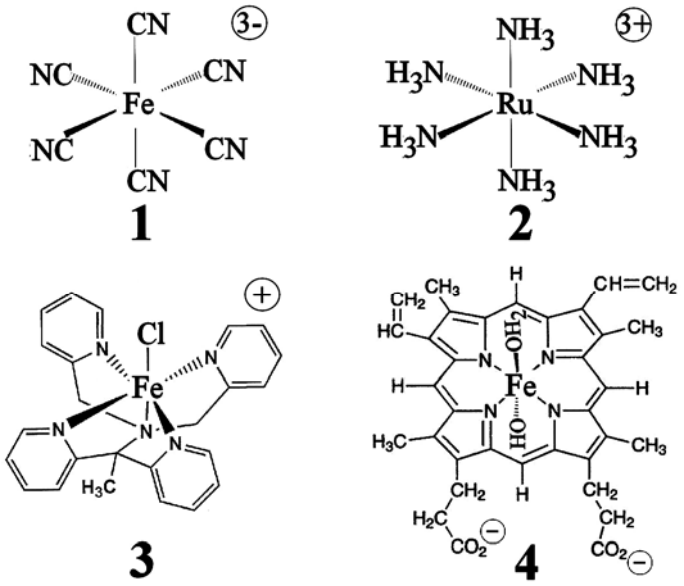

Scheme 7.1 Molecular structures of ferricyanide, $Fe(CN)_6^{3-}$ (1), hexaammine ruthenium(III), $Ru(NH_3)_6^{3+}$ (2), $[Fe(II)(N,N\text{-bis(pyridin-2-yl-methyl)-1,1-bis(pyridin-2-yl)-1-aminoethane)Cl]^+$ or $Fe(BBA)Cl^+$ (3), and $[Fe(III)(\text{proto-porphyrinato-IX})(H_2O)(OH)]^{2-}$ or hemin (4).

In this chapter natural cotton (a "standard" cotton from Phoenix Calico, woven, bleached, non-desized and non-mercerized) is employed in order to explore the ability of voltammetric methods to provide useful characterization tool for processes in textile samples. The cotton is immobilized at a graphite electrode surface with a close contact between graphite and cotton ensured by initially applying graphite flakes to the textile. It is shown that the reactivity of metal complexes can change when compared in cotton and in aqueous solution. This type of electrode is very useful for the investigation of the interaction of redox active materials with cotton and for the study of mobility within cotton. It may also be useful as a novel analytical device for the determination of analytes of high cellulose affinity.

The absorption of redox active metal complexes into the cotton fibers is investigated for a range of different redox systems (see Scheme 7.1). The ferricyanide anion, $Fe(CN)_6^{3-}$ (**1**), has been chosen as a model redox system with good stability in aqueous buffer solution and with highly reversible electron transfer. The uptake into and interaction with cotton of this redox probe is investigated and a simplistic diffusion model suggested. The cationic $Ru(NH_3)_6^{3+/2+}$ redox system has been selected based on the complementary charge. Next, a well known

bleaching catalyst [7], [Fe(II)(N,N-bis(pyridin-2-yl-methyl)-1,1-bis(pyridin-2-yl)-1-aminoethane)Cl]$^{+}$ or Fe(BBA)Cl^{+} (see Scheme 7.1), is investigated. Finally, the well known anionic proto-porphyrinato-IX complex hemin (see Scheme 7.1) has been investigated. Hemin has been studied with electroanalytical methods when immobilized at electrode surface [8], in the form of polymerized films [9] or dissolved in ionic liquids [10]. Hemin is a potent electrocatalysts for many redox reactions in aqueous media. The reduction of oxygen [11], the reduction of hydrogen peroxide [12] or catalase activity [13], or processes involving trichloroacetate [14] or nitrite/NO [15] are only some representative examples. Voltammetry of these metal complexes in the presence of cotton textile is employed to investigate absorption, diffusion, and reactivity within cotton.

7.2. Experimental

7.2.1. Reagents

Hemin chloride, Na_2CO_3, $NaHCO_3$, KCl, $Ru(NH_3)_6Cl_3$, $K_4Fe(CN)_6$, and graphite powder (1-2 micron) were obtained from Aldrich and used without further purification. (N,N-bis(pyridin-2-yl-methyl)-1,1-bis(pyridin-2-yl)-1-aminoethane) chloro iron(II) chloride, [Fe(BBA)Cl]Cl, was supplied by Unilever (Port Sunlight, UK). Demineralised and filtered water was taken from an Elgastat water purification system (Elga, High Wycombe, Bucks) with a resistivity of not less than 15 MOhm cm. Cotton samples (Phoenix Calico, US) were woven, bleached, non-fluorescent, non-desized (not washed to remove any residuals), and non-mercerized.

7.2.2. Instrumentation

For voltammetric studies a microAutolab II potentiostat system (EcoChemie, Netherlands) was employed with a Pt gauze counter electrode and a saturated Calomel (SCE) reference electrode (Radiometer, Copenhagen). The working electrode was a 4.9 mm diameter basal plane pyrolytic graphite electrode ("Pyrocarbon", Le Carbone UK). Scanning electron microscopy (SEM) images were obtained with a JEOL JSM6310 system. Experiments were conducted after de-aerating with high purity argon (BOC) for at least 15 minutes. The temperature during experiments was 20 ± 2 ^{o}C.

7.2.3. Procedures

Cotton discs of ca. 5.2 mm diameter and ca. 0.27 mm thickness (measured by placing the disc between two glass slides) were cut from fabric and stored in a closed container at 4 ^{o}C. Individual cotton fibers have a diameter of typically 10 μm (see Figure 7.1). Prior to electrochemical experiments, graphite powder was applied to one side of the dry cotton disc (the textile was completely covered with graphite to maximize the electrical contact to the electrode) which is then placed in contact with a 4.9 mm diameter basal plane pyrolytic graphite electrode and firmly immobilized with a coarse Lycra^{TM} membrane. Prior to immersion into the aqueous buffer phase, the cotton modified electrode was kept in an

atmosphere of argon (ca. 10 minutes) to remove residual oxygen from within the cotton fibers. The graphite flakes (see Figure 7.1D) allow processes within the cotton material to be observed and the voltammetric signals from the solution phase to be minimized.

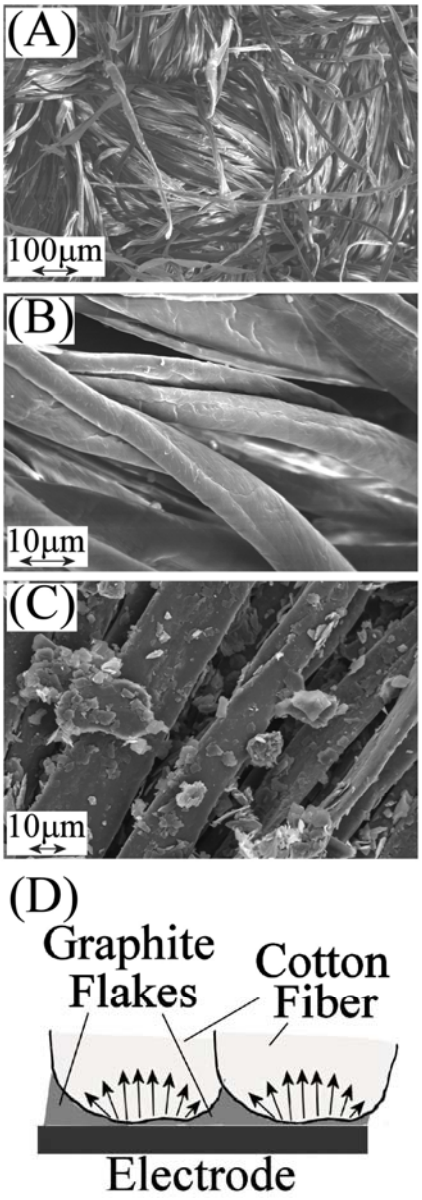

Figure 7.1 Scanning electron microscopy (SEM) images for (A,B) **cotton textile fibers and** (C) **cotton with graphite flakes immobilized on the surface.** (D) **Schematic representation of the graphite flakes helping to improve the cotton to electrode contact.**

In order to modify the cotton fibers, cotton discs were soaked in a solution of the metal complex under investigation dissolved in aqueous carbonate buffer (pH 10). The soaking time

was chosen to ensure equilibration and complete diffusion throughout the sample. The cotton disc was then placed on filter paper (Whatman), dried in air, and stored at 4 ^{o}C. These modified cotton samples were subsequently treated following the same procedure of first applying graphite flakes and then immobilization at a graphite electrode.

7.2.4. Analysis of Diffusion Data

Voltammetric experiments with cotton textile immobilized at the electrode surface provide information about the concentration and mobility of metal complexes within the cotton fiber. Amorphous cellulose provides a hydrophilic environment for water and ions to diffuse into. Cotton discs of ca. 5.2 mm diameter and 270 μm thickness represent a thick membrane and the voltammetric experiment (for a reversible redox system) can be assumed to cause only a minor perturbation whilst providing concentration data as a function of time. Both the diffusion of reagents into the cotton sample and the "leaching" of metal complexes from the cotton sample into clean buffer environment were monitored. The charge under the voltammetric response was used as a measure of the concentration of metal complex within the cellulose structure.

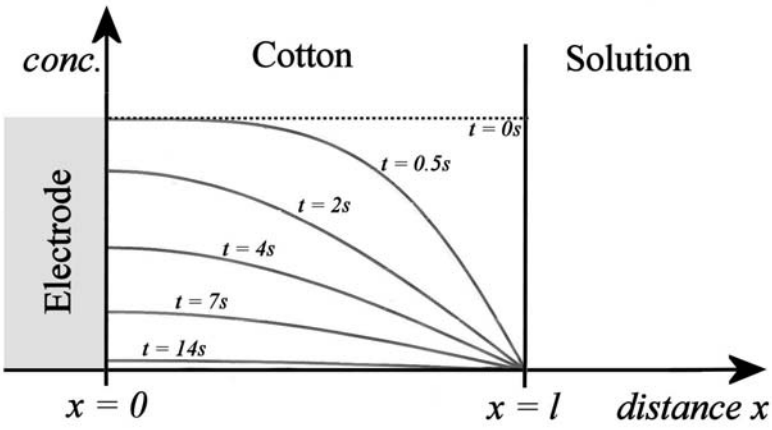

Figure 7.2 Schematic representation of the concentration profile within a membrane (cotton) during a leaching process as a function of time (assumed in this plot are a 100 μm thick membrane (*l*) and a diffusion coefficient of $D = 10^{-9}$ m^2s^{-1}; equation 1 has been employed to calculate concentrations as a function of distance and time).

A simple model for the diffusion process was chosen based on the assumption of diffusion within a homogeneous membrane in contact with the electrode surface (see Figure 7.2) and a fixed concentration within the solution in contact with the cotton sample. In a typical

"leaching" experiment the concentration at the electrode surface will change with time in a characteristic way depending on the thickness of the membrane (parameter *l* in Figure 7.2). An approximate equation for this case was derived by Carslaw and Jaeger [16] (see Equation 7.1).

Equation 7.1

$$\frac{Q}{Q_0} \approx \frac{C}{C_0} = 1 - \left[\exp(-\beta t) \frac{\cos x(\beta/D)^{1/2}}{\cos l(\beta/D)^{1/2}} \right] - \frac{16\beta l^2}{\pi} \sum_{n=0}^{\infty} \left[\frac{(-1)^n \exp(-D(2n+1)^2 \pi^2 t / 4l^2)}{(2n+1)\{4\beta l^2 - D\pi^2 (2n+1)^2\}} \cos \frac{(2n+1)\pi x}{2l} \right]$$

In this equation C is the concentration of the diffusing reagent, C_0 is the initial concentration, β denotes the time constant for a fast step of the solution concentration to a new non-equilibrium value, D is the diffusion coefficient, l is the thickness of the membrane, x is the position for which the concentration is calculated, and n denotes the degree of the term used in this approximation. The charge under a voltammetric peak, Q, is generally proportional to the concentration of the redox active compound and therefore it is assumed here that $\frac{Q}{Q_0} \approx \frac{C}{C_0}$. In this study calculations with n = 3 gave satisfactory results and data fitting (manual optimization of D and Q_0) was possible with a Microsoft Excel spreadsheet. Three weaknesses of this approximate data analysis approach are (i) heterogeneity of cotton is disregarded, (ii) diffusion within the aqueous solution phase is assumed to be fast and not rate limiting, and (iii) the effect of a partitioning equilibrium between cotton and aqueous phase on the rate of absorption of leaching out is not considered.

7.2.5. Elemental Analysis of Iron Content in Cotton Samples

The cotton samples were reproduced in different concentrations to be analyzed for their iron elemental content. This was achieved by soaking 10 samples in each different concentration of metal complex for a minimum of four hours to ensure equilibrium, which were then dried under ambient conditions for a further hour period. The samples were then put in a 'Carbonlite' furnace for 45 minutes at 1200K in a platinum crucible, oxidizing any iron and combusting any cellulosidic material. The remaining ash was then dissolved in 50% nitric acid then 35% hydrochloric acid to ensure complete solvation of the oxidized iron. This was then

made up into a solution and the mass of iron per disc measured using a Varian AA-275 series atomic absorption spectrometer. Having measured the mass of iron, m_A, present in each cotton disc sample the associated hypothetical maximum charge (where all present electrochemically active species are able to electron transfer at the electrode surface), Q_{max}, was calculated using Equation 7.2 (F is the Faraday constant and Z_A is the atomic mass of the element deposited, in this case iron).

Equation 7.2

$$Q_{max} = \frac{m_A F}{Z_A}$$

7.3. Results and Discussion

7.3.1. Electrochemical Reactivity of $Fe(CN)_6^{3-}$ Absorbed into Cotton and Immersed in Aqueous Buffer Solution

Initially, standard redox systems are employed to explore the effect of cotton on the mobility and reactivity of metal complexes. The ferricyanide anion, $Fe(CN)_6^{3-}$, is readily soluble in aqueous 0.1 M carbonate buffer (pH 10) and stable over prolonged periods. Rotating disc voltammetry (RDE) experiments conducted with a 4.9 mm diameter basal plane pyrolytic graphite electrode allow a well defined one electron reduction process (Equation 7.3) to be observed with a half wave potential of 0.18 V vs. SCE. The diffusion coefficient for $Fe(CN)_6^{3-}$ in 0.1 M carbonate buffer, $D_{Fe(CN)_6^{3-}} = 0.5 \times 10^{-9}$ m^2s^{-1} (at 20 ^oC, data not shown), is obtained from a plot of the mass transport controlled limiting current versus the square root of the rate of rotation [17].

Equation 7.3 $Fe(CN)_6^{3-}(aq) + e^- \rightleftharpoons Fe(CN)_6^{4-}(aq)$

Cotton samples, when exposed to $Fe(CN)_6^{3-}$ solution in 0.1 M carbonate buffer, quickly take on a yellow colour depending on the concentration of $Fe(CN)_6^{3-}$ in the treatment solution. Immobilization of the cotton sample at the electrode surface, immersion into clean 0.1 M carbonate buffer solution (pH 10) and scanning the potential from 0.5 V vs. SCE to -0.1 V vs. SCE allows characteristic voltammetric responses for the $Fe(CN)_6^{3-}$ within the cotton sample to be observed (see Figure 7.3). The half wave potential is observed at 0.18 V vs. SCE.

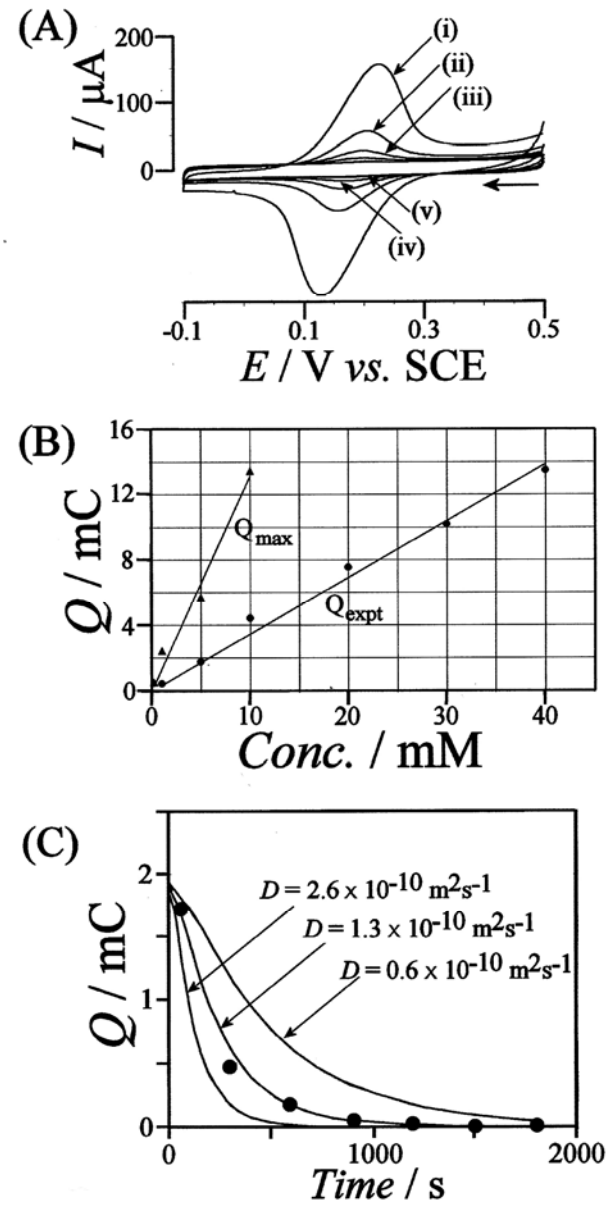

Figure 7.3 (A) **Cyclic voltammograms (scan rate 10 mV s^{-1}) for the reduction and re-oxidation of ferricyanide (**1**) absorbed into a cotton fabric (absorption conditions 5 mM ferricyanide in 0.1 M carbonate buffer pH 10, measurement time (i) 60s, (ii) 300s, (iii) 600s, (iv) 900s, and (v) 1200s after immersion of the cotton disc).** (B) **Plot of the initial charge, Q_{expt}, and the hypothetical maximum charge, Q_{max}, under the voltammetric peak for the ferricyanide reduction as a function of the concentration of ferricyanide in the absorption solution.** (C) **Plot of the change of the charge under the voltammetric peak for the ferricyanide reduction (filled circles) as a function of time during diffusion of ferricyanide from the cotton fabric into a clean 0.1 M carbonate buffer solution. Lines are calculated based on equation 7.1 (see text).**

In Figure 7.3A a typical set of voltammograms is shown. The voltammetric response for ferricyanide can be observed to get weaker over a period of 20 minutes (see Figure caption).

Simultaneously, the colour of the cotton sample changes from yellow to white. Figure 7.3B shows a typical plot for the charge under the reduction peak observed during the first potential cycle and for a range of different $Fe(CN)_6^{3-}$ concentrations in the treatment solution. It can be seen that an approximately linear increase in the voltammetric signal occurs as the $Fe(CN)_6^{3-}$ concentration increases. Physically, this behaviour is consistent with a simple "trapping" effect. Solution phase together with cations and anions penetrates into the amorphous regions of the cellulose structure and remains within the cotton fiber (in amorphous cellulose) after drying. Based on the linear plot in Figure 7.3B no strong specific interaction of the $Fe(CN)_6^{3-}$ cation occurs (vide infra). The amount of $Fe(CN)_6^{3-}$ within the cotton is linearly proportional to the concentration of $Fe(CN)_6^{3-}$.

In order to further confirm this interpretation, elemental analysis for Fe in the cotton disc sample was performed and the charge corresponding to a complete conversion, Q_{max}, evaluated. The hypothetical maximum charge, Q_{max}, and the experimentally detectable charge, Q_{expt}, for the electron transfer process in Equation 7.3 have been plotted against concentration of $Fe(CN)_6^{3-}$ during absorption (see Figure 7.3B). As expected, the relationship for both Q_{max} and Q_{expt} is linear and approximately 30% of the $Fe(CN)_6^{3-}$ present in the cotton sample is converted with a scan rate of 10 mV s^{-1}. From the elemental analysis data the "average concentration" of $Fe(CN)_6^{3-}$ in the cotton disk (assuming a homogeneous disk of 270 μm thickness) is calculated to be 2.5 × higher compared to the aqueous solution concentration during immobilisation. This value suggests a weak accumulation effect.

Figure 7.3C shows the change of the charge under the voltammetric reduction response with "leaching time". A characteristic decay is observed and an approximate equation (see experimental, Equation 7.1) is employed to parameterize the data. If a thickness of the membrane, l = 270 μm, is assumed, an approximate diffusion coefficient can be obtained of $D_{Fe(CN)_6^{3-}} = 0.13 \times 10^{-9}$ m^2s^{-1}. This value is only slightly lower when compared to the diffusion coefficient for $Fe(CN)_6^{3-}$ in aqueous buffer solution, $D_{Fe(CN)_6^{3-}} = 0.5 \times 10^{-9}$ m^2s^{-1}, which is probably due (at least in part) to the reduced volume available for the diffusion process within the cotton fiber. This value has to be considered as very approximate because of the

combination of intra-fiber diffusion (assumed here) and inter-fiber diffusion (ignored in the model).

7.3.2. Electrochemical Reactivity of $[Ru(NH_3)_6]^{3+}$ Absorbed into Cotton and Immersed in Aqueous Buffer Solution

In order to explore the effect of charge of the ionic species diffusing within the cellulose matrix, the cationic $Ru(NH_3)_6^{3+/2+}$ redox system is employed. $Ru(NH_3)_6^{3+}$ is readily dissolved in aqueous 0.1 M carbonate buffer solution, but at pH 10 the metal complex is stable only for ca. 1-2 hours. Rotating disc voltammetry experiments were conducted and a one-electron reduction with a half wave potential of -0.25 V vs. SCE was observed (Equation 7.4). The diffusion coefficient for $Ru(NH_3)_6^{3+}$ in 0.1 carbonate buffer was determined as $D_{Ru(NH_3)_6^{3+}} = 0.44 \times 10^{-9}$ m^2s^{-1} (at 20 ^oC, data not shown).

Equation 7.4 $$Ru(NH_3)_6^{3+}(aq) + e^- \rightleftharpoons Ru(NH_3)_6^{2+}(aq)$$

When cotton discs treated with $Ru(NH_3)_6^{3+}$ were immobilised at the electrode surface and immersed in clean carbonate buffer solution, characateristic voltammetric responses were observed with a half wave potential of -0.25 V vs. SCE (see Figure 7.4A). The decay of the voltammetric signal with time is consistent with the leaching process. Figure 7.4B shows typical values for the charge under the reduction signal with time. Analysis of the diffusion process with equation 1 allows the diffusion coefficient for $Ru(NH_3)_6^{3+}$ within cotton to be estimated as $D_{Ru(NH_3)_6^{3+}} = 0.11 \times 10^{-9}$ m^2s^{-1}.

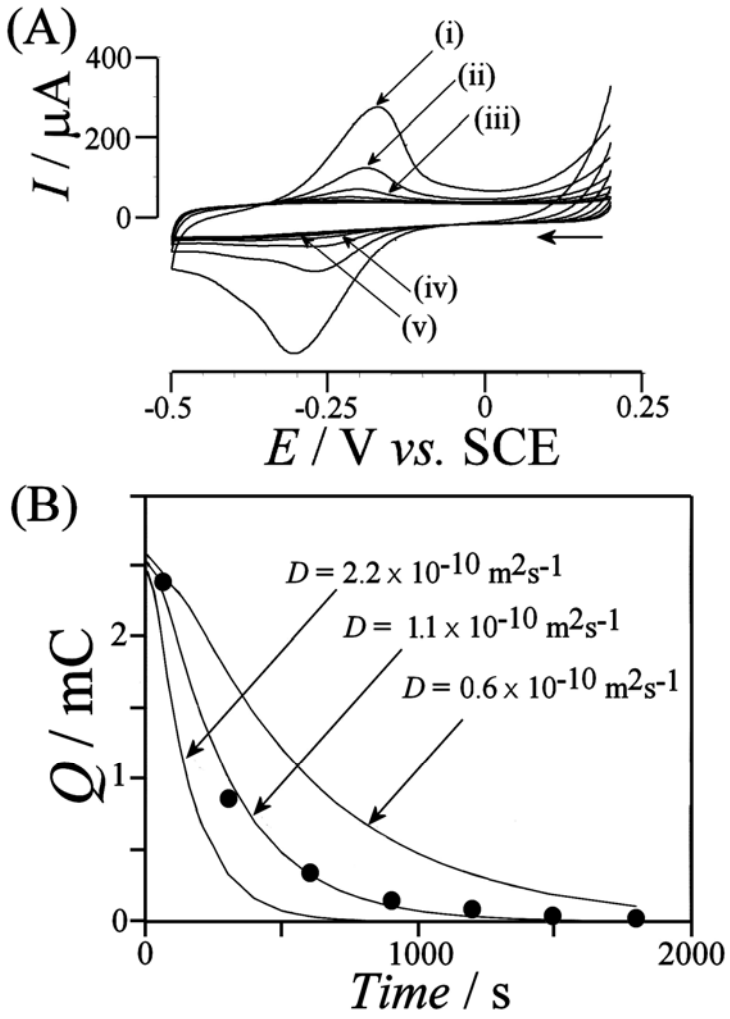

Figure 7.4 (A) **Cyclic voltammograms (scan rate 10 mV s^{-1}) for the reduction and re-oxidation of $Ru(NH_3)_6^{3+}$ (2) absorbed into a cotton fabric (absorption conditions 5 mM $Ru(NH_3)_6^{3+}$ in 0.1 M carbonate buffer pH 10, measurement time (i) 60s, (ii) 300s, (iii) 600s, (iv) 900s, and (v) 1200s after immersion of the cotton disc).** (B) **Plot of the change of the charge under the voltammetric peak for the $Ru(NH_3)_6^{3+}$ reduction (filled circles) as a function of time during diffusion of $Ru(NH_3)_6^{3+}$ from the cotton fabric into a clean 0.1 M carbonate buffer solution. Lines are calculated based on Equation 7.1 (see text).**

Both redox systems, $Fe(CN)_6^{3-}$ and $Ru(NH_3)_6^{3+}$ are highly hydrophilic and show very similar characteristics when immobilized into a cotton fabric. Adsorption for both types of ions appears to occur without strong specific interaction with the amorphous cellulose and the rate of diffusion for both ions within the amorphous cellulose appears to be similar (approximately one order of magnitude slower than in solution). Next, two redox systems with higher affinity to amorphous cellulose and their electrochemistry within the cellulose matrix are investigated.

7.3.3. Absorption and Electrochemical Reactivity of (N,N-bis(pyridin-2-yl-methyl)-1,1-bis(pyridin-2-yl)-1-aminoethane)chloro iron(II) [Fe(BBA)Cl]$^+$ in Cotton Immersed in Aqueous Buffer Solution

The metal complex $[Fe(BBA)Cl]^+$ (see Scheme Chapter 7:.1) is readily soluble in aqueous 0.1 M carbonate buffer at pH 10. The pale red solution is indefinitely stable under argon and stable for several hours in the presence of oxygen. The Fe(II) center in this metal complex is readily oxidized and rotating disc voltammograms have been recorded in order to characterize this process (see Figure 7.5A). The one-electron oxidation (see Equation 7.5) in solution occurs at a half wave potential of 0.0 V vs. SCE and the diffusion coefficient is determined as $D_{Fe(BBA)Cl^+} = 0.6 \times 10^{-9}\ m^2s^{-1}$.

Equation 7.5 $Fe(BBA)Cl^+(aq) \rightleftharpoons Fe(BBA)Cl^{2+}(aq) + e^-$

It is interesting to compare the results from rotating disc voltammetry studies in the absence and in the presence of cotton fabric samples at the electrode surface. Figure 7.5B shows voltammograms obtained in the same solution as those in Figure 7.5A. There are several effects of the cotton fabric on the voltammetric responses: (i) the magnitude of the mass transport controlled limiting currents is much reduced due to slow diffusion through the fabric, (ii) peak-shaped features are observed in addition to the sigmoidally shaped responses, and (iii) a new oxidation feature is observed as a peak at 0.5 V vs. SCE without significant contribution to the sigmoidally shaped anodic signal. Further quantitative analysis of this complex rotating disk voltammetric signal appears unwarranted.

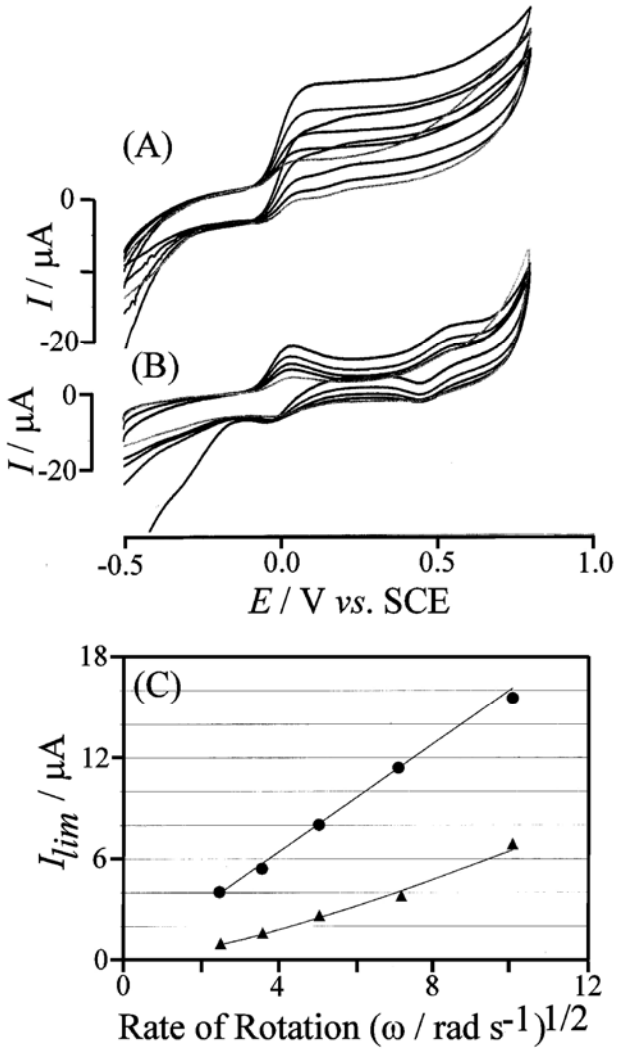

Figure 7.5 (A) **Cyclic voltmmograms (scan rate 10 mVs^{-1}) for the oxidation of 0.2 mM Fe(BBA)Cl^{+} (3) dissolved in aqueous 0.1 M carbonate buffer pH 10 obtained at a rotating 4.9 mm diameter graphite electrode at rotation speeds between 0 Hz and 16 Hz.** (B) **Cyclic voltammograms obtained under the same conditions as those in (A) but with a cotton disc immobilized at the electrode surface.** (C) **Plot of the mass transport controlled limiting current versus the square root of the rate of revolution ("Levich plot") demonstrating the diffusion effects in the absence (circles) and in the presence (triangles) of cotton textile.**

The observation of a new redox system in the presence of cotton (or cellulose) is suggesting a change in chemical behaviour of Fe(BBA)Cl^{+} in the cotton environment. The magnitude of the first voltammetric peak at 0.0 V vs. SCE indicates accumulation of Fe(BBA)Cl^{+} into the cotton fiber and the fact that the magnitude of the second voltammetric peak signal is similar suggests a follow-up redox process. Currently, the chemistry associated with the second redox system is not well understood and therefore the process is tentatively assigned to a second one-electron transfer or a dimer formation within the cotton matrix.

In order to investigate the accumulation and mobility of $Fe(BBA)Cl^+$ in cotton, further voltammetric experiments were conducted. Both "leaching" and absorption of $Fe(BBA)Cl^+$ into the cotton fabric occur and a quantitative study of the absorption process suggests a much slower rate of diffusion for this metal complex. Figure 7.6A shows typical voltammetric responses recorded with a 4.9 mm diameter basal plane pyrolytic graphite electrode with a cotton disc immobilized and immersed in stationary solution containing 0.1 mM $Fe(BBA)Cl^+$ in 0.1 M carbonate buffer pH 10. Initially, no significant voltammetric signal is observed and the characteristic double peak for $Fe(BBA)Cl^+$ only appears over a period of one hour. The slow uptake of $Fe(BBA)Cl^+$ from the solution into the cotton can be understood based on the diffusion model (see Figure 7.2) and based on equation 1. Theoretical lines indicated in the plot in Figure 7.6B have been obtained for $D_{Fe(BBA)Cl^+} = 2.5 \times 10^{-11}$ m^2s^{-1}. This suggests that the rate of diffusion is approximately a factor 24 slower when compared to that in aqueous solution.

In Figure 7.6C it can be seen that absorption of $Fe(BBA)Cl^+$ for a concentrations up to 10 mM obeys a Langmuir isotherm trend. When comparing the maximum charge based on elemental analysis, Q_{max}, to the electrochemically observed charge, Q_{expt}, a similar trends are observed and the binding constant $K = 500$ dm^3 mol^{-1} for $Fe(BBA)Cl^+$ on cotton can be estimated. During cyclic voltammetry with 10 mV s^{-1} scan rate approximately 12% of the $Fe(BBA)Cl^+$ within the cotton disc is electrolysed.

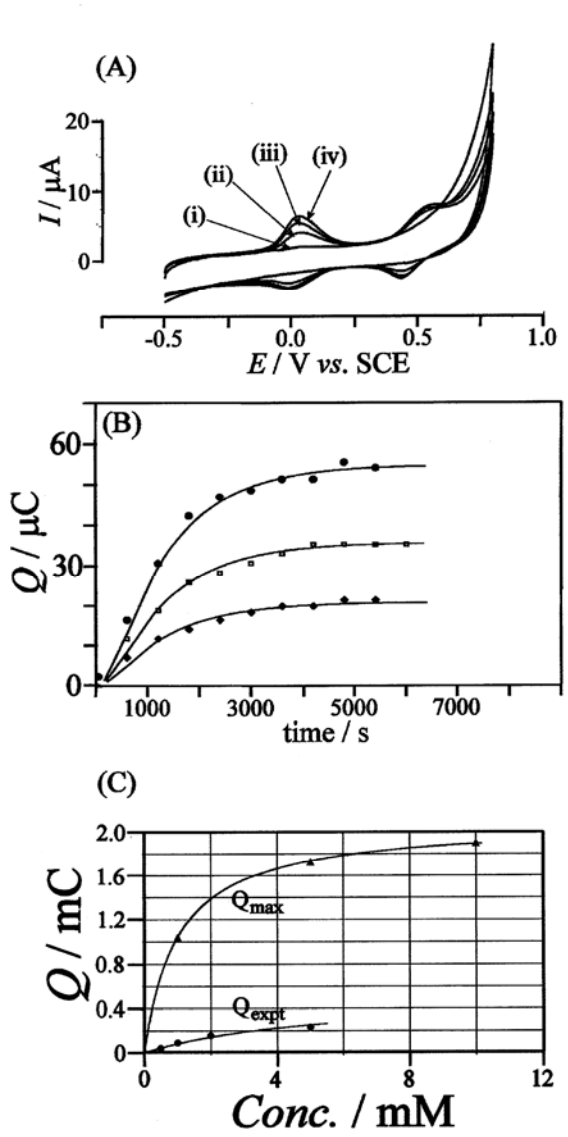

Figure 7.6 (A) Cyclic voltammograms (scan rate 10 mV s^{-1}) monitoring the absorption process for 0.1 mM $Fe(BBA)Cl^+$ at a 4.9 mm diameter basal plane pyrolytic graphite electrode with cotton disc immobilized and immersed in 0.1 M carbonate buffer pH 10. The absorption times are (i) 100s, (ii) 1200s, (iii) 2400s, and (iv) 4800s. (B) Plot of the charge under the anodic peak as a function of time during $Fe(BBA)Cl^+$ absorption from 0.1 mM, 0.05 mM, and 0.025 mM solutions. Lines have been fitted employing equation 1 and a diffusion coefficient of $D_{Fe(BBA)Cl^+} = 2.5 \times 10^{-11}$ m^2s^{-1}. (C) Langmuir plot for the amount of $Fe(BBA)Cl^+$ absorbed and electrochemically detected (Q_{expt}) or determined by elemental analysis (Q_{max}) as a function of concentration.

The $Fe(BBA)Cl^+$ redox system clearly demonstrates that (i) depending on the structure of metal complexes accumulation into cotton may occur, (ii) the (electro-)chemical behaviour of the metal complex in amorphous cellulose may differ from solution characteristics, and (iii) the mobility of species within the cellulose matrix is governed by the interaction with binding

sites. Next, the interaction of cotton with a further type of metal complex, hemin, with a negative charge is investigated.

7.3.4. Absorption and Electrochemical Reactivity of [(protoporphyrinato-IX)Fe(H_2O)(OH)]$^{2-}$ Hemin in Cotton Immersed in Aqueous Buffer Solution

Hemin forms dark green solutions in 0.1 M carbonate buffer at pH 10. The dark green colour has been attributed to the [(protoporphyrinato-IX)Fe(III)(H_2O)(OH)]$^{2-}$ complex anion which is formed by deprotonation of the parent di-aquo metal complex with a pK_A of 5.5 [18]. Hemin solubility is strongly pH dependent and even at pH 10, hemin is highly surface active (surface tension lowering) and tends to adsorb onto hydrophobic surfaces. Initial experiments were conducted with a solution of 0.5 mM Hemin in 0.1 M buffer and with a basal plane pyrolytic graphite electrode. Figure 7.7 shows typical rotating disc voltammograms indicating that both hemin reduction and hemin oxidation occurs in different potential zones.

Perhaps surprisingly, under rotating disc conditions the expected one-electron Fe(III/II) reduction of hemin (Equation 7.6) appears to give a peak-shaped response independent of the rate of electrode rotation whereas the anodic process shows the expected increase in current approximately linear with the square root of electrode rotation (see Figure 7.7C). The behaviour during reduction can be explained by an anodic deposition process involving hemin consistent with a recent report by Yang et al. [19] where the anodic "electropolymerisation" of hemin is proposed. After prolonged use of the basal plane pyrolytic graphite electrode, removal from the solution and rinsing, a strongly coloured blue film deposit is clearly observed. Therefore experiments were repeated (see Figure 7.7B) with a freshly polished electrode and avoiding potential positive of 0.2 V vs. SCE. In the resulting rotating disc voltammograms both the cathodic limiting current for hemin in solution (P1) and broad peak features probably for adsorbed hemin are observed. The limiting currents observed for the reduction when plotted versus the square root of the rotation rate (see "Levich" plot in Figure 7.7C) show a linear dependence and the approximate diffusion coefficient, $D_{hemin} = 0.5 \times 10^{-9}$ m^2s^{-1}, is calculated.

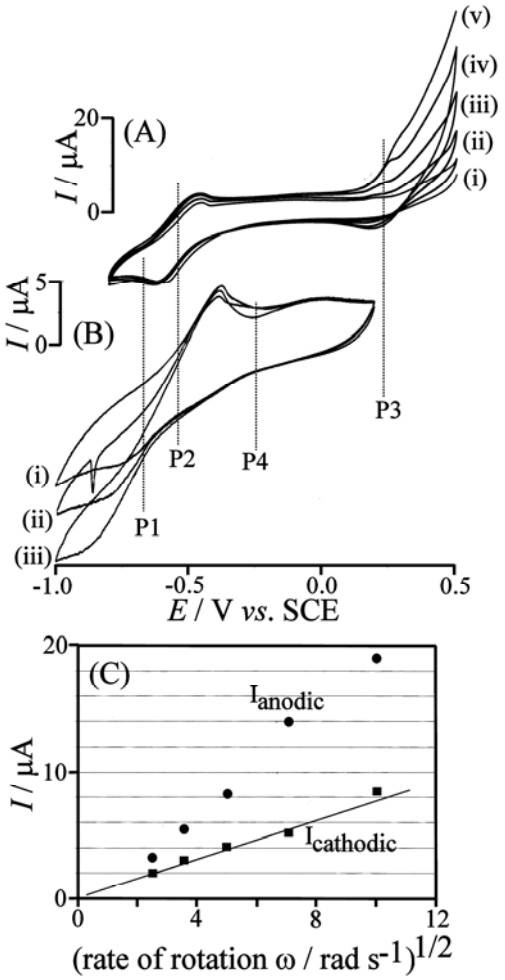

Figure 7.7 Cyclic voltammograms (scan rate 10 mV s^{-1}) obtained for the reduction of 0.5 mM hemin in 0.1 M carbonate buffer pH 10 at a rotating 4.9 mm diameter basal plane pyrolytic graphite electrode. (A) The potential is scanned from 0.5 V to -0.7 V vs. SCE with (i) 1 Hz, (ii) 2 Hz, (iii) 4 Hz, (iv) 8 Hz, and (v) 16 Hz rate of rotation. (B) The potential is scanned from +0.25 V to -1.0 V vs. SCE with (i) 1 Hz, (ii) 4 Hz, and (iii) 16 Hz rate of rotation. (C) Plot of the limiting current versus the square root of the rate of revolutions.

The voltammetric characteristics for hemin when explored over a wider potential window are relatively complex. The reduction at a fresh graphite electrode surface (P1) may be identified as a one-electron process based on a Fe(II/III) redox system (Equation 7.6).

Equation 7.6 P1: $[(\text{protoporphyrinato-IX})\text{Fe(III)}(H_2O)(OH)]^{2-} + e^- \rightleftharpoons [(\text{protoporphyrinato-IX})\text{Fe(II)}(H_2O)(OH)]^{3-}$

The anodic process (P3) appears to involve an overall two-electron process (Equation 7.7) and is causing the formation of a deposit at the electrode surface.

Equation 7.7 P3: $[(\text{protoporphyrinato-IX})\text{Fe(III)}(H_2O)(OH)]^{2-} \rightleftharpoons [(\text{protoporphyrinato-IX})\text{Fe(II)}(H_2O)(OH)]_{\infty} + 2\ e^-$

The resulting deposit at the graphite electrode surface is electrochemically active and observed as a highly reversible peak feature (P2) which is very likely to be based on a metal centered Fe(III/II) reduction. Finally, a further very weak voltammetric response (P4) can be observed at ca. -0.25 V vs. SCE and with a peak-to-peak separation of ca. 200 mV. This voltammetric response is much more pronounced in the presence of oxygen and it appears to correspond to an electro-catalytically active form of hemin adsorbed at the electrode surface.

The absorption of hemin into cotton was achieved by soaking cotton discs in solutions of various concentrations of hemin in aqueous 0.1 M carbonate buffer pH 10. The cotton discs were then dried between two filter papers under ambient conditions. When concentrations of 0.1 mM, 1.0 mM, and 10 mM hemin were used clearly different amounts of hemin were adsorbed onto the cotton sample as indicated by the variation in dark green colour of the cotton. UV/Vis reflectance spectroscopy was applied in order to characterize the samples. Absorbance peak features characteristic for $[(\text{protoporphyrinato-IX})\text{Fe(III)}(H_2O)(OH)]^{2-}$ were observed at 410nm and at 610 nm (consistent with literature spectra [20]). Absorption of hemin is likely to occur into the amorphous region of the cellulose.

Both slow "leaching" of the dark green hemin colour into clean buffer solution and the uptake of hemin from a hemin solution into a cotton sample occur and the absorption process is studied here in more detail. Figure 7.8A shows typical voltammograms obtained in stationary solution. A peak consistent with the presence of dioxygen entrapped in the cotton (P4) was observed initially but quickly decreased. An increasing reduction peak at ca. -0.6 V vs. SCE (P2) can be attributed to the absorption of hemin into the cotton textile.

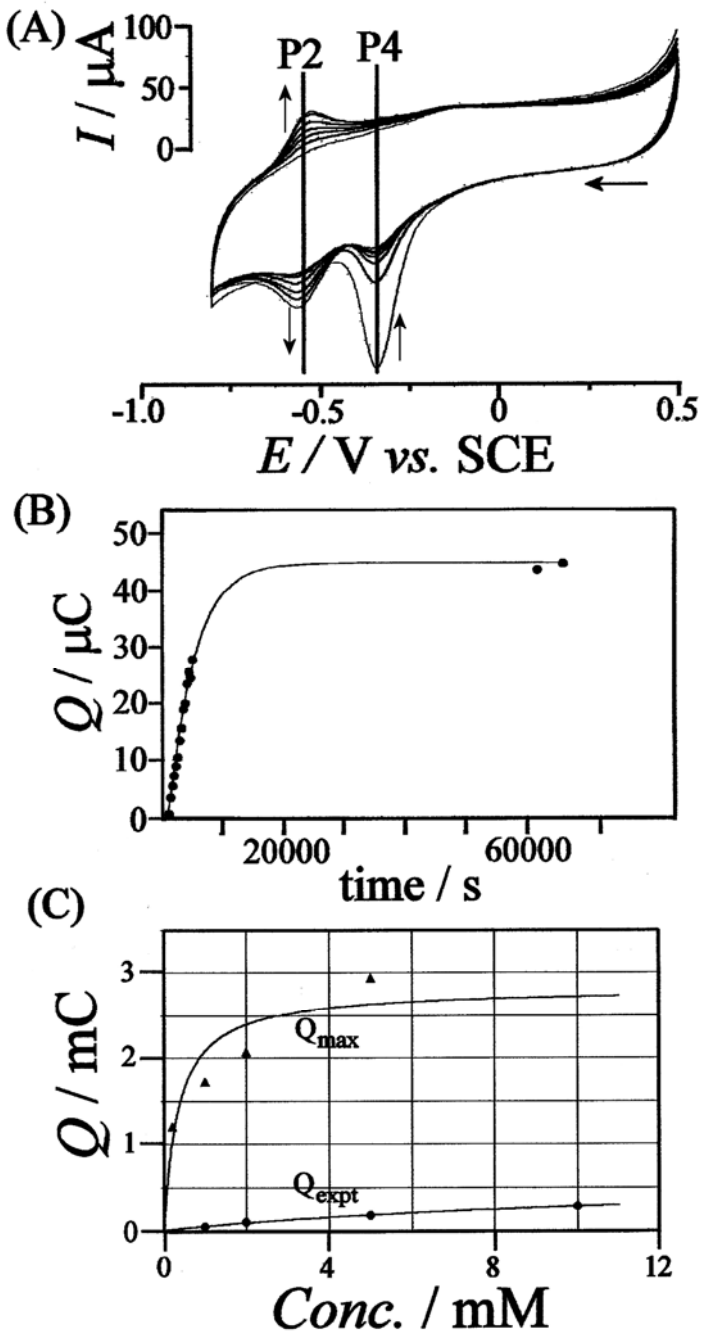

Figure 7.8 (A) **Cyclic voltammograms (scan rate 10 mV s^{-1}) for the reduction and re-oxidation of 0.1 mM hemin in aqueous 0.1 M carbonate buffer solution at pH 10. The 4.9 mm diameter basal plane pyrolytic graphite electrode had a clean cotton disc sample immobilized at the surface and the absorption of hemin into the cotton is monitored with time. Prior to immersion into the solution, the cotton sample was kept in argon atmosphere to minimize the amount of oxygen in the sample.** (B) **Plot of the charge under the hemin reduction response as a function of time.** (C) **Plot of the charge under the reduction signal for hemin absorbed into cotton (by soaking for 24h at different hemin concentrations) and immersed into 0.1 M carbonate buffer solution (pH 10).**

Figure 7.8C summarises data for the charge under the voltammetric peak Q_{expt} and for the maximum charge based on Fe elemental analysis, Q_{max}, as a function of hemin solution concentration. Hemin appears to absorb into cotton at lower concentrations and then further accumulate into cotton at higher concentration (possibly due to aggregation). The percentage of hemin electrochemically converted during potential sweeps is approximately 7%.

The uptake of hemin from the buffer solution into the cotton sample was relatively slow and a plot of the charge under the reduction peak versus time is shown in Figure 7.8B. The solid line has been calculated based on Equation 7.1 with an estimated diffusion coefficient $D_{hemin} = 0.7 \times 10^{-11}$ m^2s^{-1}. That is, the rate of diffusion of hemin within the cotton material is approximately by a factor 70 slower compared to that in solution. Table 7.1 summarises the results obtained for different redox systems.

Table 7.1 Diffusion coefficients in 0.1 M carbonate buffer pH 10 at 20±2 ^oC determined in solution (by rotating disc voltammetry) and within cotton samples (by monitoring voltammetric responses with time).

Metal complex	**In solution:** [a] **D / m^2s^{-1}**	**In cotton:** [b] **D / m^2s^{-1}**	**$D_{solution}/D_{cotton}$**
$Fe(CN)_6^{3-}$	0.50×10^{-9}	0.13×10^{-9}	4
$Ru(NH_3)_6^{3+}$	0.44×10^{-9}	0.11×10^{-9}	4
$Fe(BBA)Cl^{+}$	0.60×10^{-9}	0.25×10^{-10}	24
Hemin	0.50×10^{-9}	0.70×10^{-11}	70

[a] obtained from the analysis of rotating disc voltammetry data and by employing the Levich expression.

[b] obtained from the analysis of the time dependence of diffusion into or out of cotton disc samples and the approximate diffusion model resulting in Equation 7.1.

7.4. Conclusions

It has been shown that processes within cotton (cellulose) can be monitored with relatively simple voltammetry experiments. Information about (i) the uptake and binding of metal complexes into the cellulose matrix, (ii) the mobility and rate of diffusion, (iii) and chemical

reactivity within the amorphous cellulose environment has been obtained. The procedure based on graphite flakes applied to a cotton textile sample is highly reproducible and versatile. In future this methodology could be applied for a wider range of redox systems and under varying conditions (textile pre-treatment, solution pH, composition, and temperature) to provide information about the chemical processes within cotton and other textiles. Although providing a range of important insights, the methodologies developed and employed here remain more qualitative than quantitative. In future, better experimental and data analysis approaches (for example by comparing leaching out and absorption processes) will be required in order to address more complex questions concerning the mechanism of processes and to overcome problems with the heterogeneity of samples.

7.5. References

[1] P. John, "Biosynthesis of the major crop products", *Wiley, New York*, **1992**, p.76.

[2] H.A. Krässig, "Cellulose", *Gordon and Breach Science Publishers, Amsterdam,* **1993**, p.70.

[3] A.C. O'Sullivan, *Cellulose* 4 **1997**, 173.

[4] C. Woodings, "Regenerated cellulose fibers", *CRC Press, Cambridge*, **2000**.

[5] F. Scholz, "Electroanalytical methods", *Springer, Berlin,* **2002**.

[6] P. Westbroek, G. Priniotakis, P. Kiekens, "Analytical electrochemistry in texiles", *Woodhead Publishing Ltd., Cambridge,* **2005**.

[7] R. Hage, A. Lienke, *Angewante Chemie International Edition* 44, **2005**, 2.

[8] T. Lötzbeyer, W. Schuhmann, H.L. Schmidt, *Journal of Electroanalytical Chemistry* 395, **1995**, 341.

[9] Q.X. Yang, G.L. Gao, X.L. Wang, *Acta Physica Chimica Sinica* 16, **2000**, 741.

[10] D.L. Compton, J.A. Laszlo, *Journal of Electroanalytical Chemistry* 520, **2002**, 71.

[11] Y. Gao, J. Chen, *Journal of Electroanalytical Chemistry* 578, **2005**, 129.

[12] See for example S. Yabuki, F. Mizutani, Y. Hirata, *Electrochemistry* 71, **2003**, 408.

[13] See for example L.N. Grinberg, P.J. O'Brien, Z. Hrkal, *Free Radical Biological*

Mediation 27, **1999**, 214.

[14] A.G. de la Rosa, E. Castro-Quezada, S. Gutierrez-Granados, F. Bedioui, A. Alatorre-Ordaz, *Electrochemical Communications* 7, **2005**, 853.

[15] M.T. de Groot, M. Merkx, A.H. Wonders, M.T.M. Koper, *Journal of the American Chemical Society* 127, **2005**, 7579.

[16] J. Crank, "The mathematics of diffusion", *Oxford University Press, Oxford* **2004,** p. 53.

[17] See for example C.M.A. Brett, A.M.O. Brett, "Electrochemistry, principles, methods, and applications", *Oxford University press, Oxford,* **1993**.

[18] S. Mazumdar, O. K. Medhi, S. Mitra, *Inorganic Chemistry* 27, **1988**, 2541.

[19] Q.X. Yang, G.L. Gao, X.L. Wang, *Acta Physica Chimica Sinica* 16, **2000**, 741.

[20] S. Mazumdar, O.K. Medhi, S. Mitra, *Inorganic Chemistry* 27, **1988**, 2541.

Chapter 8: Cellulose Material Electrodes II

Catalase Absorption & Reactivity in Cotton

8.1. Introduction

Voltammetric measurements have been generally employed throughout this thesis to provide information about heterogeneous systems e.g. solids in contact with electrolyte solutions [1]. In this chapter voltammetric measurements are employed to investigate processes at the solid – liquid interface for cotton in contact with aqueous electrolyte. More specifically, I aim to explore the redox properties and catalase reactivity of metal complexes when adsorbed onto or into the cotton (or cellulose-I) material and in contact with hydrogen peroxide. This technique would provide precursory information about catalytic activity occurring within cotton materials during laundry processes.

Conventional voltammetric experiments with redox active materials dissolved in the solution phase rely on planar diffusion to and from the electrode surface (see Figure 8.1A) whereas processes at solid surfaces, e.g. a cotton surface, immobilized at an electrode surface are mechanistically more complex (see Figure 8.1B). For cotton fibers in contact with an electrode, heterogeneous electron transfer is limited to regions of direct contact and diffusion processes are possible both "inter-fiber" (in pores and spaces in between fibers) and "intra-fiber" (within amorphous regions in the cellulose-I structure [2], see Figure 8.1B). The experiments designed in chapter 7 are repeated here to explore electrochemical processes at cotton surfaces and within the cotton material by applying a graphite flake coating to the textile in contact with the electrode (see Figure 8.1C). The graphite flakes minimize the effects of inter-fiber diffusion and allow processes within the cotton material to be observed in situ (e.g. the absorption and reactivity of metal complexes with catalase or bleaching activity) as a function of the aqueous buffer environment or as a function of time. The direct electrochemical contact between graphite flakes and cotton is demonstrated.

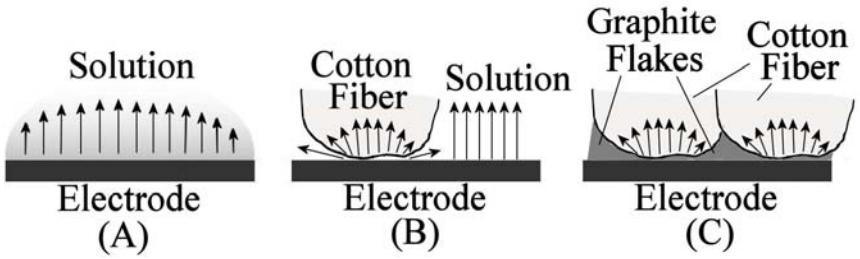

Figure 8.1 Schematic representation of electrochemical processes at (A) **an electrode in solution and** (B) **an electrode in contact with a cotton fiber in solution. Arrows indicate possible pathways for diffusion e.g. "inter-fiber" and "intra-fiber" diffusion. In** (C) **the contact between electrode and cotton has been optimized with graphite flakes.**

Cotton is a natural product formed from relatively pure cellulose-I microfibrils packed to give a structure with crystalline (ca. 60%, ca. 7-9 nm crystal size) and amorphous regions [3]. Cotton has excellent adsorbent properties due to the amorphous regions. Modified cotton has been used, for example, for the removal of toxic metal ions from water [4]. When immobilized at the electrode surface, cotton acts as an electrical insulator. However, the ability of cotton to adsorb molecules and ions from solution creates ionic conductivity. In this chapter cotton fabric is immobilized at a graphite electrode and the interwoven fibers are shown to partially block and limit access to the electrode surface. The adsorption of redox active materials onto the cotton surface (and into the cellulose fibers) results in characteristic current responses with kinetic and thermodynamic information about binding and reactivity. It is shown that voltammetric methods are highly sensitive and allow even small amounts of absorbates to be detected and monitored. Changes in molecular reactivity upon absorption from the solution phase into the cotton material are observed.

Bleaching, peroxidase-, or catalase-type processes are observed when peroxo-intermediates are activated to result in oxygen transfer [5], radical processes [6], or simply peroxide dismutation [7]. Reactive intermediates formed during peroxide activation attack and de-colorize dyes or organic matter [8]. A wide range of catalysts (often based on iron, copper, or manganese metal complexes) for this type of processes exists in nature [9,10,11] or has been developed specifically for technical processes [12]. Here, a well known dinuclear manganese complex, Wieghardt's $[Mn(IV)_2(\mu\text{-}O)_3L_2](PF_6)_2$ with L = 1,4,7-trimethyl-1,4,7-triazacyclononane [13,14,15] (see Structure), which may be considered as a mimic of an

important family of naturally occuring di-nuclear manganese complexes [16,17] is employed to demonstrate catalase activity and voltammetric measurements at cotton surfaces immersed in aqueous buffer media.

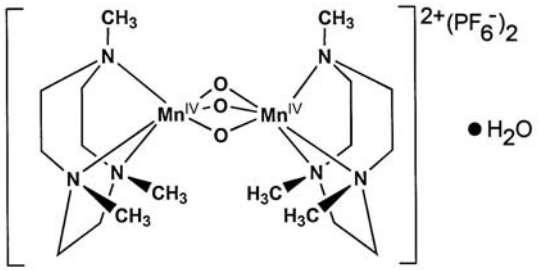

Figure 8.2 Structure of$[Mn(IV)_2(\mu\text{-}O)_3L_2](PF_6)_2$ (with L = 1,4,7-trimethyl-1,4,7-triazacyclononane)

The metal complex $[Mn(IV)_2(\mu\text{-}O)_3L_2](PF_6)_2$ has been demonstrated to act as a precursor for a family of highly active epoxidation [18,19], alkane oxidation [20], cis-dihydroxylation [21], and bleaching catalysts [22]. The catalytic activity of this relatively inert di-manganese precursor complex has been demonstrated to depend on co-catalysts (such as acetate [23]) and to require an initial reduction step by one [24] or two electrons [25]; the latter mechanism proposes that the resulting fluxional Mn(III) species enters into a catalytic cycle. In electron spin resonance [26,27] and electro-spray mass spectrometry experiments [28] the one electron reduced $[Mn(III)Mn(IV)(\mu\text{-}O)_3L_2]^+$ cation has been identified. The composition of the reaction mixture, e.g. the presence of carboxylate anions [23] strongly affects the oxygenation chemistry. Equilibria involving monomeric and tetrametric manganese complexes (formed for example in aqueous solutions of Mn^{2+} salts and triazacyclononane ligands) have been shown to cause dramatic changes in reactivity towards hydrogen peroxide [29].

In this chapter, the electrochemistry of cotton textile surfaces immersed in aqueous buffer media is investigated by voltammetric methods. Different types of redox systems are employed to interact with the cotton and voltammetric measurements are undertaken in stagnant solution and under rotating disc conditions. It is shown that voltammetry provides new powerful tools for the study of the surface chemical processes at cotton surfaces and within cotton textiles. Changes in reactivity of the $[Mn(IV)_2(\mu\text{-}O)_3L_2](PF_6)_2$ metal catalyst system in the presence and in the absence of cotton suggest an active part of cellulose matrix in the catalytic process.

8.2. Experimental

8.2.1. Reagents

Chemical reagents such as Na_2CO_3, $NaHCO_3$, KCl, $K_4Fe(CN)_6$, and graphite powder (1-2 micron) were obtained from Aldrich and used without further purification. $[Mn(IV)_2(\mu\text{-}O)_3L_2](PF_6)_2$ was provided by Unilever Research and Development, Port Sunlight, UK. Demineralised and filtered water was taken from an Elgastat water purification system (Elga, High Wycombe, Bucks) with a resistivity of not less than 15 MOhm cm. Cotton samples (Phoenix Calico, US) were woven, bleached, non-fluorescent, non-desized (not washed to remove any residuals), and non-mercerized.

8.2.2. Instrumentation

For voltammetric studies, a microAutolab II potentiostat system (EcoChemie, Netherlands) was employed with a Pt gauze counter electrode and a saturated Calomel (SCE) reference electrode (Radiometer, Copenhagen). The working electrode was a 4.9 mm diameter basal plane pyrolytic graphite electrode ("Pyrocarbon", Le Carbone UK). An Agar sputter coating unit was employed for platinum coating. A sputter duration of 6s was chosen to deposit approximately 500 ng onto the 5.2 mm diameter cotton fabric disc. Scanning electron microscopy (SEM) images were obtained with a JEOL JSM6310 system. Experiments were conducted after de-aerating with high purity argon (BOC) for at least 15 minutes. The temperature was 22 ± 2 ^oC.

8.2.3. Procedures

Standard cotton discs (Phoenix Calico, US) of ca. 5.2 mm diameter and 0.27 mm thickness were cut from fabric and stored in a closed container at 4 ^oC. Prior to electrochemical experiments, graphite powder (Aldrich, 1-2 micron flakes) was applied to one side of the cotton disc (the surface was fully covered to give a shiny graphite surface) which is then placed in contact with a 4.9 mm diameter basal plane pyrolytic graphite electrode and immobilized with a coarse Lycra^{TM} membrane. Prior to immersion into the aqueous phase the cotton modified electrode was kept in an atmosphere of argon (ca. 10 minutes) to remove

residual oxygen from within the cotton fibers. In order to modify the cotton surface, two strategies were followed. A high surface loading was achieved by soaking in 3.5 mM solution of catalyst in demineralised water, 24h drying, rinsing with water, and further drying. A more controlled surface loading was achieved by 30 minute soaking in catalyst solution (a suitable concentration of catalyst dissolved in 0.1 M carbonate buffer at pH 9.8) followed by removal of excess liquid by pressing between filter papers and drying.

8.3. Results and Discussion

8.3.1. Voltammetric Measurements in the Absence and in the Presence of Cotton

In order to investigate the electrochemistry of cotton surfaces, an electrically conducting contact to a suitable substrate electrode has to be achieved. Here, graphite "flakes" were directly applied to the cotton surface. The resulting modified surface was then immobilized in contact with the surface of a 4.9 mm diameter basal plane pyrolytic graphite disc electrode. SEM images in Figure 8.3 show the cotton surface before and after impregnation with graphite flakes. In Figure 8.2A the texture of the cotton surface can be seen as consisting of fibers (composed of microfibrils) with approximately 20 μm diameter. Figure 8.3B shows the cotton surface with small graphite particles (1 to 2 μm) immobilized. The extent of the graphite – cotton interaction is important in order to achieve a good and reproducible voltammetric signal. The graphite layer applied to the cotton surface allows molecules absorbed into the cotton to be detected by direct electrochemistry (*vide infra*).

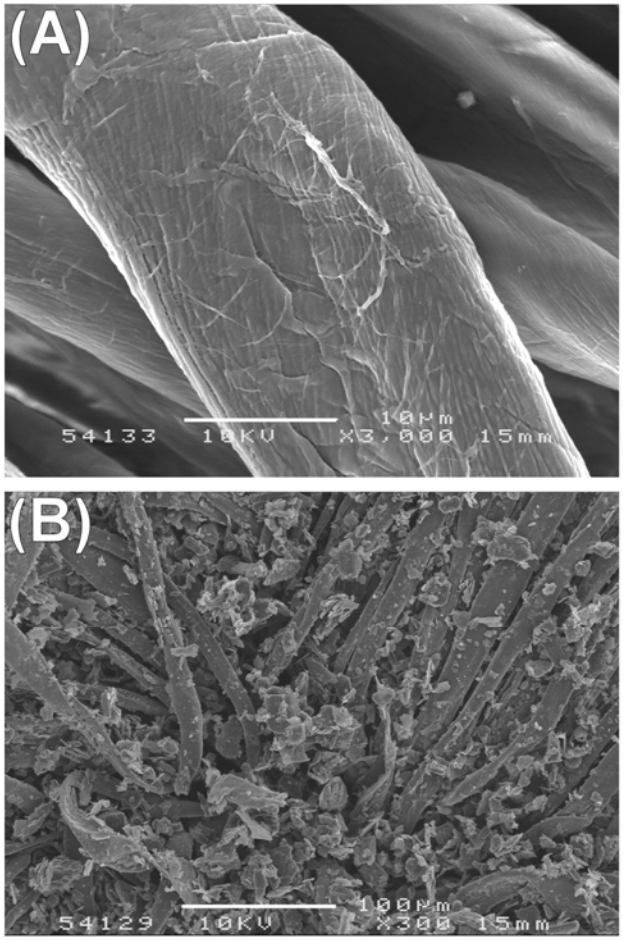

Figure 8.3 SEM images of (A) **a cotton fiber surface (scale bar 10 µm) and** (B) **cotton modified with graphite flakes of ca. 1-2 µm size (scale bar 100 µm).**

In order to assess the rate of diffusion through these cotton samples, rotating disc voltammetry experiments were conducted. The $Fe(CN)_6^{4-}$ redox system (see Equation 8.1) was chosen as a model system and initially, data was recorded in the absence of cotton. Next, a (graphite-modified) cotton disc was immobilized at the electrode surface and another set of voltammograms were recorded.

Equation 8.1 $$Fe(CN)_6^{4-} \rightleftharpoons Fe(CN)_6^{3-} + e^-$$

Figure 8.4 shows typical current data and a plot of the measured limiting currents versus the square root of the rotation rate ("Levich plot"). The "Levich" equation (Equation 8.2) describes the mass transport controlled limiting current as a function of the rate of rotation of the electrode.

Equation 8.2

$$I_{\lim} = 0.62nFAD^{2/3}\omega^{1/2}v^{-1/6}c$$

In this equation, the transport limited current, I_{lim}, is related to the number of electrons transferred per molecule diffusing to the electrode surface, n, the Faraday constant, F, the diffusion coefficient, D, the rate of electrode rotation, ω (in rad s^{-1}), the kinematic viscosity, v, and the concentration of redox active species, c. In Figure 8.4C, it can be seen that the currents obtained at the bare electrode result in a straight line plot and a theoretical line (dotted line, see Figure 8.4C) is consistent with the literature diffusion coefficient [30] for $Fe(CN)_6^{4-}$, $D_{Fe(CN)_6^{4-}} = 6.7 \times 10^{-10}$ m^2s^{-1}.

In the presence of the cotton disc a much reduced current is recorded due to the lower rate of mass transport across the cotton membrane. Two distinct transport zones can be observed:

Zone 1: for a rate of rotation up to approximately 25 rad s^{-1} a current plateau is reached with ca. 20 μA (see dashed line) and this behaviour is consistent with a stagnant solution and a membrane diffusion limited current. From the Nernst diffusion equation, $I_{membrane} = nFDAc \times \delta^{-1}$, the apparent diffusion layer thickness δ = 120 μm is obtained.

Zone 2: for a higher rate of rotation, the convection process is penetrating further into the porous cotton material and the apparent diffusion layer thickness is decreasing. Therefore the current observed at higher rates of rotation is increased.

With these calibration measurements, a quantitative understanding of the rate of mass transport across the immobilized cotton membrane can be obtained. However, the $Fe(CN)_6^{3-/4-}$ redox system is highly water soluble and measurements under these conditions are likely to probe predominantly "inter-fiber" diffusion. Current peaks observed in the presence of cotton are indicative of both a film of stagnant solution and some "intra-fiber" diffusion (*vide infra*).

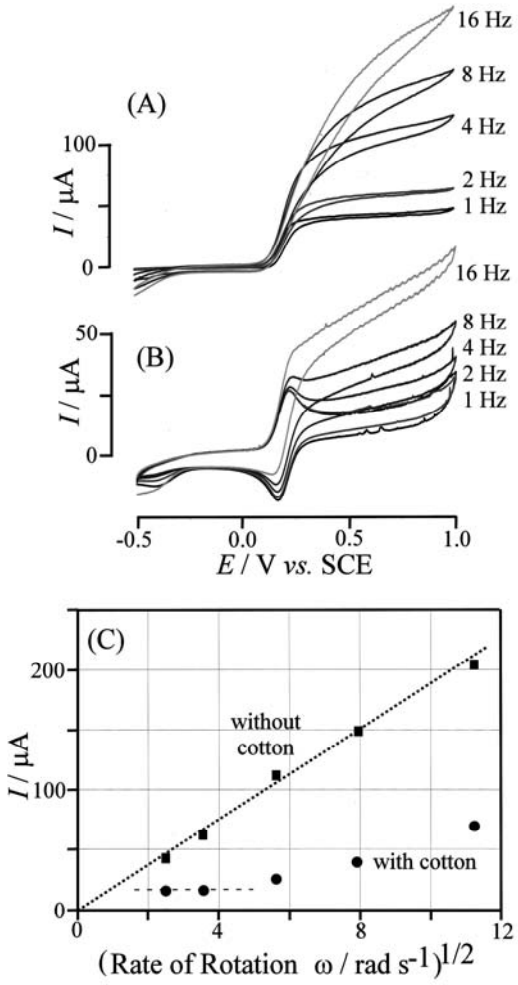

Figure 8.4 Cyclic voltammograms (scan rate 10 mV s^{-1}) obtained at a rotating 4.9 mm diameter graphite electrode immersed in 2 mM $Fe(CN)_6^{4-}$ in aqueous 0.1 M KCl (A) without and (B) with a cotton disc immobilized at the electrode surface. (C) Levich plot of the current versus the square root of the rotation rate. All limiting currents are measured by taking the current reading at 1 V *vs.* SCE.

8.3.2. Voltammetric Measurements at Platinum Modified Cotton Surfaces

The investigation of catalase activity of metal complexes can be based on their electrochemical response in the presence of peroxides. Recently, platinum has been suggested as a highly active model system for heterogeneous catalase activity [31]. Although important differences in mechanism exist, the ability to react with peroxide to give highly reactive intermediates is important in all catalase, oxygenase, or Fenton-type processes. In order to appraise the general effectiveness of a catalyst immobilized at the cotton surface, platinum metal clusters (ca. 500 ng on a 5.2 mm diameter cotton disc) sputter coated onto the fabric are

used. Platinum sputter-coated onto cotton shows excellent adhesion and no sign of transfer or removal for example when scratched with a spatula.

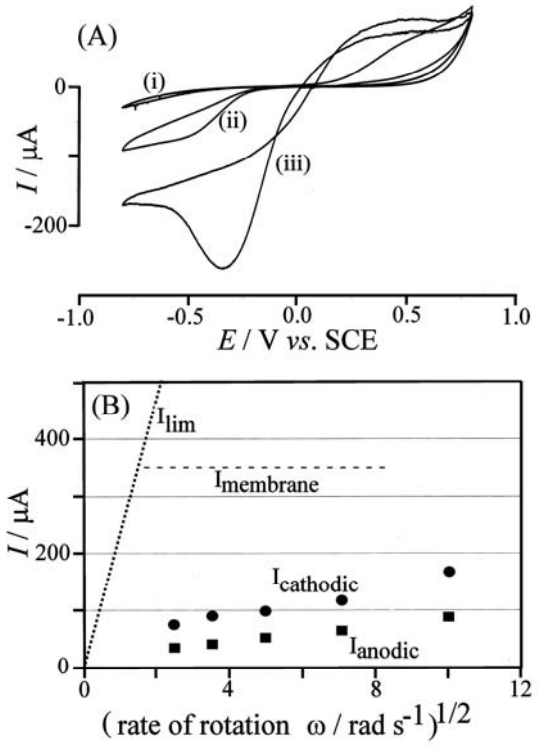

Figure 8.5 (A) Cyclic voltammograms (scan rate 10 mVs^{-1}) obtained under rotating disc conditions (100 rad s^{-1}) in 8 mM H_2O_2 in aqueous 0.1 carbonate buffer pH 9.8 for (i) a 4.9 mm diameter graphite electrode, (ii) a 4.9 mm diameter graphite electrode with cotton disc, and (iii) a 4.9 mm diameter graphite electrode with platinum modified cotton disc. (B) Levich plot for voltammetric data (scan rate 10 mVs^{-1}) obtained in 8 mM H_2O_2 in aqueous 0.1 carbonate buffer pH 9.8 at a 4.9 mm diameter rotating graphite electrode with a platinum modified cotton disc. The dotted line labeled I_{lim} indicates the expected current response (equation 8.2) at bare graphite and the dashed line labeled $I_{membrane}$ shows the current response consistent with the diffusional behaviour of $Fe(CN)_6^{4-}$ (see text).

First, the effect of cotton (alone) and of catalyst doped cotton on the electrochemical response for hydrogen peroxide are demonstrated. Figure 8.5 shows cyclic voltammograms obtained at a rotating disc (100 rad s^{-1}) and in the presence of 8 mM H_2O_2. The current response at a bare graphite electrode is negligible (curve i) and consistent with a very high overpotential for both the oxidation of H_2O_2 to O_2 and the reduction of H_2O_2 to water. With a cotton disc immobilized at the electrode surface, two interesting features are observed (see curve ii). A weak oxidation response is registered commencing at 0.3 V vs. SCE. Upon scanning to negative potentials, also a weak cathodic process consistent with the reduction of hydrogen

peroxide is observed. Both anodic and cathodic processes remain when the cotton sample is carefully lifted from the graphite surface leaving behind the imprinted graphite flake surface. Therefore, these weak anodic and cathodic processes are assigned to electrocatalytic activity at graphite flake edges rather than to pure cotton containing significant amounts of catalytic metal impurities in the natural fiber.

Next, with a small amount of platinum (ca. 500 ng on a 5.2 mm diameter disc) sputter coated onto the cotton surface, a powerful catalyst is available and the catalytic currents are clearly observed. An oxidation current (Figure 8.5, curve iii) is observed which at 0.0 V vs. SCE immediately changes into a cathodic steady state current response. An additional peak feature observed at -0.35 V vs. SCE can be identified as oxygen reduction due to oxygen diffusing through the cotton fiber interior after being formed during the anodic process. In these experiments, a simple transfer of platinum from cotton to graphite can be ruled out based on additional experiments. Rubbing the platinum modified cotton surface onto basal plane pyrolytic graphite did not result in catalytic activity of the electrode surface and a graphite flake surface carefully lifted from a platinum coated cotton sample did not show any sign of platinum activity on the imprinted surface. The graphite flake contact to the cotton surface must be intimate and electron transfer must be occurring directly to the modified cotton surface. These experiments clearly demonstrate the ability of electrochemistry to detect catalytic activity for surface immobilized catalysts on cotton and a more quantitative analysis of these data is possible when both the H_2O_2 concentration and the rate of rotation are varied.

Currents for oxidation and for reduction of hydrogen peroxide both scale linearly with concentration and increase upon increasing mass transport (the rate of rotation). Figure 8.5B shows plots of voltammetric data obtained for variable rotation rates and the effect of mass transport on both the anodic and cathodic limiting currents. Analysis by comparison with the theoretical limiting currents (350 μA membrane current expected in Zone 1, see dashed line, compare with Figure 8.4, using $D_{H_2O_2} = 1.46 \times 10^{-9}$ m^2s^{-1} [32]) expected for full conversion suggests that the process is limited by a diffusion process different to that observed for the $Fe(CN)_6^{4-}$ oxidation process (*vide supra*). H_2O_2 has to diffuse into the reaction zone where the graphite electrode is in contact with the cotton. The fact that the cathodic current is increased

when compared to the anodic current may be attributed to residual oxygen. Most important (a "benchmark") for this study is the anodic limiting current for the oxidation of 8 mM H_2O_2 at the platinum catalyst at a 100 rad s^{-1} rate of rotation which is ca. 90 μA (see Figure 8.4B). It will be shown below that this value may be considered as the diffusion limited current for hydrogen peroxide diffusion into the reaction zone independent of the catalyst system studied.

8.3.3. Voltammetric Measurements with $[Mn(IV)_2(\mu\text{-}O)_3L_2](PF_6)_2$ Modified Cotton

The dinuclear manganese complex $[Mn(IV)_2(\mu\text{-}O)_3L_2](PF_6)_2$ has been well studied as a precursor to catalytic processes [33] and proposed as a reagent to achieve bleaching [26], epoxidation [34] and similar types of oxygenation processes [29] Here, the $[Mn(IV)_2(\mu\text{-}O)_3L_2](PF_6)_2$ metal complex is shown to strongly interact with cotton (cellulose-I) surfaces and to change reactivity upon adsorption. The two Mn(IV) metal centers in this complex are known to undergo facile reduction to dinuclear Mn(IV)Mn(III) (this complex has been observed with a characteristic 16-line EPR signal) and Mn(III)Mn(III) (the III/III species is implied, not shown directly) systems [28]. Phenols, ascorbate, or catechols in aqueous environments trigger the facile reduction process and thereby initiate the catalytic activity [26].

In order to further characterize the redox properties of the $[Mn(IV)_2(\mu\text{-}O)_3L_2](PF_6)_2$ metal complex, initially conventional rotating disc voltammograms were recorded. Figure 9.5 shows typical voltammograms obtained for a solution of 0.2 mM $[Mn(IV)_2(\mu\text{-}O)_3L_2](PF_6)_2$ in 0.1 M carbonate buffer pH 9.8 at different rates of rotation (A) at a bare graphite electrode and (B) at a cotton modified graphite electrode. A well-defined reduction response is observed with a half wave potential of ca. 0.04 V vs. SCE. Data analysis based on Equation 8.2 and plotting the limiting current data versus the square root of the rotation rate allows the diffusion coefficient for $[Mn(IV)_2(\mu\text{-}O)_3L_2](PF_6)_2$, $D_{MnMn} = 0.6 \times 10^{-9}$ m^2s^{-1}, to be determined (assuming a two electron reduction). This value is in good agreement with a hydrodynamic radius of ca. 0.5 nm expected for the molecular structure of the dimer (employing the Stokes Einstein expression [35] $D = \frac{kT}{6\pi\eta r}$). Varying the pH of the buffer solution between 9.5 and 12.5 results

in a linear shift of the half wave potential of ca. 59 mV per pH unit (not shown) which implies a 2-electron reduction accompanied by fast uptake of two protons. The presence of a peak feature at slower rates of rotation (see Figure 8.6A) suggests some adsorption from the aqueous phase directly onto graphite.

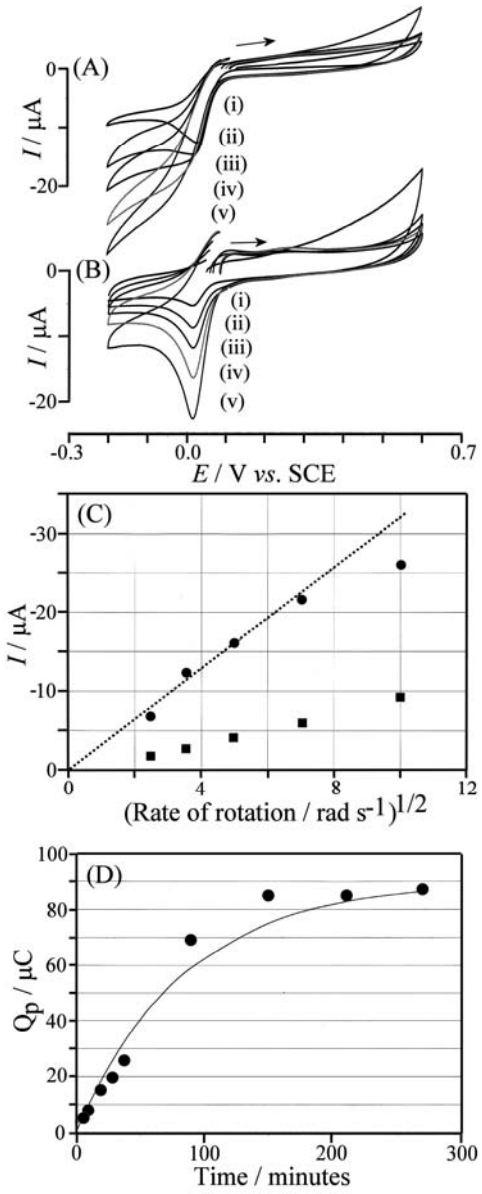

Figure 8.6 Cyclic voltammograms (scan rate 10 mVs^{-1}) obtained for the reduction of 0.2 mM $[Mn(IV)_2(\mu\text{-}O)_3L_2](PF_6)_2$ in 0.1 M carbonate buffer pH 9.8 at (A) **a rotating 4.9 mm diameter graphite electrode and** (B) **a rotating cotton modified graphite electrode with (i) 6.2, (ii) 12.5, (iii) 25, (iv) 50, and (v) 100 rad s^{-1} rate of rotation.** (C) **Levich plot of the limiting current versus the square root of the rate of rotation. Data are shown obtained without (circles) and with (squares) cotton. The dotted line shows the theoretical curve for a diffusion coefficient $D_{MnMn} = 0.6 \times 10^{-9}$ m^2s^{-1}. All limiting currents are measured by taking the current reading at -0.2 V *vs.* SCE** (D) **Plot of the charge under the reduction peak versus time for a clean cotton disc immobilized at a graphite electrode and immersed into 0.2 mM $[Mn(IV)_2(\mu\text{-}O)_3L_2](PF_6)_2$ in aqueous 0.1 carbonate buffer pH 9.8 without agitation.**

Rotating disc voltammetry experiments conducted with a cotton disc immobilized onto the graphite electrode surface show considerably diminished current responses (see Figure 8.6B and C) consistent with results observed for ferrocyanide oxidation (*vide supra*). The cotton seems to act as a membrane slowing down (inter-fiber) transport of $[Mn(IV)_2(\mu\text{-}O)_3L_2](PF_6)_2$ towards the electrode surface. However, the cathodic current peak suggests some intra-fiber diffusion and accumulation of $[Mn(IV)_2(\mu\text{-}O)_3L_2](PF_6)_2$ within the cotton. Adsorption of $[Mn(IV)_2(\mu\text{-}O)_3L_2](PF_6)_2$ onto graphite is also possible but less likely in the presence of the competing absorber cotton. In order to investigate the nature of interaction between $[Mn(IV)_2(\mu\text{-}O)_3L_2](PF_6)_2$ metal complex and cotton, additional experiments in stagnant solution were conducted.

Figure 8.6D demonstrates the effect of time on the integrated charge response (derived from the peak current) for a fresh cotton disc immobilized onto the graphite electrode and immersed in a solution of 0.2 mM $[Mn(IV)_2(\mu\text{-}O)_3L_2](PF_6)_2$. It can be seen that the peak current for the reduction of $[Mn(IV)_2(\mu\text{-}O)_3L_2](PF_6)_2$ is gradually increasing in agreement with slow uptake of $[Mn(IV)_2(\mu\text{-}O)_3L_2](PF_6)_2$ into the cotton fiber material. Figure 8.5D shows a typical pattern of the increase of the charge under the reduction peak at 0.0 V vs. SCE (following a simple exponential law $Q_p = Q_p^{\lim} \times \left[1 - \exp\left(-\frac{t}{\tau}\right)\right]$, with $\tau \approx 100$ minutes, see line) and a limit being reached only after approximately 3 hours. The time constant for uptake is independent of the solution concentration and is interpreted here as slow diffusion of $[Mn(IV)_2(\mu\text{-}O)_3L_2](PF_6)_2$ into the active region between graphite and cotton. It seems likely that slow diffusion through the amorphous regions of cellulose-I (intra-fiber) dominates.

Figure 8.7A shows typical cyclic voltammetric responses for $[Mn(IV)_2(\mu\text{-}O)_3L_2](PF_6)_2$ soaked and dried into the cotton surface from an aqueous solution followed by rinsing to remove excess (see Experimental). When immobilized into cotton fibers, $[Mn(IV)_2(\mu\text{-}O)_3L_2](PF_6)_2$ shows an open circuit potential of ca. 0.1 V vs. SCE and a currently unidentified anodic peak at ca. 0.4 V vs. SCE (in part due to a fresh graphite background current). A well defined reduction response occurs with a peak potential of ca. 0.0 V vs. SCE consistent with rotating

disc voltammetry data in Figure 8.6 and approximately consistent with literature reports of redox activity in aqueous buffer media [36]. Therefore, in alkaline carbonate buffer solution, this reduction can be identified as a two electron process (*vide supra*) which is followed by a chemical process (possibly the formation of a derivative with carbonato ligands). The reduction observed during the first voltammetric scan is followed by two smaller oxidation responses with peak potential of 0.08 V and 0.30 V vs. SCE. During the second cycle the reduction response for $[Mn(IV)_2(\mu\text{-}O)_3L_2](PF_6)_2$ is still observed although diminished.

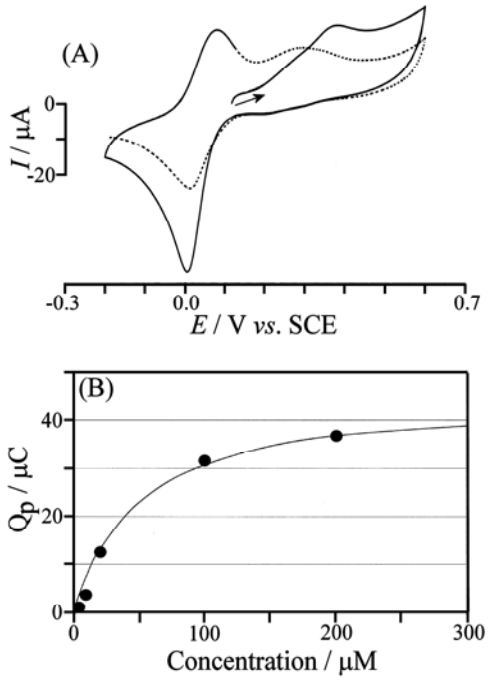

Figure 8.7 (A) **Cyclic voltammogram (scan rate 10 mVs^{-1}) for $[Mn(IV)_2(\mu\text{-}O)_3L_2](PF_6)_2$ dried on in excess and rinsed with water, dried and then investigated in 0.1 M carbonate buffer pH 9.8. The dotted lines indicate the second cycle.** (B) **Langmuir plot of the charge under the reduction peak versus $[Mn(IV)_2(\mu\text{-}O)_3L_2](PF_6)_2$ solution concentration in 0.1 M carbonate buffer pH 9.8. Cotton discs were treated by immersion (30 minutes), drying on a filter paper, immobilization at a graphite electrode, and voltammetric measurement in 0.1 M carbonate buffer pH 9.8.**

In order to obtain more reliable adsorption data and to eliminate the problem of additional adsorption directly onto the graphite surface, cotton samples were prepared first by placing them into solutions of different $[Mn(IV)_2(\mu\text{-}O)_3L_2](PF_6)_2$ concentrations in 0.1 M carbonate buffer pH 9.8, followed by drying between filter paper, impregnation with graphite, immobilization at the graphite electrode surface and immersion in clean aqueous carbonate buffer at pH 9.8 for voltammetric analysis. This procedure yields a clear dependence of the

charge Q_p under the reduction response at 0.0 V vs. SCE on the concentration of $[Mn(IV)_2(\mu\text{-}O)_3L_2](PF_6)_2$. A Langmuirian dependence (see Figure 8.7B) is observed and the binding constant, approximately $K = 2 \times 10^3$ $mol^{-1}dm^3$, is determined. At a higher concentration of 0.5 mM $[Mn(IV)_2(\mu\text{-}O)_3L_2](PF_6)_2$ the value of Q_p was observed to increase again (not shown) and this was interpreted as more extensive adsorption into multi-layers (compare the samples with $[Mn(IV)_2(\mu\text{-}O)_3L_2](PF_6)_2$ dried on followed by rinsing, Figure 8.7A). Next, the interaction of the $[Mn(IV)_2(\mu\text{-}O)_3L_2](PF_6)_2$ metal complex immobilized at the cotton surface and in contact with hydrogen peroxide is investigated.

8.3.4. Voltammetric Measurements with $[Mn(IV)_2(\mu\text{-}O)_3L_2](PF_6)_2$ Modified Cotton in the Presence of Hydrogen Peroxide

Catalase activity in the presence of hydrogen peroxide can result in both anodic or cathodic current responses (see Pt coated cotton, Figure 8.5) depending on the nature of the catalytic cycle and the reactive intermediate undergoing electron transfer. For the $[Mn(IV)_2(\mu\text{-}O)_3L_2](PF_6)_2$ metal complex, a distinct and H_2O_2 concentration dependent additional anodic current response is observed (see Figure 8.8A).

Figure 8.8A shows a three cycle (the first 3 scans) cyclic voltammogram obtained with a fresh cotton disc (with $[Mn(IV)_2(\mu\text{-}O)_3L_2](PF_6)_2$ dried on) in the presence of 8 mM H_2O_2 and at a 100 rad s^{-1} rate of rotation. Very interesting is the initial cathodic peak which is observed only during the first potential cycle. This peak is proportional to the amount of $[Mn(IV)_2(\mu\text{-}O)_3L_2](PF_6)_2$ metal complex present and demonstrates (in agreement with literature reports) that no reaction with H_2O_2 prior to reduction occurs [26]. Once activated, the catalytic process is detected as an anodic current response with a limiting current of approximately 90 μA. This value is in very good agreement with the current observed for platinum modified cotton (Figure 8.5) and therefore assigned here to the mass transport limited current for catalytic hydrogen peroxide oxidation (*vide supra*). Pronounced cathodic current peaks at ca. -0.5 to -0.6 V vs. SCE are likely to be associated with the reduction of oxygen produced in the previous anodic process. These peaks are therefore not of interest in further discussion.

Mechanistically, the rapid formation of a reduced state within the $[Mn(IV)_2(\mu\text{-}O)_3L_2](PF_6)_2$ based catalytic cycle appears to dominate the process and significant coupling of hydrogen peroxide conversion to the electrode process occurs only at positive potentials where the reduced catalyst is oxidized. In contrast, when investigated in solution the $[Mn(IV)_2(\mu\text{-}O)_3L_2](PF_6)_2$ metal complex behaves very differently. Figure 8.8B(iv) shows voltammograms obtained for the reduction of 0.2 mM $[Mn(IV)_2(\mu\text{-}O)_3L_2](PF_6)_2$ metal complex in 0.1 M carbonate buffer at pH 9.8 under rotating disc conditions and with/without hydrogen peroxide. In contrast to measurements in the presence of cotton, in solution, the metal complex is catalyzing the *electro-reduction* of hydrogen peroxide and the current for this reduction increases proportional to the H_2O_2 concentration (not shown). Intriguingly, upon cycling the potential to more positive values, initially only a very weak catalytic effect for the oxidation of hydrogen peroxide is observed which then steadily increases culminating in a peak response at ca. 0.2 V vs. SCE. This complex redox behaviour is attributed to the adsorption of a catalytically active state of the metal complex onto graphite at sufficiently positive applied potentials. It is very likely that the species adsorbing onto the graphite at positive applied potentials is closely related to the catalytically active species absorbed into the cotton. The different effects of electrode potential on processes in solution and in cotton suggest that in the presence of cotton direct adsorption onto graphite is less important. However, these mechanistic features are currently not fully resolved.

Rotating disc voltammograms shown in Figure 8.8B(i-iii) further demonstrate the catalytic effect of the $[Mn(IV)_2(\mu\text{-}O)_3L_2](PF_6)_2$ metal complex absorbed into cotton. Increasing the H_2O_2 concentration causes a linear increase in the anodic (catalytic) current response whereas no cathodic currents are observed. Next, by lowering the amount of catalyst adsorbed onto the cotton surface, a transition from diffusion control to kinetic control is observed.

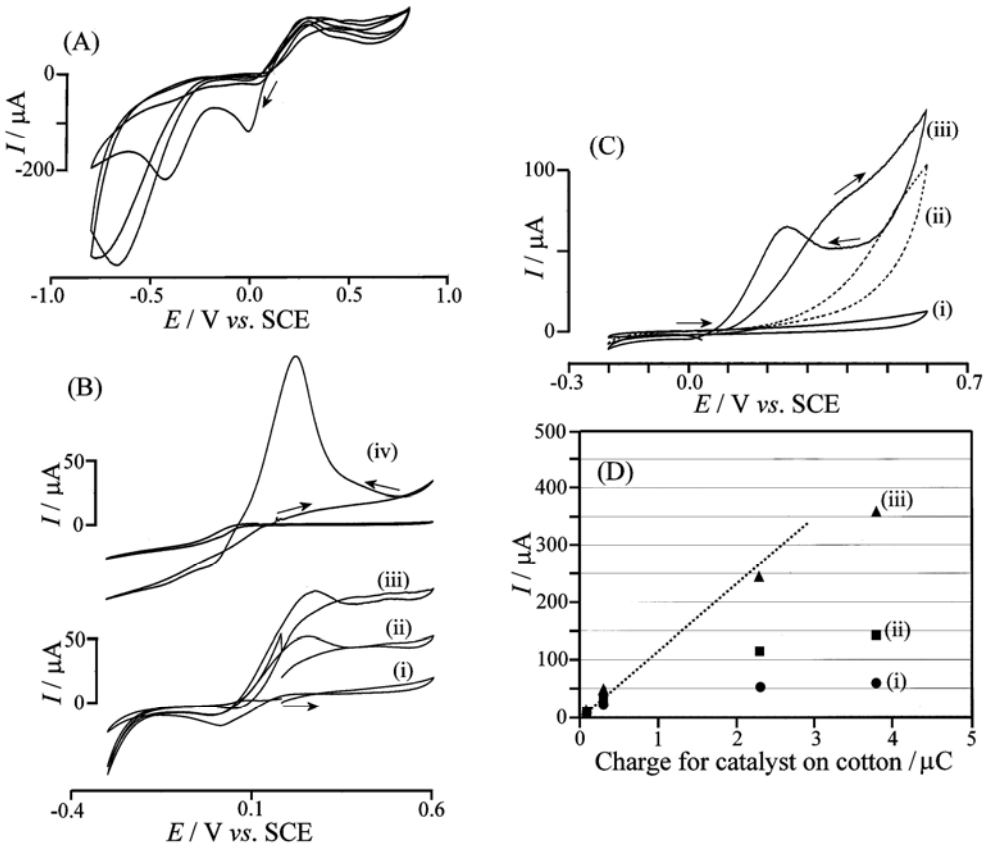

Figure 8.8 (A) **Consecutive cyclic voltammograms (scan rate 10 mVs^{-1}) obtained for cotton discs with $[Mn(IV)_2(\mu\text{-}O)_3L_2](PF_6)_2$ (dried on and rinsed) immobilized at a 4.9 mm diameter graphite electrode and immersed in 0.1 M carbonate buffer pH 9.8 in the presence of 8 mM H_2O_2. The first three voltammograms obtained with a rotating disc electrode (100 rad s^{-1} rate of rotation) are shown.** (Bi-iii) **Conditions as in (A) but with (i) 1 mM, (ii) 4 mM, and (iii) 8 mM H_2O_2 concentration. Voltammograms in (Biv) were obtained without cotton at a rotating (63 rad s^{-1}) graphite electrode immersed in 0.2 mM $[Mn(IV)_2(\mu\text{-}O)_3L_2](PF_6)_2$ in 0.1 M carbonate buffer pH 9.8 (without and with 4 mM H_2O_2).** (C) **Rotating disc cyclic voltammograms (100 rad s^{-1} rotation rate, scan rate 10 mVs^{-1}) obtained for a 4.9 mm diameter graphite electrode immersed in 0.1 M carbonate buffer pH 9.8 containing 8 mM H_2O_2 (i) bare, (ii) with clean cotton, and (iii) with 2.3 μC $[Mn(IV)_2(\mu\text{-}O)_3L_2](PF_6)_2$ on a cotton disc (adsorbed from 50 μM $[Mn(IV)_2(\mu\text{-}O)_3L_2](PF_6)_2$ in 0.1 M carbonate buffer pH 9.8).** (D) **Plot of the limiting current for the catalytic H_2O_2 oxidation versus the amount (charge) of $[Mn(IV)_2(\mu\text{-}O)_3L_2](PF_6)_2$ on the cotton surface. Data are given for (i) measured limiting currents, (ii) mass transport corrected kinetic limiting currents, and (iii) H_2O_2 depletion and mass transport corrected kinetic limiting currents. The dotted line indicates the approximately linear correlation employed for the derivation of the rate law.**

Figure 8.8C shows a cyclic voltammogram obtained at a rotating disc electrode (16 Hz, 8 mM H_2O_2) confirming that the anodic limiting current decreases with the amount of catalyst adsorbed. In the plot in Figure 8.8D data points (i) indicate the measured limiting currents as a function of the amount of catalyst on the cotton surface. In order to extract the kinetic catalytic current from this mixed diffusion – kinetic controlled current the following very approximate expression can be employed (Equation 8.3).

Equation 8.3

$$I_{\text{kinetic}} = \left(\frac{1}{I_{\text{experimental}}} - \frac{1}{I_{\text{diffusion}}} \right)^{-1}$$

In this expression I_{kinetic} is the current corrected for mass transport effects, $I_{\text{experimental}}$ is the measured anodic limiting current, and $I_{\text{diffusion}}$ refers to the limit of mass transport. Data for the kinetic limiting currents are included in the plot in Figure 8.8D (data points (ii)). Measurements with low catalyst loading and variable concentrations of H_2O_2 (not shown) confirm that the rate of H_2O_2 oxidation increases proportionally to H_2O_2 concentration, and a simple rate law for the catalytic oxidation process can be proposed (equation 8.4).

Equation 8.4

$$rate = k \times [catalyst]_{surface} \times [H_2O_2]_{surface}$$

Due to the depletion of H_2O_2 during the anodic process, the steady state concentration $[H_2O_2]_{surface}$ during rotating disc voltammetry experiments is likely to be different compared to the bulk concentration $[H_2O_2]_{solution}$ (with high catalyst loading the surface concentration becomes essentially zero at the electrode surface when the mass transport limit is reached). A further simple correction (assuming a planar diffusion profile) can be introduced to approximately compensate for this depletion effect (Equation 8.5).

Equation 8.5

$$[H_2O_2]_{surface} = [H_2O_2]_{solution} \times \frac{I_{\text{diffusion}} - I_{\text{experimental}}}{I_{\text{diffusion}}}$$

By applying this correction to data in Figure 8.8D (the current values were adjusted to be consistent with a surface concentration of 8 mM H_2O_2) a plot of kinetic limiting currents approximately linearly correlated with the surface concentration of catalyst on cotton is obtained (Figure 8.8D, data points (iii)). The dotted line is confirming the rate law (Equation 8.4) and allows the rate constant $k = 3 \times 10^4$ $dm^3s^{-1}mol^{-1}$ to be estimated (using the geometric surface area of the electrode). A further interesting general conclusion concerning the reactivity of the $[Mn(IV)_2(\mu\text{-}O)_3L_2](PF_6)_2$ metal complex is that absorption into cotton remains

strong even in the presence in the H_2O_2 and loss of catalyst into the solution phase is insignificant.

Further studies will be required to more firmly link catalyst activity to current responses observed in the presence of hydrogen peroxide. The effect of the reaction type (catalase, oxygenase, bleaching etc.) on the electrochemical behaviour remains to be explored. However, the observation that information about the adsorption and reactivity of the $[Mn(IV)_2(\mu\text{-}O)_3L_2](PF_6)_2$ metal complex on cotton is available from relatively simple voltammetric experiments is promising and may lead to further experimental developments. The voltammetric study of textiles impregnated with graphite flakes is a versatile tool and will allow catalyst activity and catalyst effects on redox active stains to be correlated under relevant conditions (e.g. in aqueous carbonate buffer media).

8.4. Conclusions

It has been shown that voltammetric measurements at cotton surfaces provide detailed insights into (i) absorption processes involving redox active species, (ii) reactivity at the cotton surface, and (iii) catalytic reactions involving hydrogen peroxide. For the case of the metal complex $[Mn(IV)_2(\mu\text{-}O)_3L_2](PF_6)_2$ a surprising difference in reactivity in the presence and in the absence of cotton has been noted and this observation highlights the need for experimental tools to assess catalyst reactivity in the presence of textiles. Voltammetry as a versatile experimental tool will be of interest not only for cotton, but possibly for a wider range of applications involving surface processes at different types of fabrics, surface modification processes, intra-fiber diffusion in cotton and fabrics, and the determination and optimization of catalyst reactivity.

8.5. References

[1] F. Scholz, U. Schröder, R. Gulaboski, "Electrochemistry of immobilized particles and droplets*" Springer: Berlin,* **2005**.

[2] D. Klemm, B. Heublein, H.P. Fink, A. Bohn, *Angewante Chemie International Edition* 44**, 2005**, 3358.

[3] H.A. Krässig, "Cellulose – Structure, Accessibility and Reactivity", *Gordon and Breach: Amsterdam,* **1993**.

[4] E.J. Roberts, S.P. Rowland, *Environmental Science & Technology* 7, **1973**, 552.

[5] H.R. Khavasi, N. Safari, *Journal of Porphyrins & Phthalocyanines* 9, **2005**, 75.

[6] F. Gozzo, *Journal of Molecular Catalysts A* 171, **2001**, 1.

[7] T. Okuno, S. Ito, S. Ohba, Y. J. Nishida, *Dalton Transactions* **1997**, 3547.

[8] D.M. Gould, M. Spiro, W.P. Griffith, *Journal of Molecular Catalysts A* 186, **2002**, 69.

[9] J. Selverstone, C.S. Valentine, A. Foote, Greenberg, J.F. Liebman, "Active oxygen in biochemistry*" Chapman & Hall: London*, **1995**.

[10] A. Sigel, H. Sigel, "Manganese and its role in biological processes", *Marcel Dekker: New York,* **2000**.

[11] S. Sinnecker, F. Neese, W. J. Lubitz, *Biological & Inorganic Chemistry 10*, **2005**, 231.

[12] J. Limburg, G.W. Brudvig, R.H. Crabtree, "Biomimetic oxidation chemistry", B. Meunier, (ed.), *World Scientific: Singapore,* **2000**, p. 509.

[13] K. Wieghardt, U. Bossek, W. Gebert, *Angewante Chemie, International Edition*. 22, **1983**, 328.

[14] K. Wieghardt, U. Bossek, B. Nuber, J. Weiss, J. Bonvoisin, M. Corbella, S.E. Vitols, J.J. Girerd, *Journal of the American Chemical Society* 110, **1988**, 7398.

[15] J.H. Koek, S.W. Russell, L. van der Wolf, R. Hage, J.B. Warnaar, A.L. Spek, J. Kerschner, L. DelPizzo, *Dalton Transactions* **1996**, 353.

[16] K. Wieghardt, K. Pohl, U. Bossek, B. Nuber, J. Weiss, *Zeitschr. Naturforsch. Sec.* B 43, **1988**, 1184.

[17] G.W. Brudvig, W.F. Beck, J.C. de Paula, *Annual Review of Biophysics & Biophysical*

Chemistry 18, **1989**, 25.

[18] A. Berkessel, C.A. Sklorz, *Tetrahedron Letters 40*, **1999**, 7965.

[19] D.E. De Vos, S. De Wildeman, B.F. Sels, P.J. Grobet, P.A. Jacobs, *Angewante Chemie, International Edition* 38, **1999**, 980.

[20] G.B. Shul'pin, G.V. Nizova, Y.N. Kozlov, I.G. Pechenkina, *New Journal of Chemistry* 26, **2002**, 1238.

[21] J.W. de Boer, J. Brinksma, W.R. Browne, A. Meetsma, P.L. Alsters, R. Hage, B.L. Feringa, *Journal of the American Chemical Society* 127, **2005**, 7990.

[22] V. Pecoraro, (ed.) "Manganese redox enzymes", *VCH: Weinheim,* **1992**.

[23] U. Bossek, M. Saher, T. Weyhermüller, K. Wieghardt, *Chemistry Communications* **1992**, 1780.

[24] R. Hage, B. Krijnen, J.B. Warnaar, F. Hartl, D.J. Stufkens, T.L. Snoeck, *Inorganic Chemistry* 34, **1995**, 4973.

[25] B.C. Gilbert, J.R. Lindsay Smith, I. Mairata, A.Payeras, J. Oakes, *Organic Biomolecular Chemistry* 2*,* **2004**, 1176.

[26] R. Hage, J.E. Iburg, J. Kerschner, J.H. Koek, E.L.M. Lempers, R.J. Martens, U.S. Racherla, S.W. Russell, T. Swarthoff, M. R. P. van Vliet, J.B. Warnaar, L. van der Wolf, B. Krijnen, *Nature* 369, **1994**, 637.

[27] K.O. Schäfer, R. Bittl, F. Lendzian, V. Barynin, T. Weyhermüller, K. Wieghardt, W. Lubitz, *Journal of Physical Chemistry B* 107, **2003**, 1242.

[28] B.C. Gilbert, J.R.I. Lindsay Smith, A. M. Payeras, J. Oakes, *Organic Biomolecular Chemistry* 2, **2004**, 1176.

[29] T.H. Bennur, D. Srinivas, S. Sivasanker, V.G. Puranik. *Journal of Molecular Catalysis A* 219*,* **2004**, 209.

[30] R.N. Adams, "Electrochemistry at solid electrodes", *Marcel Dekker: New York* **1969** p.219.

[31] J.L. Fernandez, C. Hurth, A.J. Bard, *Journal of Physical Chemistry* B 109, **2005**, 9532.

[32] S.A.G. Evans, J.M. Elliott, L.M. Andrews, P.N. Bartlett, P.J. Doyle, G. Denuault, *Analytical Chemistry* 74, **2002**, 1322.

[33] C.B. Woitiski, Y.N. Kozlov, D. Mandelli, G.V. Nizova, U. Scguchardt, G.B. Shul'pin,

Journal of Molecular Catalysis A 222, **2004**, 103.

[34] B.C. Gilbert, J.R. Lindsay Smith, I Mairata, A. Payeras, J. Oakes, I. Pons, R. Prats, *Journal of Molecular Catalysis A* 219, **2004**, 265.

[35] P.W. Atkins, J. de Paulo, "Physical Chemistry", *7th edition, Oxford University Press: Oxford* **2002**, p. 845.

[36] R. Hage, B. Krijnen, J.B. Warnaar, F. Hartl, D.J. Stufkens, T.L. Snoeck, *Inorganic Chemistry* 34, **1995**, 4973.

Chapter 9: Conclusions

The focus of this thesis examines the physical and chemical properties of cellulose and how it behaves when part of an integrated chemical system. Electrochemistry, and in particular voltammetry, has been used as the predominant chemical tool kit. This has necessitated the development of new methodologies for cellulose electrochemistry. It has been demonstrated that cellulose can be formed onto an electroactive substrate enabling the study of naturally occurring and novel cellulose architectures.

Cellulose is explored in various forms from the nano-scale through the micro- to the macro-scale. Cotton, a natural source of cellulose and refined spruce tree cellulose fibrils were used to explore forms of pure cellulose. A supply of cellulose nanofibrils by Prof. Wim Thielemans enabled the study of nanotechnology formation methodologies with addition component for form composite cellulose materials. This enabled the addition of new properties and functionality to the cellulose matrix.

The materials used to form the new cellulose structures also vary in scale. At the molecular level there has been the manipulation of dendrimer units; on the nanoscale TiO_2 nanoparticles have been used to incorporate electrical properties and to cellulose-polymer composite structures, of both natural (chitosan) and synthetic (polydiallyldimethylammonium chloride or PDDAC) origin, have been created. Due to the structural rigidity of the cellulose, nanostructural combinations are proven to form easily on electrode substrates and as free standing macroscopic materials in their own right. These new nanocellulose materials are of use as possible biological, environmental and physiological analyte sensors.

The general versatility of cellulose is due to its intrinsic inert state and structural stability. Cellulose-TiO_2 thin films can be form using layer-by-layer deposition on indium doped tin oxide (ITO) electrodes. Cellulose-TiO_2 films were used as a substrate for the immobilization of a redox protein, methemoglobin. The demetallation of methemoglobin mechanism was

discovered and explored and methods to inhibited demetallation suggested. The TiO_2-cellulose films offer a novel substrate for the facile immobilization of redox proteins and could in future be used as a biological analyte sensor.

Films of nanocellulose-PDDAC and nanocellulose-chitosan were formed on glassy carbon electrode substrates using a solvent casting technique. Both films demonstrate preferential adsorption of charged ions from the solution phase. Absorption into the films is promoted by the presence of "receptors" embedded in a "sandwich" structure which facilitates selective binding in the film. The receptor sites in the nanocellulose-PDDAC are polycationic in nature due to the presence of a positively charge nitrogen site on the PDDAC chain. The reactivity of nanocellulose-chitosan films is dominated by the chitosan component. Binding of anions is effective at a pH lower than the pK_A of chitosan (6-7) where the chitosan is protonated. The accumulation and transport of multiply charged anions such as $Fe(CN)_6^{3-/4-}$ has been examined. Voltammetric studies show that although diffusion within the cellulose-PDDAC and cellulose-chitosan structure is slow (ca. 6 orders of magnitude slower than in aqueous solution) good analytical signals are obtained. The Langmuirian binding co-efficient and upper and lower limits of detection of $Fe(CN)_6^{3-/4-}$ were measured for both films (see table 9.1) The nanocellulose-PDDAC film has more effective binding than the nanocellulose-chitosan film.

The nanocellulose-polymer composite electrodes were also shown to be able to detect well known target environmental analytes such as triclosan and sodium dodecylsulphate (SDS). Triclosan is electroactive and subsequently the film merely promotes greater sensitivity to its detection. SDS is electrochemically inert and was detected by competitively binding it into the nanocellulose-chitosan film with $Fe(CN)_6^{4-}$enabling indirect measurement. The methodology put forward is demonstrated to have low limits of detection in the region of low μM levels for both films (see table 9.1). The relatively high affinity of the nanocellulose-chitosan and nanocellulose-PDDAC to triclosan and SDS suggests that both cellulose-polymer composites could be employed in the extraction of excess biocides and surfactants for environments where they are contaminants.

Table 9.1 A summary of all of the cellulose electrodes and the respective diffusion co-efficients, Langmuir binding co-efficients and detection range for various analytes. All values have been calculated using the relevant electrochemical method.

	Analyte	Diffusion Co-efficient, D (m^2 s^{-1})	Langmuir Binding Co-efficient, K (mol^{-1} dm^3)	Detection Range (mol dm^{-3})
Electrodeposited Cellulose	$Ru(NH_3)_6^{3+}$	1.7×10^{-14}	-	-
	Methyl Viologen (MV^{2+})	3.5×10^{-15}	-	-
Nanocellulose-TiO_2	Methemoglobin	-	2×10^5	$10^{-7} – 10^{-4}$
Nanocellulose-PDDAC	$Fe(CN)_6^{4-/3-}$	$\sim 10^{-15}$	1.2×10^4	$10^{-5} – 10^{-3}$
	Triclosan	-	2.1×10^4	$10^{-6} – 10^{-3}$
Nanocellulose-Chitosan	$Fe(CN)_6^{4-}$	-	2.2×10^3	$10^{-5} – 10^{-2}$
	Triclosan	-	2.6×10^3	$10^{-6} – 10^{-3}$
	SDS	-	3×10^4	$10^{-5} – 10^{-3}$
Nanocellulose-Boronic Acid Dendrimer	Alizarin Red S	-	6×10^3	$10^{-5} – 10^{-3}$
Cotton	$Fe(CN)_6^{3-}$	1.3×10^{-10}	-	-
	$Ru(NH_3)_6^{3+}$	1.1×10^{-10}	-	-
	$Fe(BBA)Cl^+$	2.5×10^{-11}	-	-
	Hemin	7×10^{-12}	-	-
	$[Mn(IV)_2(\mu\text{-}O)_3L_2](PF_6)_2$	-	2×10^3	$10^{-6} – 10^{-4}$

Nanocellulose-boronic acid dendrimer membranes were formed by ulitizing the binding ability of boronic acids to poly-sacharride interfaces. Excess of boronic acid binding sites introduced into the film allows the absorption, diffusion and detection of analytes that are susceptible to bind to the sites. Alizarin red S, a common diol probe dye molecule which is electrochemical active was absorbed into the membrane and followed both spectrophotometrically and voltammetrically. It was possible to obtain binding information and detection limits (see table 9.1) suggesting that this might be a suitable methodology for detecting physiological analytes which often have diol functionality, for example glucose.

Plain cellulose in the form of refined spruce tree fibrils and cotton were also studied. Electro-deposition was used to form micro-porous films of spruce tree fibrils onto boron-doped diamond electrode surfaces. Accumulation of model cationic redox systems was achieved and the mass transport via diffusion within a cellulose environment was examined and diffusion co-efficient for charged cationic species obtain (see table 9.1). Diffusion was inhibited by the presence of the cellulose when compared to solution phase diffusion by approximately 5 orders of magnitude slower. It was also discovered that the cellulose matrix promotes additional chemical processes due to preferential partitioning at the cellulose solution interface. The dimerisation, when reduced, of methyl viologen was seen to be promoted by this preferential partitioning.

Finally, it has been shown that processes within cotton can be monitored using voltammetry experiments. A procedure where graphite flakes were applied to a cotton textile sample proved to be highly reproducible and versatile. Information about (i) the uptake and binding of metal complexes into cotton samples, (ii) they're mobility and rate of diffusion, (iii) and chemical reactivity (including catalytic reaction involving hydrogen peroxide) within the amorphous cellulose environment has been obtained. For the case of the metal complex $[Mn(IV)_2(\mu\text{-}O)_3L_2](PF_6)_2$ a surprising difference in reactivity in the presence and in the absence of cotton.

When comparing the diffusion of species in solution, in artificially constructed cellulose architectures and in naturally occurring cellulose structures, there is a variation by orders of magnitude in the respective diffusion co-efficients. The behaviour of the $Fe(CN)_6^{3-/4-}$ anion has been studied in all the different types of cellulose. With a diffusion co-efficient in solution of 5×10^{-10} m^2 s^{-1}, the interactive nature of the cellulose matrix upon its dynamics at an electrode surface is appreciable. In more densely packed cellulose architectures (micro- and nanocellulose modified electrodes) the diffusion co-efficient is in the order of $10^{-14} – 10^{-15}$ m^2 s^{-1}. Where this comparison becomes most interesting is the cotton case where both inter- and intra-fiber diffusion occur and the composite diffusion results in an observed composite diffusion co-efficient of 2.5×10^{-11} m^2 s^{-1}. Mass transport fluctuations and the additional change in reactivity of complexes in cellulose matrices highlights the need for experimental tools to assess reactivity in heterogeneous systems. Voltammetry as a versatile experimental

tool will be of interest not only for cotton, but possibly for a wider range of applications involving surface processes at different types of fabrics, surface modification processes, intra-fiber diffusion in cotton and fabrics, and the determination and optimization of catalyst reactivity.

In future this methodology could be applied for a wider range of redox systems and under varying conditions (textile pre-treatment, solution pH, composition, and temperature) to provide information about the chemical processes within cotton and other textiles. In future, better experimental and data analysis approaches (for example simulation of diffusion, partition co-efficients) will be required in order to address more complex questions concerning the mechanism of processes and to overcome problems with the heterogeneity of samples. It has also been shown here that the versatility of cellulose and the facile incorporation of "receptor" components into nanocellulose films will be of interest in many areas of sensor development, membrane technology, and drug release applications. The nanoscale methodologies utilised here (layer-by-layer thin film formation and solvent evaporation or casting) are both viable for scale-up due to their ease of formation, a possible route to the mass production of cellulose sensors.